The Dissertation Committee for Yongha Kim certifies that this is the approved version of the following dissertation:

Polymer Nanocomposite Foams: Fabrication, Characterization, and Modeling

Committee:

Wei Li, Supervisor

Jonathan Y. Chen

Dragan Djurdjanovic

Paulo Ferreira

Joseph H. Koo

Polymer Nanocomposite Foams: Fabrication, Characterization, and Modeling

by

Yongha Kim, BSE.; MSME.

Dissertation

Presented to the Faculty of the Graduate School of

The University of Texas at Austin

in Partial Fulfillment

of the Requirements

for the Degree of

Doctor of Philosophy

The University of Texas at Austin

December 2012

Dedication

To my lovely wife, son, and daughter: Youngmi Hong, Daniel Kim, and Irene Kim,

whose infinite love I cherish greatly

Acknowledgements

I would first like to express my sincere gratitude and appreciation to Dr. Wei Li, my advisor and chair of my Ph.D. advisory committee, for his expert guidance, mentorship, encouragement, and support. From his wish to see students' success, he has been a great mentor academically and professionally. I have learned a great deal from him, and am truly grateful.

I would also like to express my sincere thanks to my graduate advisory committee: Drs. Jonathan J. Chen, Dragan Djurdjanovic, Paulo Ferreira, and Joseph H. Koo for their service and advices. Their valuable guidance has served to improve my Ph.D. works.

I would like to thank the members of Nano and Bio Materials Processing and Manufacturing Lab: Liang Ma, Sriharsha Sundarram, Wei Jiang, Nanzhu Zhao, Russell Borduin, Jungyu Ock, Daniel Justiss, Zelalem Arega, Bryan Philpott, Changchun Zhou, Emmanuel Cua, Jordan Lee, and Jeremy Barker, for constructive discussions during this research.

Lastly, I would like to thank my parents and parents-in-law for their love and support from Korea. I would like to express my sincerest appreciation to my wife, Youngmi Hong, for her love, support, patience, and understanding. Without her grace and courage, I could have not completed this Ph.D. dissertation.

Polymer Nanocomposite Foams: Fabrication, Characterization, and Modeling

Publication No._____

Yongha Kim, Ph.D.

The University of Texas at Austin, 2012

Supervisor: Wei Li

Polymer nanocomposite foams have attracted tremendous interests due to their multifunctional properties in addition to the inherited lightweight benefit of being foamed materials. Polymer nanocomposite foams using high performance polymer and bio-degradable polymer with carbon nanotubes were fabricated, and the effects of foam density and pore size on properties were characterized. Electrical conductivity modeling of polymer nanocomposite foams was conducted to investigate the effects of density and pore size.

High performance polymer Polyetherimide (PEI) and multi-walled carbon nanotube (MWCNT) nanocomposites and their foams were fabricated using solvent-casting and solid-state foaming under different foaming conditions. Addition of

MWCNTs has little effect on the storage modulus of the nanocomposites. High glass transition temperature of PEI matrix was maintained in the PEI/MWCNT nanocomposites and foams. Volume electrical conductivities of the nanocomposite foams beyond the percolation threshold were within the range of electro-dissipative materials according to the ANSI/ESD standard, which indicates that these lightweight materials could be suitable for electro-static dissipation applications with high temperature requirements.

Biodegradable Polylactic acid (PLA) and MWCNT nanocomposites and their foams were fabricated using melt-blending and solid-state foaming under different foaming conditions. Addition of MWCNTs increased the storage modulus of PLA/MWCNT composites. By foaming, the glass transition temperature increased. Volume electrical conductivities of foams with MWCNT contents beyond the percolation threshold were again within the range of electro-dissipative materials according to the ANSI/ESD standard. The foams with a saturation pressure of 2 MPa and foaming temperature of 100 °C showed a weight reduction of 90% without the sacrifice of electrical conductivity. This result is promising in terms of multi-functionality and material saving. At a given CNT loading expressed as volume percent, the electrical conductivity increased significantly as porosity increased.

A Monte-Carlo simulation model was developed to understand and predict the electrical conductivity of polymer/MWCNT nanocomposite foams. Two different foam morphologies were considered, designated as Case 1: volume expansion without nanotube rearrangement, and Case 2: nanotube aggregation in cell walls. Simulation

results from unfoamed nanocomposites and the Case 1 model were validated with experimental data. The results were in good agreement with those from PEI/MWCNT nanocomposites and their foams, which had a similar microstructure as modeled in Case 1. Porosity effects on electrical conductivity were investigated for both Case 1 and Case 2 models. There was no porosity effect on electrical conductivity at a given volume percent CNT loading for Case 1. However, for Case 2 the electrical conductivity increased as porosity increased. Pore size effect was investigated using the Case 2 model. As pore size increased, the electrical conductivity also increased.

Electrical conductivity prediction of foamed polymer nanocomposites using FEM was performed. The results obtained from FEM were compared with those from the Monte-Carlo simulation method. Feasibility of using FEM to predict the electrical conductivity of foamed polymer nanocomposites was discussed. FEM was able to predict the electrical conductivity of polymer nanocomposite foams represented by the Case 2 model with various porosities. However, it could not capture the pore size effect in the electrical conductivity prediction. The FEM simulation can be utilized to predict the electrical conductivity of Case 2 foams when the percolation threshold is determined by Monte-Carlo simulation to save the computational time. This has only been verified when the pore size is small in the range of a few micrometers.

Table of Contents

List of Tables

List of Figures

Chapter 1. Introduction

1.1 MOTIVATION OF THIS RESEARCH

Polymer nanocomposite foams with improved electrical conductivity have recently been studied for lightweight electrostatic discharge (ESD), electromagnetic interference (EMI) shielding, and lightning-strike protection applications. It is well known that a small amount of highly conductive nanoparticles, when well dispersed, could form a conducting network in the polymer matrix. Making these polymer nanocomposites into foams would create a new class of lightweight materials that will find many applications in aerospace, automotive, and electronics applications. ESD and EMI can be serious issues for electronics due to possible spark generation by static charge build-up and emitted electromagnetic waves that interfere with the operation of the electronic equipment [1]. To prevent ESD and EMI, metal-based materials either thin sheet metals or metal coated plastics, have been used traditionally. However, these materials suffer from problems such as being heavy, prone to corrosion, and difficult to process. Conductive polymer nanocomposite foams have distinct advantages compared to metal based materials, especially for ESD and EMI applications in aircrafts, space crafts, and automobiles due to their desirable lightweight properties.

A variety of polymer matrices have been used to create foams with conducting fillers, including multiwall carbon nanotubes (MWCNTs), graphene platelets, and carbon nanofibers (CNFs) [2-10]. A key objective of recent studies is to improve the electrical conductivity, since it is the most important characteristic for ESD and EMI shielding applications. Although their electrical conductivities are high enough, the matrix materials used in previous studies all have a low service temperature and may not be suitable for high performance applications, such as aircraft interior. Therefore, it is needed to fabricate conductive nanocomposite foams using high performance polymer to take the advantages of matrix material properties such as the high glass transition temperature.

Environmental issues have been considered as an important factor in plastic manufacturing, due to the increased demand to reduce land fill. Plastic consumption is subjected to increase by a factor of three in the current decade [11]. Especially, the lifetime of electronics is becoming shorter. Currently the average lifetime of consumer electronics is approaching to just several months [11]. Plastics used in these products start to become waste faster. Utilizing biodegradable polymers is considered to be a solution to reducing the plastic wastes. Therefore, in the area of conductive polymer nanocomposite foams, biodegradable polymers can be applied for lightweight ESD and EMI shielding applications.

Electrical conductivity modeling of nanocomposite foams would be useful for understanding and predicting the electrical property. However, little effort has been found in literature. In spite of the lack of theoretical studies on conductive foamed polymer nanocomposites, there are many research efforts devoted to understanding and predicting the electrical behaviors of unfoamed polymer nanocomposites with fibrous fillers using Monte-Carlo simulation. In this study the Monte-Carlo simulation method is applied to model the electrical conductivity of polymer nanocomposite foams.

Monte-Carlo simulation requires lengthy computational time. To reduce the computational load, the finite element analysis (FEA) method is investigated for electrical conductivity prediction for foamed polymer nanocomposites. If this approach is feasible, the electrical conductivity prediction of foamed polymer nanocomposites could be done more efficiently.

1.2 RESEARCH OBJECTIVES

The goal of this research is to investigate the effects of foam density and morphology such as pore size on electrical properties of polymer nanocomposite foams through both experimental and theoretical studies. Specifically, the following objectives have been identified.

- To fabricate and characterize electrically conductive polymer nanocomposite foams with a high temperature polymer matrix and MWCNTs,
- To fabricate and characterize electrically conductive polymer nanocomposite foams with a biodegradable polymer matrix and MWCNTs,
- To model electrical conductivity of foamed polymer nanocomposites with fibrous nanofillers using Monte-Carlo simulation, and
- To investigate the feasibility of using the finite element analysis method to predict electrical conductivity of polymer nanocomposite foams.

1.3 ORGANIZATION OF THIS DISSERTATION

This thesis is organized into seven chapters. Chapter 1 is a brief introduction to the motivation and objectives of this research. Chapter 2 provides a literature review on the state of the art of polymer nanocomposite foams research and electrical conductivity modeling of unfoamed polymer nanocomposites systems using 3-D Monte-Carlo simulation. The purpose of the simulation is to understand and predict electrical conductivity of foamed polymer nanocomposite foams. In Chapter 3, fabrication and characterization of polymer nanocomposite foams using a high performance polymer and carbon nanotubes were discussed. In Chapter 4, fabrication and characterization of polymer nanocomposite foams using a biodegradable polymer and carbon nanotubes were discussed. The foaming mechanisms of the nanocomposite foams discussed in Chapters 3 and 4 are different. In Chapter 5, electrical conductivity modeling of polymer nanocomposite foams was discussed using the Monte-Carlo simulation method for different foaming mechanisms. Chapter 6 describes the feasibility of using the finite element analysis method to predict the electrical conductivity of polymer nanocomposite foams. Finally, Chapter 7 provides a summary, including conclusions of the current research and recommendations for future work.

Chapter 2. Literature Review

2.1 POLYMER NANOCOMPOSITES

Polymer nanocomposites are materials that are composed of polymer matrices and small amounts (a few wt% of polymer matrices) of nanometer-sized additives [12]. The purpose of producing polymer nanocomposites is to achieve great property improvement of polymer matrices such as mechanical, thermal, and electrical properties. A great amount of interfacial area between polymer matrices and nanometer-sized fillers is the fundamental to distinguish polymer nanocomposites from traditional polymer composites such as carbon fiber-reinforced polymer composites. Polymer nanocomposites could exhibit high performance characteristics beyond what traditional polymer composites had [12].

2.1.1 Types of nanofillers in the polymer nanocomposites

Koo [12] classified nanofillers into three types: one nano-scale dimension (nano-platelet), two nano-scale dimension (nano-fiber), and three nano-scale dimension (nano-particulate), depending on how many dimensions are nano-scaled. For example, nanofibers are two nano-scale dimension nanofillers, since their length is in the micron

scale among the three dimensions. Nanofillers with appropriate physical and dimensional properties can be selected depending on the application.

Among various nanofillers, carbon nanotubes (CNTs), since their discovery in 1991 [13], haven been considered as novel nanofillers and used extensively in both science and engineering due to their exceptional properties [14]. They showed a combination of excellent mechanical, thermal, and electrical properties, which any previous materials could not display [14]. There are two main types of CNTs, single-walled carbon nanobutes (SWCNTs) and multi-walled carbon nanotubes (MWCNTs) depending on the number of rolled cylinder-shaped graphene sheets in the CNTs, and SWCNTs possess better physical properties in general [15]. Applications of CNTs in various technical areas such as automotive, aerospace, energy, and medicine include gas adsorbents, actuators, composite reinforcements, catalyst support, and chemical sensors [15]. Due to the excessively expensive material cost of SWCNTs (100 times more than that of MWCNTs) [12], MWCNTs could be a better alternative in various applications to be economically feasible.

2.1.2 Synthesis methods of polymer nanocomposites

To synthesis polymer nanocomposites by incorporating polymer matrices and nanofillers, there are three representative methods, which are solution blending, melt blending, and in-situ polymerization [16]. In the solution blending method, nanofillers and polymer are mixed in a suitable solvent, and then the solvent is evaporated to form a composite. In general, mixing is performed by magnetic stirring and ultrasonication. A good solvent needs to be selected for polymer chain disentanglement [17]. A solution blending method is preferred especially for high temperature polymers due to the needs of high temperature for effective polymer flow in the melt blending process [18]. In spite of the advantage of this method, there are a few drawbacks. Residual solvent could affect the performance of the product, such that additional solvent removal processing is needed, which is time and energy consuming [19]. In addition, since large quantity of solvent needs to be used, this method would not be applicable for industrial applications due to economic and environmental issues.

In the melt blending method, thermoplastic polymers and nanofillers are mixed by shear force created by single or twin screw extruder above the glass transition temperature for amorphous polymers and melting temperature for some semi-crystalline polymers [14]. The advantages of this method are its simplicity and compatibility with current industrial techniques [20]. However, the drawback of this method is that this

method is only limited to processing thermoplastic polymers. Some high temperature polymers need high processing temperature which might not be applicable with the existing industrial melt blending techniques. In addition, unexpected polymer degradation could happen in the presence of nanofillers under a high shear rate [21].

The in-situ polymerization method is especially important for insoluble and thermally unstable polymers, which the solution blending or melt blending technique cannot process [14]. Nanofillers are mixed with a low viscosity monomer solution, and mechanical treatment such as ultrasonication is used to achieve filler dispersion [22]. The advantage of this technique is that monomers having high diffusivity could infiltrate into the filler agglomerates to enhance their dispersion [23]. This method can be applied to process almost any kind of polymer composites [14], however, complexity of the chemical process is the drawback of this method.

2.2 POLYMER FOAMS

Polymer foams are materials consisting of a solid polymer matrix and gaseous pores in the structure. Polymer foams are found almost everywhere in our life, such as disposable packaging of fast-food and cushioning of the furniture. Applications of polymer foams can be divided based on the density of foams [24]. High density foams, whose density is about 75 % - 90 % of the unfoamed polymers, are generally used as structural applications, such as battery cases, air-conditioner housing and bases, and washer tops and doors, where certain rigidity is need with weight reduction [24]. Low density foams, whose density is about 10 % to 20 % of the unfoamed polymers, are used in heat and sound insulation, shock mitigation, and floatation, and cushioning applications in automotive, marine, and construction applications [24].

For foam synthesis, use of blowing agents is the most common method. Blowing agents are materials that create gaseous phase in the polymer. They can be divided into chemical and physical blowing agents. Blowing agents can be incorporated into polymer melt for a continuous foaming process where polymers go through gas saturation and foaming simultaneously, or into solid polymer with high pressure for a batch foaming process where polymers experience two separate steps, foaming agent saturation and actual foaming [16].

2.2.1 Chemical foaming agents

Foaming agents can be classified into chemical and physical blowing agents. Chemical foaming agents produce gaseous phases through heat-induced decomposition [24]. There are two types of chemical blowing agents, exothermic and endothermic. Exothermic blowing agents generates heat during the chemical reaction to produce gas, while endothermic blowing agents require heat to react [24]. Manufacturing polyurethane foams is an example to use chemical foaming agents, where isocyanate group reacts with water to produce amine and carbon dioxide (CO_2) [25]. Using chemical foaming agents is especially beneficial to foam thermoset polymers such as polyurethane. It is because thermosets cannot be processed after curing. Adding chemicals in monomers enable foaming during curing. The drawback is the chemical residue. Using chemical blowing agents including azodicabonamide may not be suitable for food or biomedical device containers [24].

2.2.2 Physical foaming agents

Physical foaming agents do not involve any chemical reactions during foaming. Physical foaming agents include atmospheric gases or volatile liquids that evaporate at certain conditions [24]. Nitrogen, CO_2, helium, and argon are examples of permanent gas blowing agents. Chlorofluorocarbons (CFCs), hydrocarbons such as butanes and propanes, and chlorinated hydrocarbons such as dichloromethane (DCM) are examples of volatile liquid blowing agents [24]. CFCs were most widely used physical blowing agent

in industry; however, due to the depletion of the ozone layer by CFCs, it became illegal to use in the US from the year of 2010 according to the Montreal Protocol [26, 16]. Inert gases such as nitrogen and CO_2 have attracted interests nowadays due to their environmentally friendly nature, especially CO_2 for its higher solubility in polymers than that of nitrogen [27].

2.2.3 Continuous foaming process

Foaming processes can be classified by their continuity, to continuous and non-continuous foaming processes. In continuous foaming process, blowing agent saturation and foaming are coupled in a one-step process. Extrusion foaming is a representative example of a continuous foaming process [28]. Polymer (thermoplastic) melt is saturated with a blowing agent (usually physical blowing agent), in a specially designed extruder barrel to withstand high pressure and temperature, and foamed when it exits through the die of the extruder. Phase separation and cell nucleation happen for highly pressurized homogeneous polymer/blowing agent system at ambient environment at extruder die by a rapid pressure drop, creating pores in polymer matrix. Pores grow until the temperature of the polymer/blowing agent system drops to its glass transition temperature (T_g), and a solid foam structure is obtained below T_g of the system [16, 23, 29]. Continuous foaming is the most commonly used method in industry, due to its high productivity [16].

2.2.4 Non-continuous foaming process

In a non-continuous foaming process, blowing agent saturation and foaming steps are decoupled into two separate procedures. Batch foaming is an example of non-continuous foaming process. In a batch foaming process, polymer is saturated with a blowing agent under certain pressures and temperatures. If the saturation temperature is higher than T_g of the blowing agent saturated polymer, the release of pressure would result in cell nucleation and growth due to super saturation and softening of the system. If the saturation temperature is lower than the effective T_g of the polymer/blowing agent system, even though there is a super saturation due to the release of the pressure, the cell is not able to nucleate and grow. In this case, temperature needs to be raised above the effective T_g of the polymer/blowing agent system for foaming to occur. In spite of the low productivity of the process, de-coupled processing steps of non-continuous foaming allow independent manipulation of saturation and foaming steps, resulting in higher process flexibility [16].

2.2.5 Solid-state foaming

Solid-state foaming is one of batch foaming processes, which saturate solid polymer with inert gases at a high pressure and form porous foams by a rapid drop in pressure or a rapid increase in temperature. CO_2 is mostly used inert gas as the blowing agent in solid state foaming due to its non-toxicity, non-flammability, low environmental impact, and affordability [30, 31]. Solid-state foaming allows to process small batches of material, such that it is optimum for laboratory research where there is limited

accessibility to the material due to high cost or complicated sample preparation [31]. In addition, because solid-state foaming is one of non-continuous foaming process, saturation and foaming steps can be manipulated separately, providing precise control over various foaming-related parameters. Separate manipulation of the process parameters would allow study of the effects of each parameter on foam morphology or material properties, which is also an important characteristics for laboratory experiments [31].

2.3 POLYMER NANOCOMPOSITE FOAMS

Polymer nanocomposite foams are literally foamed polymer nanocomposites, and they have attracted tremendous interests due to their improved mechanical, thermal, and electrical properties, in addition to the inherited lightweight benefit of foamed materials [16]. Small amounts of well-dispersed nano additives not only improve material properties from the functionality of nano additives, but also facilitate the bubble nucleation since they create more nucleation sites in the polymer. Compared to the conventional macro or micro-sized fillers, nanofillers generate large amounts of nucleation sites with relatively low filler loading [32], resulting higher cell density (number of cells in a unit volume) and smaller cell size, thus larger surface area in the foam structure. Polymer nanocomposite foams having unique combinational properties are a new class of materials, which could be solutions to problems which conventional materials could not resolve.

2.3.1 Nucleation theory in polymer nanocomposite foams

The classical nucleation theory is used to describe bubble nucleation in polymer nanocomposite foams. The nucleation process can be divided into homogeneous nucleation and heterogeneous nucleation, depending on the existence of the nucleation site. The basic difference between homogeneous and heterogeneous nucleation is the required activation energy for nucleation, which is Gibbs free energy (ΔG). Activation energy for heterogeneous nucleation (ΔG_{het}) is proportional to that of homogeneous nucleation (ΔG_{hom}), by a factor of $S(\Theta)$ which is a function of the contact angle (Θ) between gas and polymer/particle interface. Equation 2-1 shows the relationship between ΔG_{het} and ΔG_{hom}, and Equation 2-2 gives the function of $S(\Theta)$ [23, 33].

$$\Delta G_{het} = \Delta G_{hom} \cdot S(\Theta) \qquad (2\text{-}1)$$

$$S(\Theta) = (1/4)(2 + \cos\Theta)(1 - \cos\Theta)^2 \qquad (2\text{-}2)$$

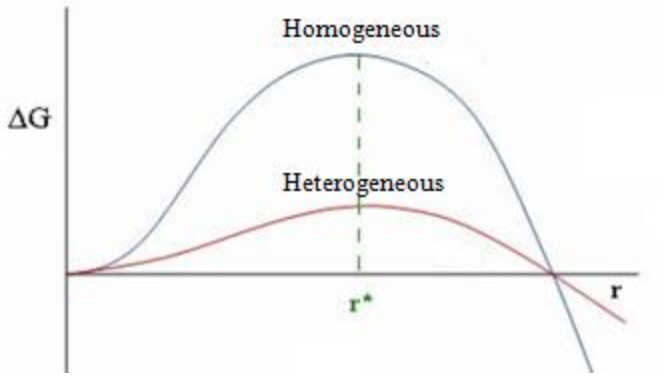

Figure 2-1. Difference in free energy of nucleation for homogeneous and heterogeneous nucleation [23, 33]. r^* is the critical nucleus size to proceed in a spontaneous nucleation process (From r^*, growth in cluster size is not limited by nucleation, but by diffusion [34]).

Since $S(\Theta) < 1$, ΔG_{het} has to be less than ΔG_{hom}. Figure 2-1 shows the ΔG difference graphically. Reduced free energy for heterogeneous nucleation due to existing nucleation sites results in increase in nucleation density [16]. A higher nucleation density for a system having nucleation sites such as those in a polymer nanocomposite system would result in a higher cell density (# of pores in a unit volume of a foam structure) than that of a single phase system, thus small pores under the same foaming condition.

2.3.2 Thermosetting polymer-based nanocomposite foams

Polyurethane (PU)/MWCNT nanocomposite foams were fabricated by Xu et al. [7]. To synthesize nanocomposite foams, a variety of components were employed, such as polyether polyol, polyisocyanate, silicone glycol copolymer, triethanolamine, dibuyltin dilaurate, distilled water, and MWCNTs. MWCNTs were incorporated with polyether polyol separately. Polyisocyanate and distilled water reacted in the system, and gave CO_2 to form pores in the structure. Additional curing process was performed for polymer chains to cross-link. They fabricated PU/MWCNT foams with a porosity of 96% and the electrical conductivity of 10^{-7} S/cm. Further increase in porosity resulted in transition from conductor to insulator.

Nanocomposite foams using elastomer were fabricated by Fletcher et al. [8] for flexible ESD and EMI shielding applications. MWCNTs were added to Fluorocarbon (FKM) and cured by Viton A Bisphenol. Celogen CE was used as the blowing agent. Percolation threshold was found at the MWCNT loading of 2 wt% for unfoamed and 4 wt% for foamed nanocomposites. The maximum electrical conductivity of 10^{-6} S/cm and EMI shielding effectiveness of 20 dB was obtained with a MWCNT loading of 8 wt%. They achieved density reduction of around 23 to 30% for elastomer nanocomposite foams, while maintaining a good electrical conductivity and EMI shielding effectiveness.

2.3.3 Thermoplastic polymer-based nanocomposite foams

Many research efforts have been found regarding thermoplastic polymer nanocomposite foams with a variety of conventional polymer matrices having melting points of 100 to 250 °C and glass transition temperatures of around 100 °C or below. Polystyrene (PS) [35], polypropylene (PP) [36, 37], polycarbonate (PC) [38], poly(methyl methacrylate) (PMMA) [39], and polyethylene (PE) [40, 41] served as polymer matrices with nanoclay as nanofillers. Most of those research efforts focused on the effect of clay on foam morphology. It was found that addition of a small amount of nanoclay increased cell density and reduced cell size significantly [35-41]. Lee et al. [41] found that the dispersion of nanoclay is an important factor to achieve high cell density of PE/nanoclay nanocomposite foams. Fu et al. [39] found that addition of 0.5 wt% of nanoclay improved mechanical property of the nanocomposite foam, but more addition of nanoclay worsened the mechanical property due to the worse dispersion. They concluded that the optimum amount of nanofiller has to be selected to achieve improved mechanical performance.

PS/carbon nanofibers (CNFs) nanocomposite foams were synthesized. Lee et al. [42] found that the addition of 0.1 wt% of CNFs to PS matrix decreased pore size from 20 to 7.1 μm, and the addition of 1 wt% of CNFs decreased it down to 2.6 μm due to the higher nucleation density facilitated by the addition of CNFs. Yang et al. [6] used CNFs as nanofillers to improve the electrical conductivity of foams for lightweight polymeric EMI shielding applications. They achieved EMI shielding effectiveness of around 20 dB, which is required for commercial applications [5], with the addition of 20 wt% of CNFs. However, the density information of the foam was not provided.

PMMA/MWCNT nanocomposite foams were fabricated by solid state foaming, and the effect of filler aspect ratio on morphology was investigated by Chen et al. [43]. They found that the foams with MWCNTs having a low aspect ratio of 130 showed higher cell density than a high aspect ratio of 380. With a lower CO_2 saturation pressure of 11.6 MPa, the difference of cell density between the two foams having different filler aspect ratio was around 4 times. As saturation pressure went up, the cell density difference became smaller, and it became less than 2 times when the saturation pressure reached 15.8 MPa. They concluded that with a lower saturation pressure, nucleation sites are formed at the filler end region, such that a lower filler aspect ratio gave a higher cell density due to the larger number of nucleation sites at the filler ends. As saturation pressure increased, nucleation sites were able to be formed not only at the filler ends, but also on the filler wall region. As a result, the difference of cell density from the two foam groups having different filler aspect ratios became smaller.

PS/MWCNTs nanocomposite foams were fabricated using a chemical foaming agent, (2,2'-azoisobutyronitrile, AIBN), and their EMI shielding effectiveness was found to be 20 dB with the MWCNT content of 7 wt% [5]. Density reduction of the foam was around 50%. Table 2-1 shows the comparison of the EMI shielding effectiveness of PS based nanocomposites with CNFs [6] and MWCNTs [5]. It was found that the use of MWCNTs showed a higher EMI shielding effectiveness than CNFs at the same filler loading. This was due to the larger filler surface area to interact with the electromagnetic waves, in addition to a higher electrical conductivity of MWCNT-based nanocomposites.

Since their size is significantly smaller than that of CNFs, MWCNTs yield much large filler surface area when dispersed in the polymer foams.

Table 2-1. Comparison of the EMI shielding effectiveness of PS-based nanocomposites with different nanofillers

Filler content (wt%)	EMI shielding effectiveness (dB)	
	PS/MWCNTs foams [5]	PS/CNFs foams [6]
0.5	2.84	0.41
1	5.73	0.73
3	10.30	3.09
7	18.56	8.53
20		20.51

PE/MWCNTs nanocomposite foams were fabricated and their electrical conductivity analyzed by Rizvi et al. [44]. They achieved electrical conductivity of $6X10^{-8}$ S/cm with the MWCNTs content of 5 wt%. The Young's modulus of the composites was increased by 100% and the strength by 37% with the addition of 5 wt% MWCNTs to solid PE. However, foam mechanical properties were not reported.

PMMA/graphene nanocomposites foams were fabricated using solid state foaming by Zhang et al. [2]. Specific mechanical properties (properties divided by density) were characterized. It was found that specific moduli and strength of PMMA/graphene nanocomposites decreased by foaming; however elongation at break and specific tensile toughness improved with addition of only 1 wt% graphene. Excellent

electrical conductivity of $3X10^{-2}$ S/cm and EMI shielding effectiveness of 18 dB was obtained with the addition of 1.8 volume % of graphene.

2.3.4 High performance polymer-based nanocomposite foams

Polymer nanocomposite foams with conventional polymer matrices were discussed in Section 2.3.3. However, their service temperatures are limited, and may not be suitable for applications such as automotive and aerospace, where the resistance to high temperature is needed [45]. High performance polymers could be used instead of conventional polymers, such that the resultant nanocomposite foams could be used in a more stringent environment where high service temperature is required.

Recently, Sorrentino et al. [45] fabricated poly(ether sulfone) (PES) based polymer nanocomposite foams with the solid state foaming method using CO_2 as the blowing agent. PES is an amorphous polymer having a glass transition temperature of 225 °C and a density of 1.37 g/cm^3 [46]. Nano graphite and SiO_2 nanoparticles were used as nanofillers. PES based nanocomposites were saturated at a pressure of 8 MPa at 50 °C and foamed. They investigated the effects of both nano graphite (0.1 to 2.5 wt%) and SiO_2 nanoparticle (0.1 to 2 wt%) loadings on the density of PES based nanocomposite foams. First of all, as SiO_2 nanoparticle loading increased from 0 wt% to 2.0 wt%, the relative density of PES/SiO_2 nanocomposite foams increased from 20% to 30% for

samples foamed at 240 °C. However, for PES/nano graphite nanocomposite foams foamed at 240 °C, as nano graphite loading increased from 0 wt% to 0.1 wt%, the relative density decreased from 20% to 15%. Further increase in nano graphite from 0.1 wt% to 2 wt% increased the relative density from 15% to 33%. In general, addition of nanofillers prevented cell growth causing higher density due to high viscosity. Decrease in density with the addition of 0.1 wt% nano graphite was not explained.

2.3.5 Biodegradable polymer-based nanocomposite foams

Biodegradable polymers can be utilized to fabricate polymer nanocomposite foams in order to take advantages of their functionality for tissue engineering and light-weight, biodegradable electronics applications. For tissue engineering applications, porous biodegradable polymers such as poly(glycolic acid) (PGA) and poly(lactic acid) (PLA) were commonly used for tissue engineering scaffolds [47]. However, the mechanical property of those porous scaffolds showed insufficient stiffness and compressive strength compared to human bone, such that the use of nanofillers is considered to improve the property [47]. In addition to the mechanical property, having electrical conductivity in the biodegradable scaffold plays a role to direct cell growth, because electricity stimulus can be conducted into the tissue healing process. Therefore, conductive nanofillers such as CNTs are considered to reinforce biodegradable polymer foams [47].

Having electrical conductivity in biodegradable polymer nanocomposite foams can also be utilized in the area of lightweight biodegradable ESD and EMI shielding applications, which could be beneficial for environment when disposed after the end of device life. Thomassin et al. fabricated PCL/MWCNTs nanocomposite foams for EMI shielding applications using solid-state foaming with CO_2 as a blowing agent [3]. Poly(caprolactone) (PCL) is one of biodegradable polymers. They achieved EMI shielding effectiveness of 60 to 80 dB with MWCNTs contents of only 0.25 vol%, with the density reduction of around 70% from the unfoamed. It was observed that foamed PCL/MWCNT nanocomposites showed high EMI absorption capability than reflection which could prevent damage or interference of devices from reflected electromagnetic waves. It is because dielectric constant of the material by foaming decreased from 3.5 to 1.2, which is close to the value of air (dielectric constant of air is one), such that mismatch between the dielectric constants of the materials and surrounding atmosphere (air) reduced, causing the low reflection but high absorption [3]. Foaming biodegradable PCL/MWCNT nanocomposites resulted in lightweight electromagnetic wave absorber maintaining the biodegradability of the host matrix.

Pilla et al. fabricated PLA/MWCNTs nanocomposite foams, and their specific mechanical properties were characterized [48]. They found that addition of 1.5 wt% of MWCNTs decreased specific toughness, specific strength, and strain-at-break of foamed

samples due to potentially poor filler dispersion, which might cause stress concentration or weak interfacial interactions between the matrix and fillers. However, there was no significant loading effect found on specific Young's moduli of foamed samples.

Rizvi et al. fabricated PLA/MWCNTs nanocomposite foams using solid-state foaming method with CO_2 as a blowing agent [49]. They have investigated effect of MWCNTs loading on porosity, pore size, and cell density. It was found that as MWCNT loading increased, porosity increased in general due to the fact that higher viscosity of the nanocomposites suppressed pore collapse during the foaming process. Smallest pore size (50 μm) and the highest cell density were found with a medium MWCNT loading of 0.5 wt% due to the best filler dispersion.

2.4 ELECTRICAL PROPERTY MODELING OF POLYMER NANOCOMPOSITES

Electrical properties of polymer nanocomposite foams are an interest of research for tissue engineering and lightweight ESD and EMI shielding applications. Theoretical study on electrical properties of polymer nanocomposite foams would be an interesting topic in order to predict properties such as percolation threshold or electrical conductivity. However, no research effort has been found on modeling of electrical property of polymer nanocomposite foam systems. In spite of the lack of theoretical studies on foamed polymer nanocomposites, there are many research efforts to understand and predict electrical behaviors of unfoamed polymer nanocomposites with fibrous fillers using Monte-Carlo simulation. The Monte-Carlo simulation method to understand electrical conductivity behaviors with randomly distributed fibrous fillers consists of three steps in general: model generation, equivalent network construction, and electrical conductivity calculation.

To model the electrical conductivity of a polymer nanocomposite foam system, it is needed to have a good understanding on electrical property modeling of unfoamed nanocomposite systems. In this section, the Monte-Carlo method, which is a common technique to model the electrical property of insulator/fibrous conducting filler composite systems such as polymer nanocomposites, is reviewed.

2.4.1 Two dimensional Monte-Carlo simulation of insulator/fibrous conducting filler composite systems

Pioneered work of electrical percolation modeling in a 2D space was done by Pike and Seager [50]. They considered nanofillers as straight sticks having a fixed length and zero width. They assigned a constant number of sticks and varied their length to determine the minimum required length to achieve percolation. Based on the work by Pike and Seager, Balberg et al. obtained the actual resistance from a resistor network transformed from a conducting stick system, as shown in Figure 2-2 [51]. Only contact resistance was considered to construct the resistor network. They assigned a constant number of sticks and attempted to find the resistance change depending on the different length of sticks. As the stick length increased, resistance decreased. They found a linear relationship between $(L-L_c)^2$-1 vs. 1/resistance, where L is the length of the sticks and L_c is a critical length for percolation.

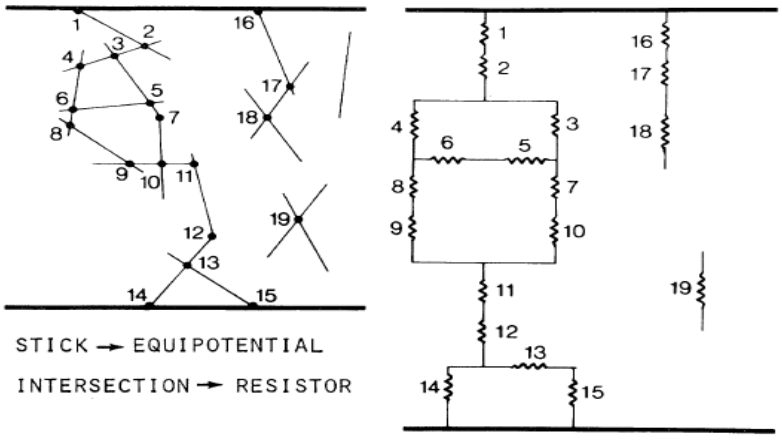

Figure 2-2. The transformation of a conducting stick system to a resistor network [51].

Du et al. [52] investigated the effect of carbon nanotube alignment on electrical conductivity of composites at percolation. Carbon nanotubes were considered as zero width sticks in a 2D space. Alignment of the tubes was determined by an angle Θ with respect to the y axis. Figure 2-3 (a) shows 50 sticks having angles between -90° to 90°, and (b) shows highly aligned 100 sticks having angles between -5° to 5°, and (c) shows 100 sticks having angles between -90° to 90°, which formed a percolation path. It was found that in general, alignment of fillers gave worse electrical properties such as a high percolation threshold and a low electrical conductivity. However, it was found that the maximum electrical performance was found at around $-80° < \Theta < 80°$, showing that a little degree of anisotropy improved electrical performance.

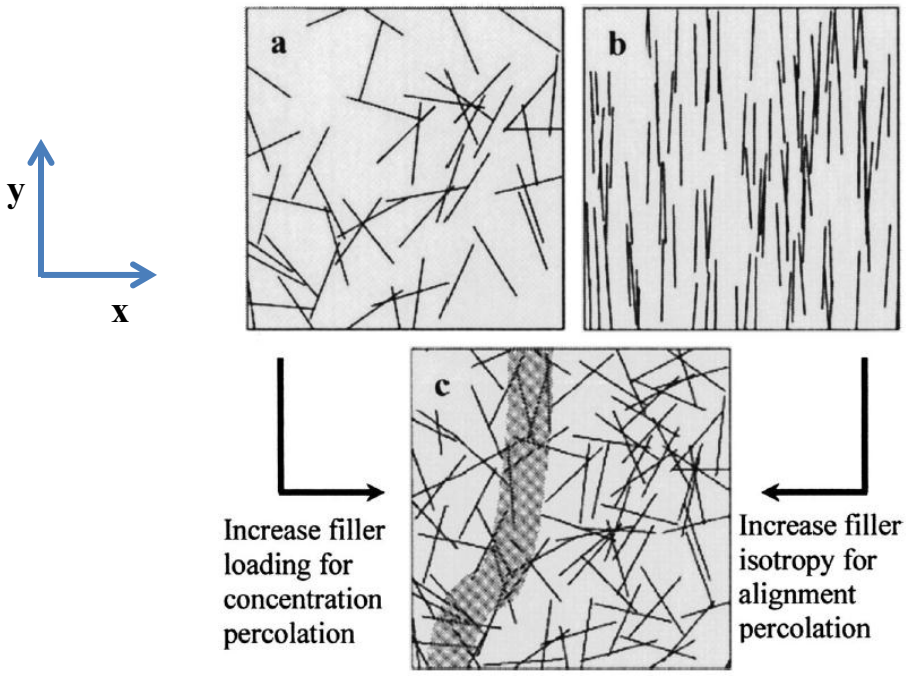

Figure 2-3. Sticks in a unit square. (a) 50 sticks having angles between -90° to 90° with respect to y axis, (b) 100 sticks having angles between -5° to 5°, and (c) 100 sticks having angles between -90° to 90°, which formed a percolation path [52].

2.4.2 Three dimensional Monte-Carlo simulation of insulator/fibrous conducting filler composite systems

Research efforts regarding electrical percolation and conductivity modeling using the Monte-Carlo method were found in a 3D space, which could yield more realistic results. The first Monte-Carlo simulation with sticks in a 3D space was done by Balberg et al. [53] in 1984. They investigated the effects of filler aspect ratio (length/radius) and anisotropy on electrical performance. They found a linear relationship between the aspect ratio and $1/N_c$, where N_c is the critical concentration at percolation. For the anisotropy effect, they found that the effect of orientation randomness in 3D is more significant than that in 2D.

Ounaies et al. [54] used 3D Monte-Carlo simulation to predict the percolation threshold of polyimide/single walled carbon nanotube (SWCNT) nanocomposites. They created cylinders in a cube structure for the simulation, as shown in Figure 2-4. The percolation threshold from numerical simulation was higher than the value from experiment. They speculated that the discrepancy was because that in the simulation SWCNTs could penetrate each other, whereas in real case they could not. Overlapping volume by tube penetration increased the percolation threshold.

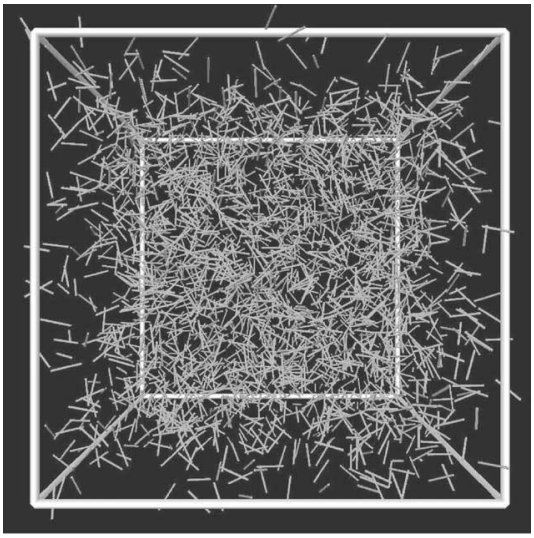

Figure 2-4. Numerical model with randomly distributed sticks [54].

In a real polymer/CNT nanocomposite system, nanofillers cannot be straight sticks or cylinders, but have certain waviness. Yi et al. introduced the effect of fiber waviness on electrical percolation threshold by setting fibers as a sinusoidal curves (y=Asin(wt)) [55]. They found that increase in waviness of nanofillers increased the percolation threshold, suggesting that more nanofillers would be needed for electrical percolation if the fibers were curved.

Hu et al. [56] performed 3D Monte-Carlo simulation to investigate the effect of filler waviness and aggregation on electrical percolation and conductivity. Their fiber generation method was different from the one in Yi et al. As shown in Figure 2-5, they created connected straight sticks having a certain angle which determine the fiber waviness. As reported by Yi et al., increased filler waviness increased the percolation threshold and decreased the electrical conductivity of nanocomposites. To investigate the

effect of filler aggregation, they created spherical aggregates using the Box-Muller method, which generates fillers in confined spheres with a normal distribution as shown in Figure 2-6. They found that high degree of aggregation increased the percolation threshold and decreased the electrical conductivity.

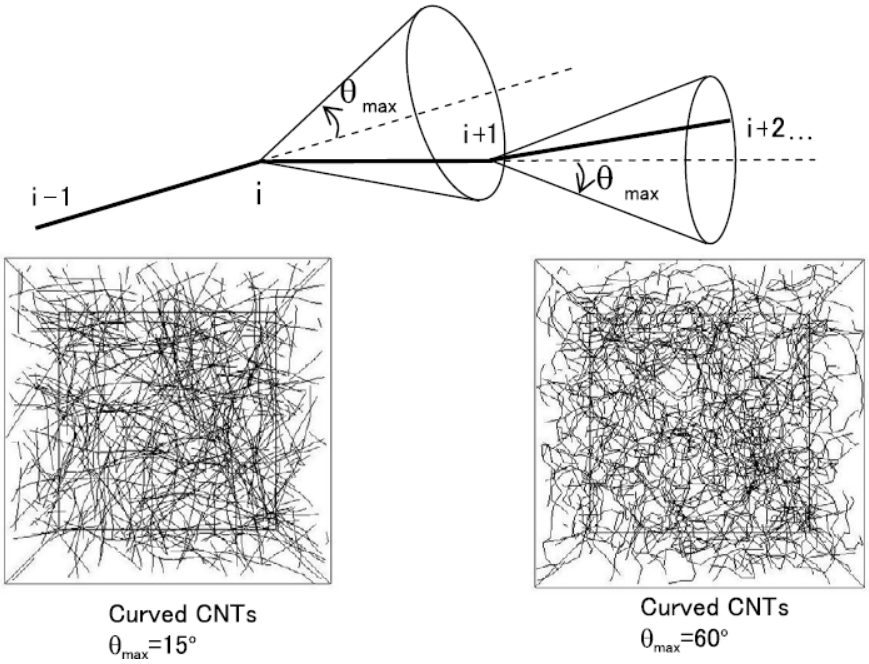

Figure 2-5. Numerical model with randomly distributed fibers having different waviness [56].

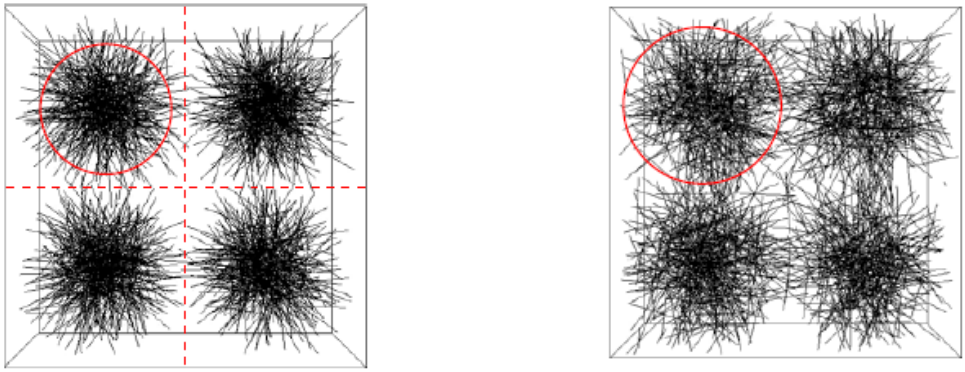

Figure 2-6. Numerical model with aggregated fibers having different degree of aggregation (higher δ: low degree of aggregation) [56].

Chapter 3. Polyetherimide/Carbon Nanotube Nanocomposite Foams: Fabrication and Characterization

3.1 INTRODUCTION

Polymer nanocomposite foams have attracted tremendous interests due to their improved mechanical, thermal, and electrical properties, in addition to the inherited lightweight benefit from foamed materials [16]. A large amount of research has been conducted, with early work focusing on improving the foam morphology and mechanical properties, such as the elastic modulus and strength. Nanoparticles such as nanoclay, carbon nanofiber (CNF), and carbon nanotubes (CNTs) were used with a wide range of polymer matrices [35-38,57-65], and have been shown able to increase the nucleation density and reduce the cell size of the polymer foams. Polymer foams reinforced with CNF and CNTs exhibited substantially improved mechanical properties compared to their neat polymer counterparts [16].

Polymer nanocomposite foams with improved electrical conductivity have recently been studied for lightweight electrostatic discharge (ESD), electromagnetic interference (EMI) shielding, and lightning-strike protection applications. It is well known that a small amount of highly conductive nanoparticles, when well dispersed, could form a conducting network in the polymer matrix. Making these polymer nanocomposites into foams would generate a new class of lightweight materials that will

find many applications in aerospace, automotive, and electronics applications. ESD and EMI can be serious issues for electronics due to possible spark generation by static charge build-up and emitted electromagnetic fields that interfere with the operations of the electronic equipment [1]. To prevent ESD and EMI, metal-based materials either thin sheet metals or metal coated plastics, have been used. However, these materials suffer from problems such as being heavy, prone to corrosion, and difficult to process. Conductive polymer nanocomposite foams have distinct advantages compared to metal based materials, especially for ESD and EMI applications in aircrafts, spacecrafts, and automobiles due to their desirable lightweight properties.

A variety of polymer matrices have been used to create foams with conducting fillers, including multiwall carbon nanotubes (MWCNTs), graphene platelets, and CNF. A key objective of recent studies is to improve the electrical conductivity, since it is the most important characteristic for ESD and EMI shielding applications. Table 3-1 provides a summary of the recent studies found in literature on conductive polymer nanocomposite foams. Most of the matrix materials were thermoplastics with the glass transition temperature (T_g) ranging from -110 to 105 °C and the melting temperature from 65 to 240 °C. The pore size ranged from sub-micron to a few hundreds of micrometers. Most of the foams have a relative density between 4-85%, which corresponds to 96-15% porosity. Thermoset foams usually have large pore sizes,

sometimes on the millimeter scale. The electrical conductivity varied dramatically among different studies, from 0.1 S/cm to $6x10^{-8}$ S/cm, depending on the filler type, loading, pore size, and relative density. Graphene based materials seemed to have a higher electrical conductivity than CNT based ones. A higher loading of the conducting phase generally contributed to a higher composite conductivity. Several studies also included mechanical property testing, which is noted in the table. Although their electrical conductivities are high enough for ESD or EMI shielding applications, the matrix materials all have a low service temperature and may not be suitable for high performance applications, such as aircraft interior.

In this chapter, polyetherimide (PEI)/multi-wall carbon nanotube (MWCNT) nanocomposite foams were fabricated and their electrical and mechanical properties were characterized. PEI is a high performance polymer with a glass transition temperature of 217 °C and a melting temperature of 340 °C. By using PEI as the matrix material, the resultant nanocomposite foams could be used in a more stringent environment where a high service temperature is required. In addition, PEI performs well with low flammability and low levels of smoke generation while it burns. The fabricated composite foams could be used for aerospace and automotive components to satisfy the lightweight, ESD prevention, as well as fire safety requirements.

Table 3-1. Summary of polymer nanocomposite foams with conductive nanofillers

Matrix	*Matrix Tg (°C)*	*Matrix Tm(°C)*	*Filler type*	*Pore size (um)*	*Relative density (%)*	*Electrical conductivity*	*Ref*
TPU	-20 to 20	180	MWCNT	5	30	NA	[9]
PVDF	-35C	177	Graphene	0.5-2	NA	10^{-1} S/cm (2 wt%)	[10]
PMMA	105	160	Graphene	5	50-65	$3x10^{-2}$ S/cm (1.8Vol%)	[2]
PMMA	105	160	MWNT	0.5-2.5	25-30	NA	[43]
PMMA	105	160	MWCNT	5-30	NA	NA	[66]
LDPE	-110	121	MWCNT	100-200	75	$6x10^{-8}$ S/cm (5 wt%)-AC	[4]
PCL	-60	65	MWCNT	50-100	15-30	$4x10^{-2}$ S/cm (0.25 vol%)-AC	[3]
PS	95	240	MWCNT	40-170	NA	10^{-2} S/cm (7 wt%)	[5]
PS	95	240	CNF	50-150	NA	10^{-3} S/cm (20 wt%)	[6]
PU	Thermosetting		MWCNT	200-1000	4-60	$2x10^{-6}$ S/cm (2 wt%)	[7]
FKM	Thermosetting		MWCNT	NA	NA	10^{-6} S/cm (8 wt%)	[8]

3.2 EXPERIMENTAL

3.2.1 Materials

PEI powder (ULTEM 1010P) was supplied by SABIC Innovative Plastics Co. PEI is a semi-transparent thermoplastic material with high strength and stiffness. The molecular structure of PEI is shown in Figure 3-1. The density, mechanical and thermal properties are shown in Table 3-2. Carboxyl group (COOH) functionalized multiwall CNTs (MWCNTs) were used in this study to improve the dispersion of nano additives by electrostatic repulsion of the functional groups. The functionalized MWCNTs were purchased from Cheap Tubes Inc. (Purity > 95%; diameter ~20 nm; length 10-50 μm; and the COOH group content 2.5%). Scanning electron microscopy (SEM) images of Cheap Tubes are shown in Figures 3-2 and 3-3 with different magnifications. Dichloromethane (DCM) from Fisher Scientific was used as the solvent to fabricate the PEI/MWCNT nanocomposites. For foaming, CO_2 was used as the blowing agent.

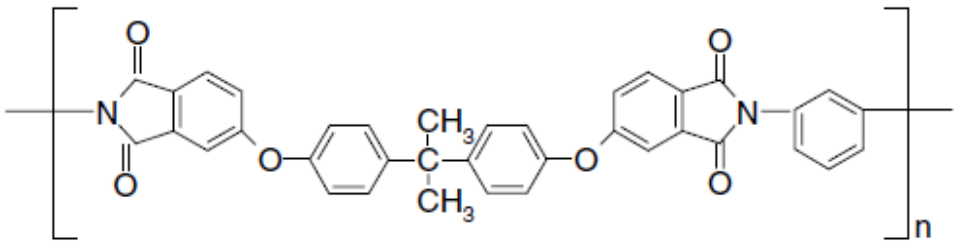

Figure 3-1. The molecular structure of PEI [67].

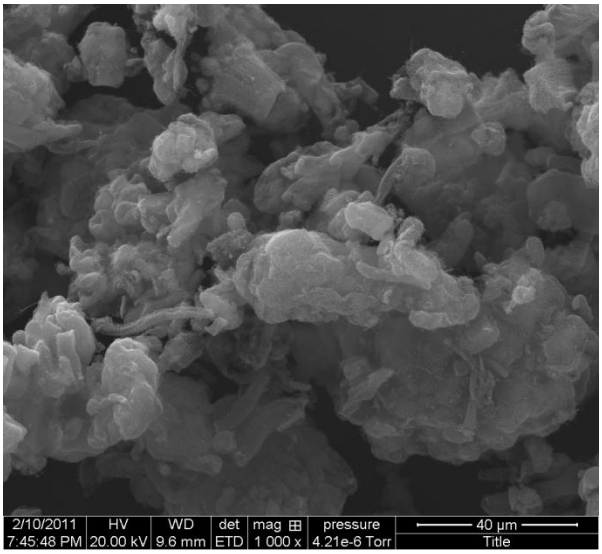

Figure 3-2. An SEM image of Cheap tubes with the scale bar 40 µm.

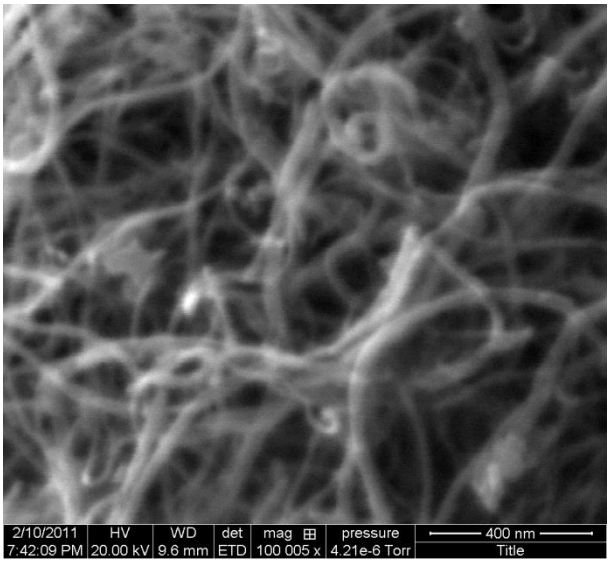

Figure 3-3. An SEM image of Cheap tubes with the scale bar 400 nm.

Table 3-2. Properties of PEI (ULTEM 1010 P)

Property	Value
Density (g/ cm^3)	1.27
Tensile stress at yield (MPa)	110
Tensile strain at yield (%)	7
Glass transition temperature (°C)	216
Service temperature (°C)	170
Processing temperature (°C)	350
Thermal conductivity (W/m-°C)	0.22

3.2.2 PEI/MWCNT Composite Fabrication

PEI/MWCNT nanocomposites were fabricated using a solvent casting method. A schematic of the nanocomposite fabrication procedures is shown in Figure 3-4. The PEI powder was dissolved in 90ml DCM with a weight ratio of PEI:DCM = 1:7. Selected amounts of MWCNTs were dissolved in 45ml DCM separately. Probe-type sonication (VC 750, Sonics and Materials Inc., USA) was used to disperse the CNTs at a power of 150W for 30 minutes. Then the 90ml PEI solution was added to the 45ml DCM/MWCNT suspension. The mixture was stirred with a magnetic stirrer at room temperature for 45 minutes. The solution was then probe sonicated again for 45 minutes at a power of 150W. The resultant PEI/MWCNT/DCM solution was cast in a Teflon-coated metal mold (400 cm^2) at room temperature and left dry overnight.

Cua [23] found that the use of DCM was not preferred for solvent casting of PEI because of the rough surface texture as shown in Figure 3-5(a). Because of the volatility of DCM, the solvent evaporation rate is high on the top surface compared to the bottom in the cast. Fast solvent evaporation at the surface causes de-swelling and rearranging of the polymer chains due to the favorable interactions with other like chains, resulting in surface contraction. A paper cover was used to slow down the evaporation rate, and smooth samples were obtained as shown in Figure 3-5(b). The thickness of obtained nanocomposite samples after solvent extraction ranged from 300 to 400 μm.

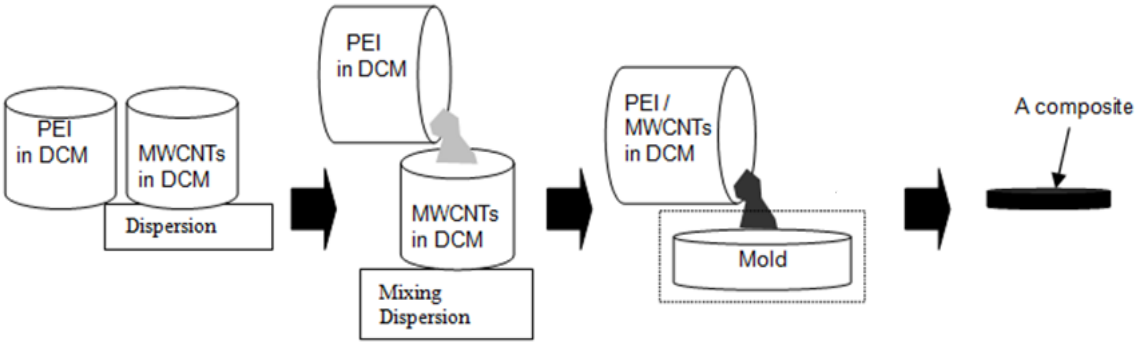

Figure 3-4. Nanocomposite fabrication procedures.

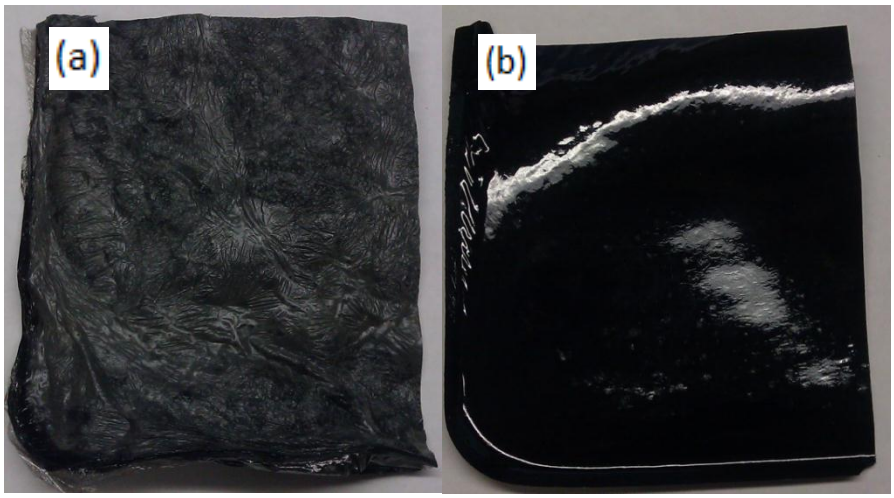

Figure 3-5. Solvent casted PEI/MWCNTs without a paper cover (a) and with a paper cover (b) on the mold.

3.2.3 Residual Solvent Extraction

Residual solvent needs to be removed from the nanocomposite samples to ensure the mechanical property and foam-ability. For the first step of solvent extraction, nanocomposite samples dried overnight in the mold were saturated in supercritical CO_2 ($ScCO_2$) until the equilibrium. When it is above the critical point (7.4 MPa and 31 °C as shown in Figure 3-6), CO_2 behaves like a fluid with a high diffusivity. A syringe pump (Teledyne ISCO 260D, USA) was used to compress CO_2 up to the desired pressure. This system was used for gas saturation for foaming as well later. The temperature of the pressure vessel is adjusted by a heater attached to the pressure vessel. In this experiment, 8 MPa and 35 °C were chosen to achieve a supercritical state of CO_2. In the $ScCO_2$ saturation step, the DCM molecules attained increased diffusivity due to the plasticizing effect of the saturated CO_2. The DCM could diffuse out with the CO_2 influx [19,68]. The $ScCO_2$ saturation step at 8 MPa and 35 °C took less than 1 day. CO_2 saturated samples were then placed in a vacuum oven for one day (MTI, USA) at 100 °C to extract CO_2. The duration of this treatment was determined by a mass loss study on solvent fabricated PEI films, as shown in Figure 3-7. The vacuum oven treatment itself was not effective, while the introduction of 1 day $ScCO_2$ saturation followed by 1 day vacuum oven treatment showed superior performance compared to 2 days of vacuum oven treatment alone. Additional time of $ScCO_2$ saturation and vacuum oven treatment did not help

solvent extraction further, such that 1 day $ScCO_2$ and 1 day vacuum treatment was chosen for solvent extraction in this study. It was showed that the average total weight loss during solvent extraction was around 13-14% of the initial sample weight.

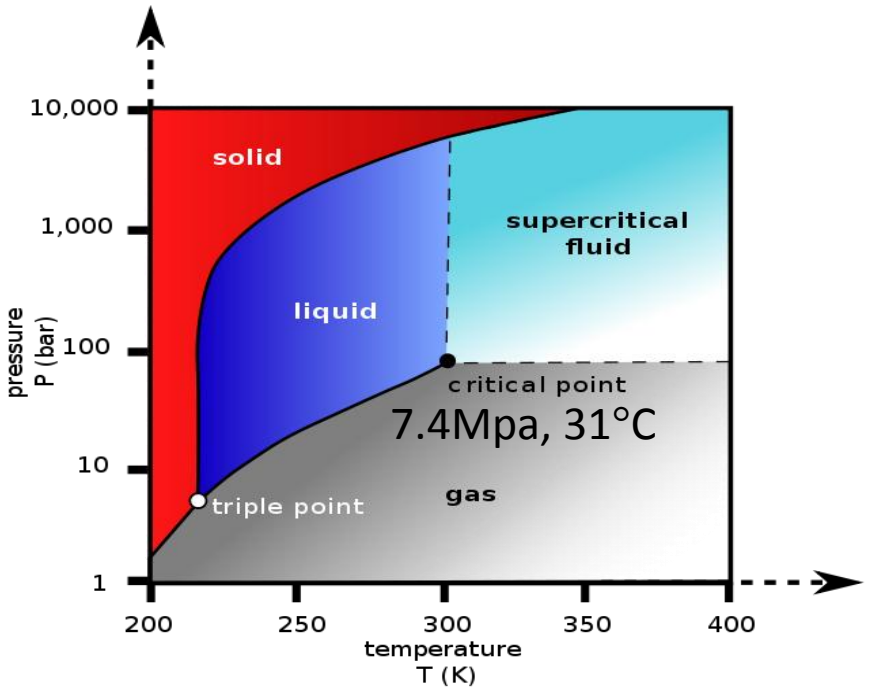

Figure 3-6. CO_2 pressure-temperature phase diagram [69].

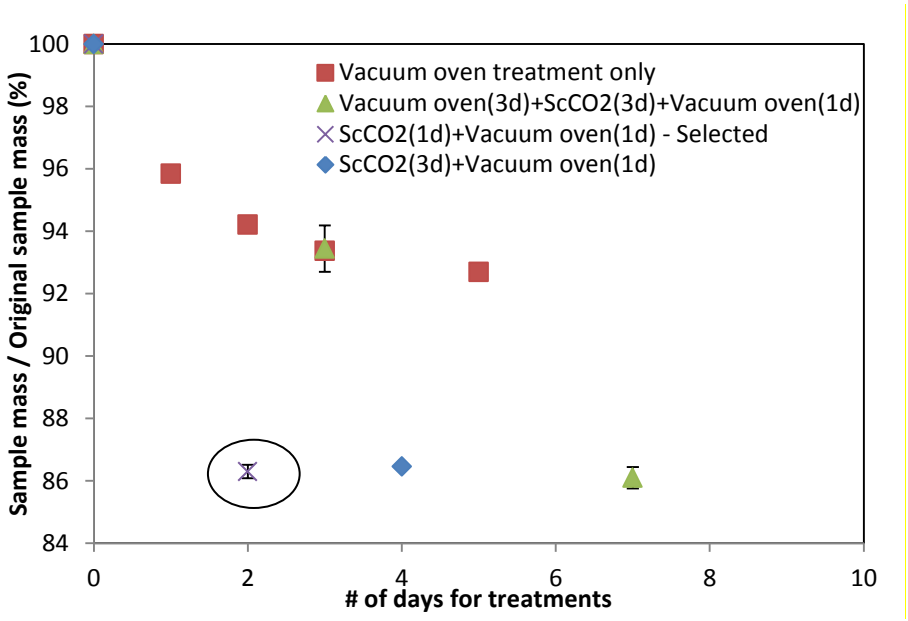

Figure 3-7. Samples mass loss% for different solvent extraction treatments.

Figure 3-8 shows dynamic mechanical analysis (DMA) tests for neat PEI before and after solvent extraction treatments. It was shown that after solvent extraction, storage modulus increased to 2.5 GPa, and the glass transition temperature increased to around 215 °C which is close to the reference value. This confirms that the residual solvent was reduced to an acceptable amount.

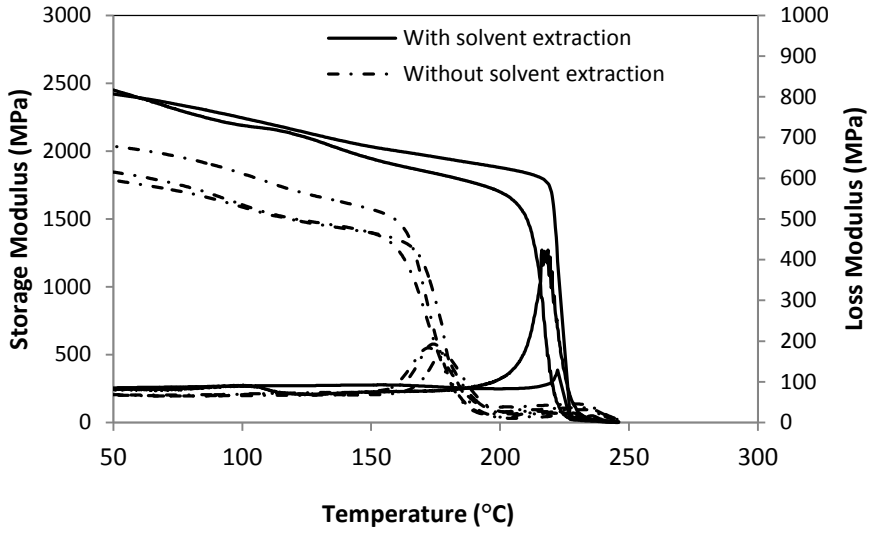

Figure 3-8. Mechanical and thermal property of PEI before and after solvent extraction.

3.2.4 Foaming of Nanocomposites

The PEI/MWCNT nanocomposites were foamed using a solid-state foaming method as shown in Figure 3-9. Solid-state foaming is a two-stage process, consisting of gas saturation and foaming. In the gas saturation stage, a sample is placed in a high pressure vessel connected to a syringe pump for gas saturation for 24 hours with CO_2 in this study. After 24 hours of saturation, CO_2 uptake of samples saturated at 4 MPa and 8 MPa were around 8 wt% and 10 wt%, respectively. The gas-saturated samples were retrieved from the pressure vessel. The elapsed time from the sample retrieval to foaming is termed as desorption time. In the actual foaming stage, by introducing a rapid heat increase, bubbles nucleate and grow due to thermodynamic instability. There are two

representative solid state foaming methods, hot platen foaming and hot bath foaming. The former produces flat samples for easy material characterization, whereas the latter provides uniform and rapid heat transfer to the samples. For ease of characterization, the hot platen foaming method with additional weight of 6.8 kg was used in the study. Figure 3-10 shows the hot platen foaming setup. Table 3-3 shows the experimental factors for the foaming study.

Table 3-3. Experimental factors for foaming

Factors	**Values**			
	Set 1	Set 2	Set 3	Set 4
Saturation pressure	4 MPa	4 MPa	8 MPa	8 MPa
Foaming temperature	155 °C	185 °C	155 °C	185 °C
Saturation time 24 hours, saturation temperature 20 °C, desorption time 20 min, and foaming time 20 sec				

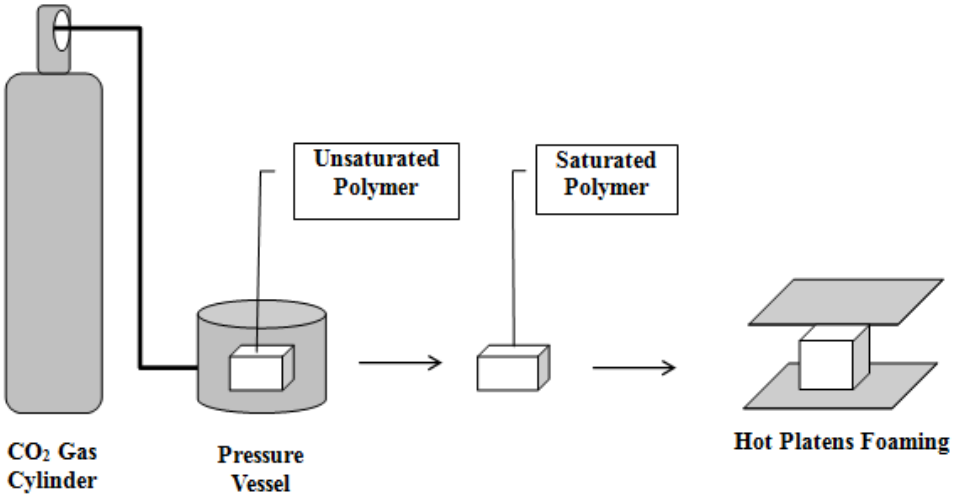

Figure 3-9. A schematic of the solid state foaming process.

Figure 3-10. The heated platen foaming setup.

3.2.5 Characterization

Volume DC electrical conductivities of samples were measured with a commercial multimeter (HHM93, Omega, USA) for low resistivity and an Ohmmeter (Super Megohmmeter, Hioki 8220, Japan) for high resistivity with a set of high resolution electrodes (SME 8311, Hioki, Japan). Densities of the samples were obtained based on the ASTM D792-00 standard using Equation (3-1), as shown below.

$$Density = \frac{Wa}{Wa - Ww}(0.9975)\ \text{g/cm}^3 \qquad (3\text{-}1)$$

where W_a is the sample weight in air, and W_w is that when immersed in water. Weight measurements were performed with a precision lab balance (ML53, Mettler Toledo, Switzerland). The ratio of the foamed sample density to that of the unfoamed is defined as the relative density of the foam.

Microstructures of the samples were observed using a Quanta 650 FEG scanning electron microscope (FEI Company, USA). The samples were freeze-fractured in liquid nitrogen to avoid damage of the imaging surface by shear force from tools like scissors. The surfaces to be observed were coated with gold and palladium (Au/Pd) using a sputter coater (EMS 500X, Electron Microscopy Sciences, USA) to prevent charging on the surface, which is not preferred for imaging.

Cell size measurement was conducted with the SEM images using Image J, which is imaging software from National Institutes of Health. Cell diameters of 20 cells were measured and the average and standard deviation were calculated. Cell density (N_f,

number of bubbles per cm^3) of each set of the samples were obtained using the following equation [35].

$$N_f = \left(\frac{n \cdot M^2}{A}\right)^{\frac{3}{2}} \qquad (3\text{-}2)$$

where

n = number of bubbles in a micrograph

A = area of the micrograph, cm^2

M = magnification factor of the micrograph

Thermo-mechanical properties were characterized using a dynamic mechanical analyzer (DMA) (Q800, TA instruments, USA) with a temperature ramp rate of 3°C/min, and a frequency of 1 Hz. DMA was used to determine the stiffness and the glass transition temperature of the materials.

3.3 RESULTS AND DISCUSSION

3.3.1 Microstructure observations

SEM images of unfoamed neat PEI are shown in Figures 3-11 and 3-12, and SEM images of PEI with 2 wt% of MWCNTs are shown in Figures 3-13 and 3-14 at different magnifications. There was no MWCNTs aggregation found from low magnification SEM images as shown in Figure 3-13. Dispersed MWCNTs throughout the polymer matrix were found, as seen in Figures 3-14. Those observations confirmed good nanofiller dispersion in the polymer matrix.

SEM images of nanocomposite foams with various foaming conditions and MWCNT loadings are shown in Figures 3-15 and 3-16. Different cell sizes were found for different foaming conditions. Foams with conditions of Set 1 and Set 2 (saturation pressure of 4 MPa) had cell sizes around 750 nanometers and those with conditions of Set 3 and Set 4 (Saturation pressure of 8 MPa) had cell sizes around 450 nanometers. The pore size measurement results are shown in Figure 3-17. It was found that the cell size depended on saturation pressure and that foaming temperature did not affect the cell size. Those behaviors could be explained using Eqn. (3-3) [16] regarding nucleation density. Sets 3 and 4 had a higher gas concentration (C) than Sets 1 and 2 due to the higher saturation pressure. Therefore, the nucleation density was higher, leading to more nuclei and smaller cell size. Sets 1 and 2 have the same saturation pressure, but different foaming temperature. Higher foaming temperature would play a role to increase the

nucleation density according to Eqn. (3-3). However, the higher foaming temperature could have caused larger final cell sizes.

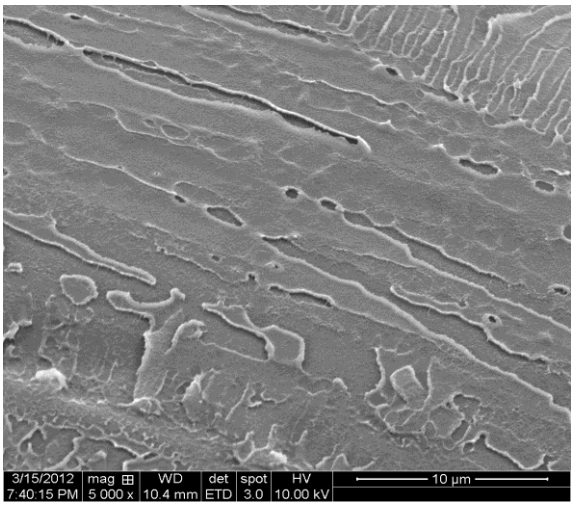

Figure 3-11. Neat PEI, scale bar: 10 µm.

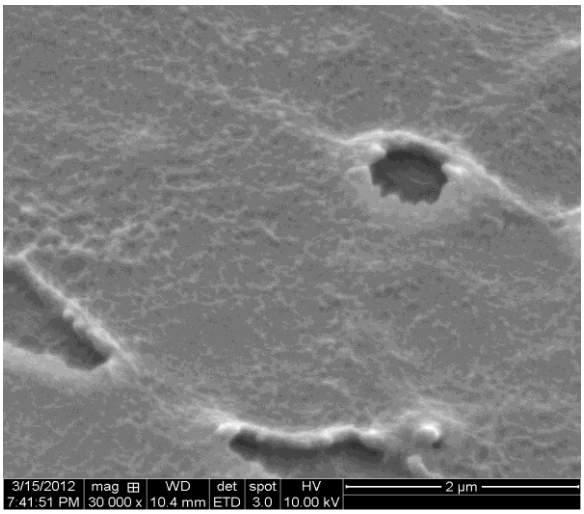

Figure 3-12. Neat PEI, scale bar: 2 µm.

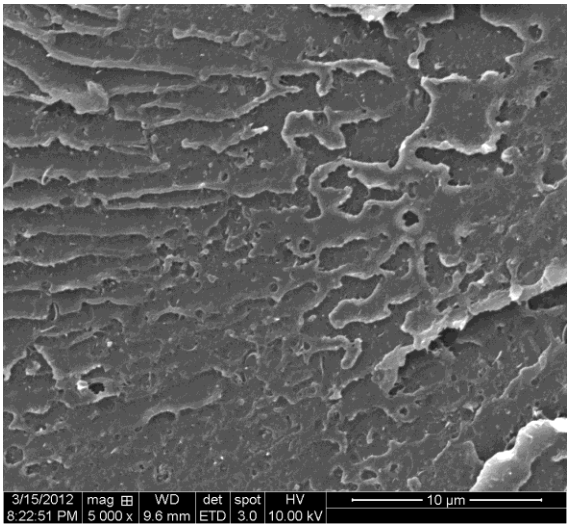

Figure 3-13. PEI/MWCNTs (2 wt%), scale bar: 10 µm.

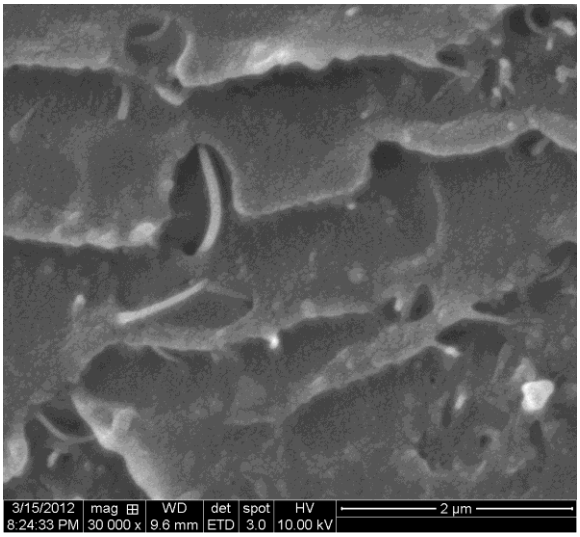

Figure 3-14. PEI/MWCNTs (2 wt%), scale bar: 2 µm.

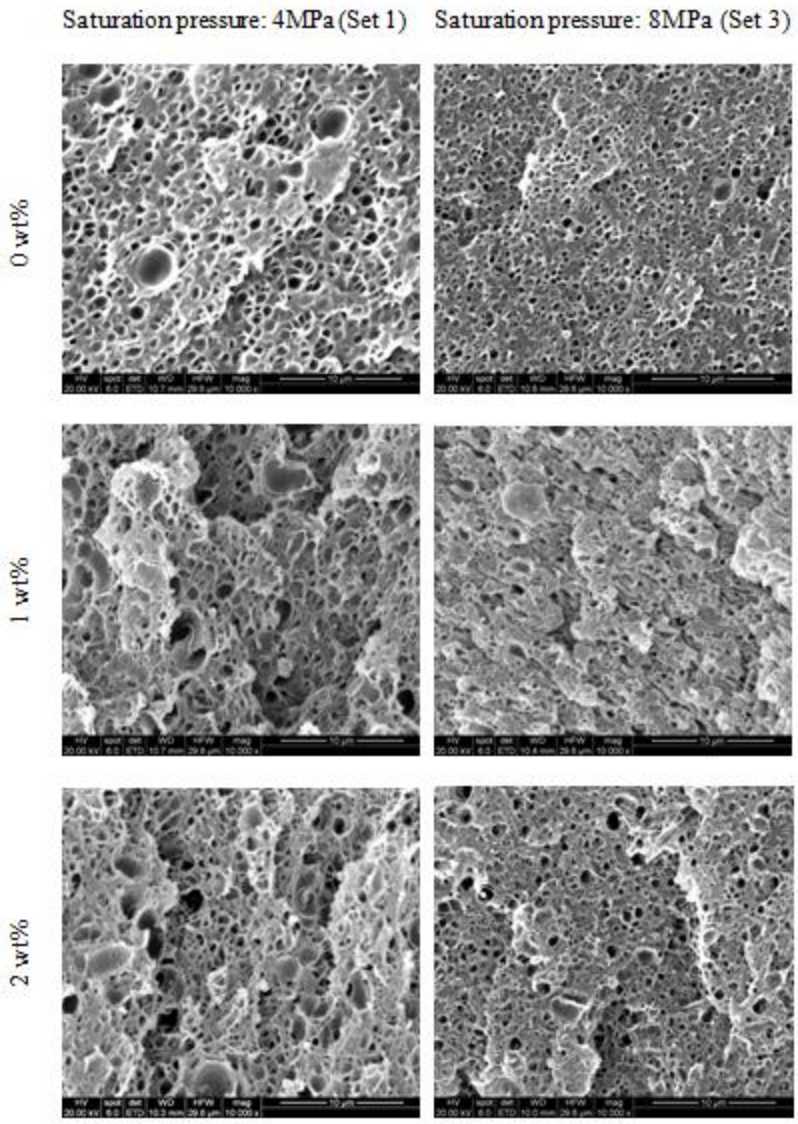

Figure 3-15. SEM images of foamed samples (Sets 1 and 3) with various MWCNT levels foamed at 185 °C. Scale bars: 10 μm.

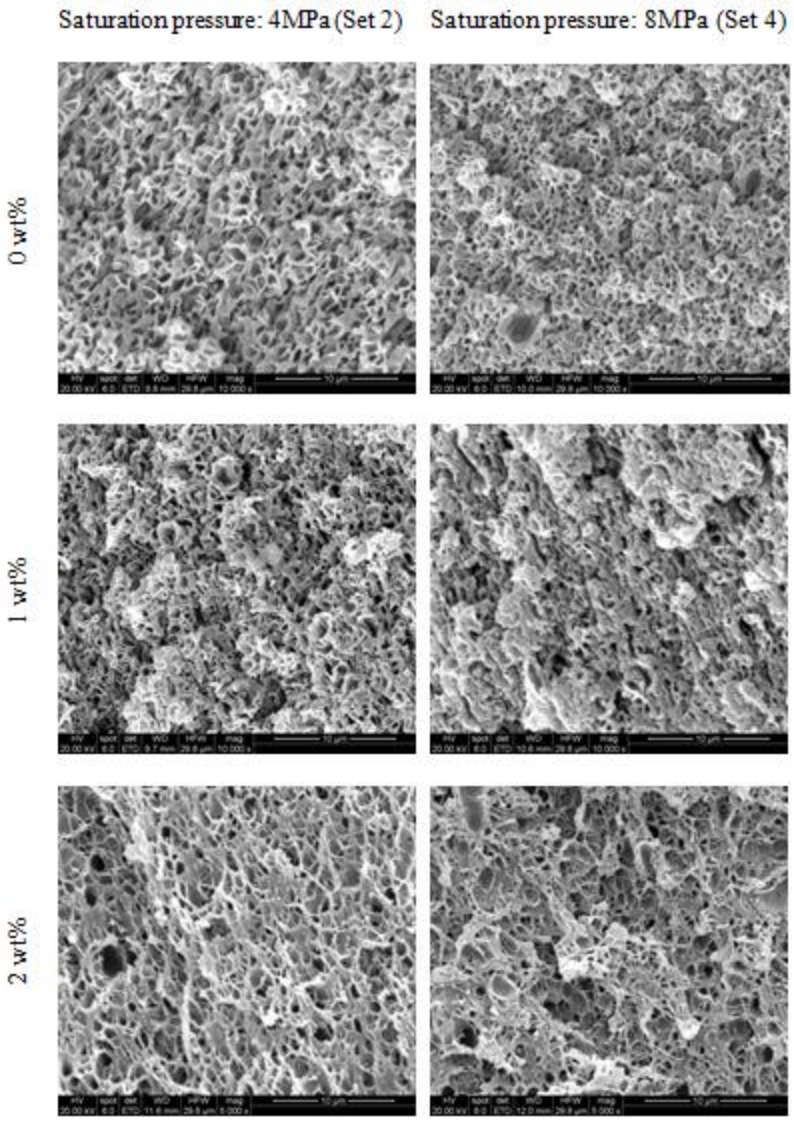

Figure 3-16. SEM images of foamed samples (Sets 2 and 4) with various MWCNT levels foamed at 185 °C. Scale bars: 10 μm.

Cell density of nanocomposite foams mainly depended on the saturation pressure, as shown in Figure 3-18. However, it was also found that the foams obtained at higher foaming temperatures had a relatively higher cell density than those foamed at lower foaming temperatures. This could be explained by Equation (3-3) as well. Even though the final cell sizes are the same for foams foamed at different foaming temperatures under the same saturation pressure, the wall thickness of the cells foamed at the higher foaming temperature is much thinner, meaning that there were more pores in the unit volume.

$$N = C \cdot f \cdot \exp\left(\frac{-\Delta G}{k \cdot T}\right) \qquad (3\text{-}3)$$

where

N = nucleation density

C = #of gas molecules dissolved in unit volume

f = kinetic pre-exponential factor

ΔG = Gibbs free energy for nucleation

k = Boltzmann's constant

T = absolute temperature

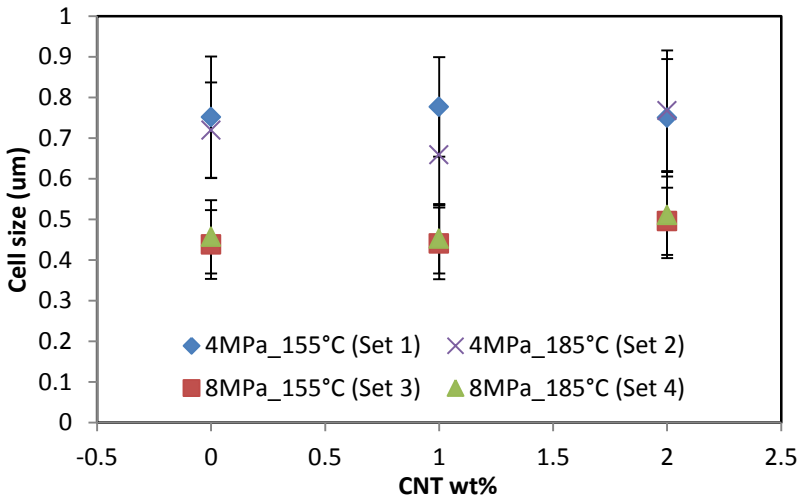

Figure 3-17. Foam cell size plot for each experimental set (20 cells are measured for each condition).

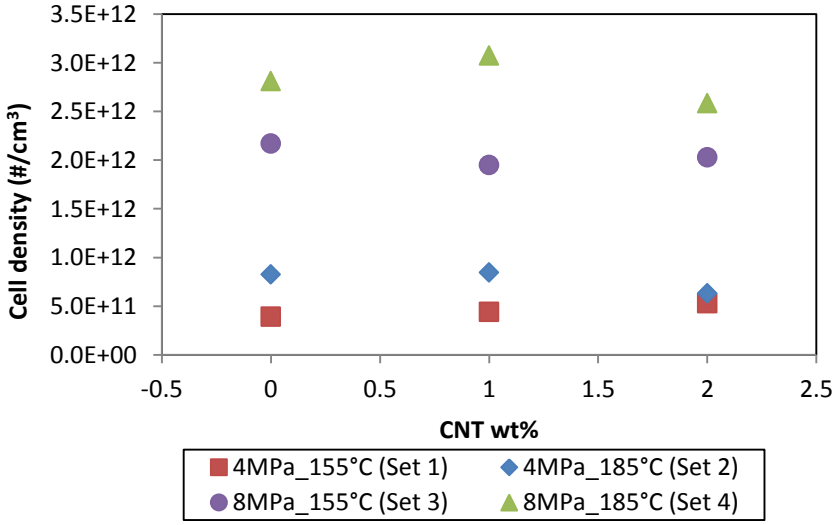

Figure 3-18. Foam cell density plot for each experimental set.

Another observation from the cell density result is that as MWCNT content increased there was no change in cell density. It is not common to the heterogeneous nucleation phenomenon under existence of reinforcements in a system. In a heterogeneous nucleation process, ΔG decreases due to the existence of extra nucleation sites, resulting in a high nucleation density [33]. It is believed that there were still some DCM molecules left to interact with MWCNT functional groups even though the amount of them was negligible by weight. As the amount of CNT increased, the number of functional group also increased, yielding a higher chance for DCM to interact with them. Because of the higher number of DCM molecules left, they also contributed to pore creation, since DCM is a well-known chemical blowing agent. This could result in collapsing of the pores created by CO_2. Therefore, even though ΔG was lowered, cell density did not increase due to the pore collapsing.

Relative densities of the nanocomposite foams were measured and the results are shown in Figure 3-19. Relative density mainly depended on foaming temperature. The higher the foaming temperature, the lower the density in general. In addition, it was found that foams with a higher saturation pressure showed a higher density. Conventionally, the more the blowing agent is in the material, the more total expansion there will be in the material. However, due to the hot press foaming method used in this study, the opposite phenomenon was found. With a higher gas concentration in the system, the effective glass transition temperature (T_g') decreases accordingly due to the plasticizing effect. Therefore, at the same foaming temperature, if the material has more gas in it, the stiffness of the materials is lower than that of the counterpart. Softer material

is more likely to be affected by pressure, resulting in less cell growth and thus higher density.

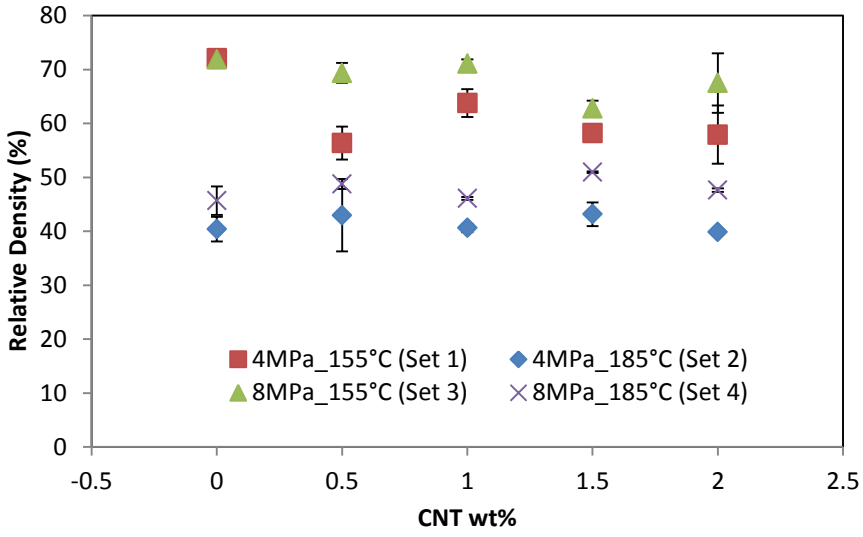

Figure 3-19. Foam relative density plot for each experimental set.

3.3.2 Thermal and Mechanical Properties of Nanocomposites and Foams

Mechanical and thermal properties of PEI/MWCNTs nanocomposites with various MWCNTs loadings were examined with DMA tests as shown in Figure 3-20. Storage moduli at 50 °C and T_g's of these samples are shown in Figures 3-21 and 3-22, respectively. The storage modulus of neat PEI samples was around 2.7 GPa. It increased to around 2.8 GPa as MWCNTs were added. However, this increase may not be statistically significant. The T_g's of the nanocomposites were found around 210 °C showing that the solvent casted PEI/MWCNT nanocomposites maintained the excellent thermal property of neat PEI and could be used in high temperature situations.

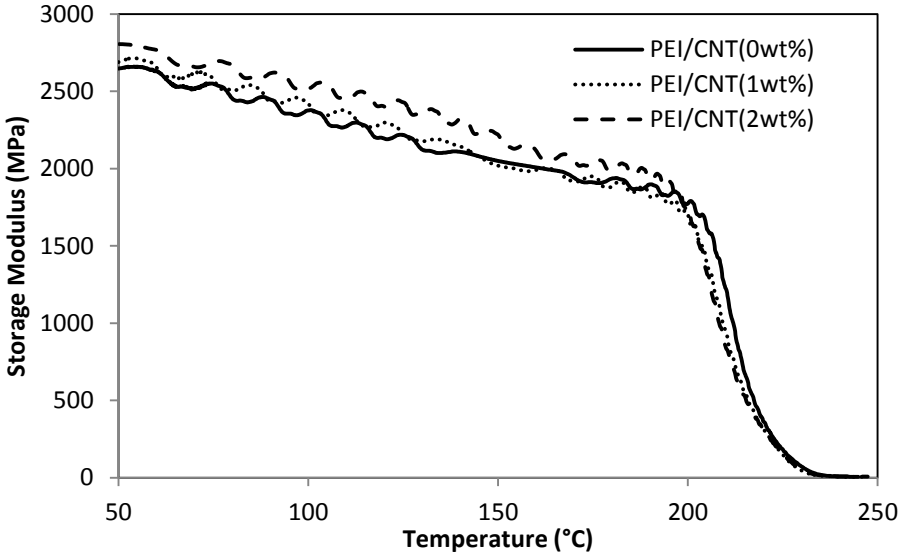

Figure 3-20. Mechanical and thermal properties of PEI/MWCNT nanocomposites.

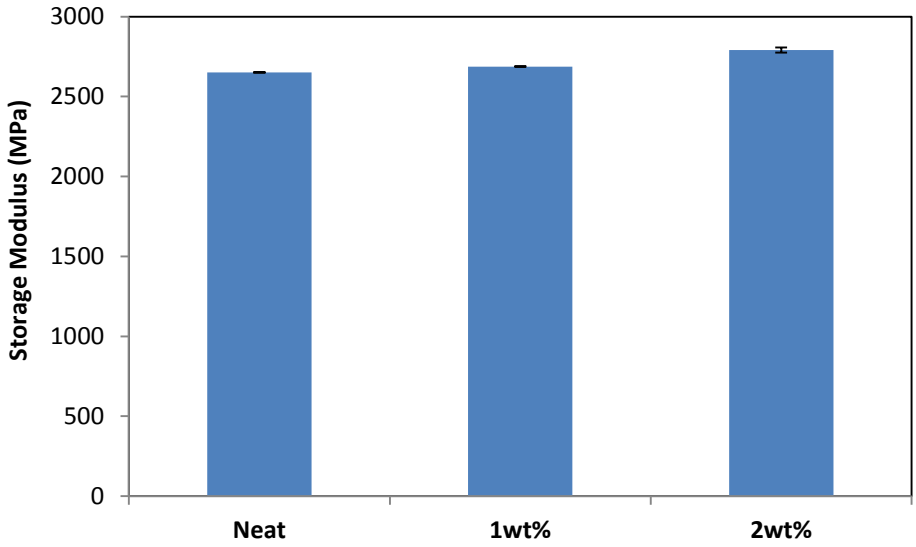

Figure 3-21. Storage moduli of unfoamed PEI with various MWCNT loadings (2 samples were tested for each condition).

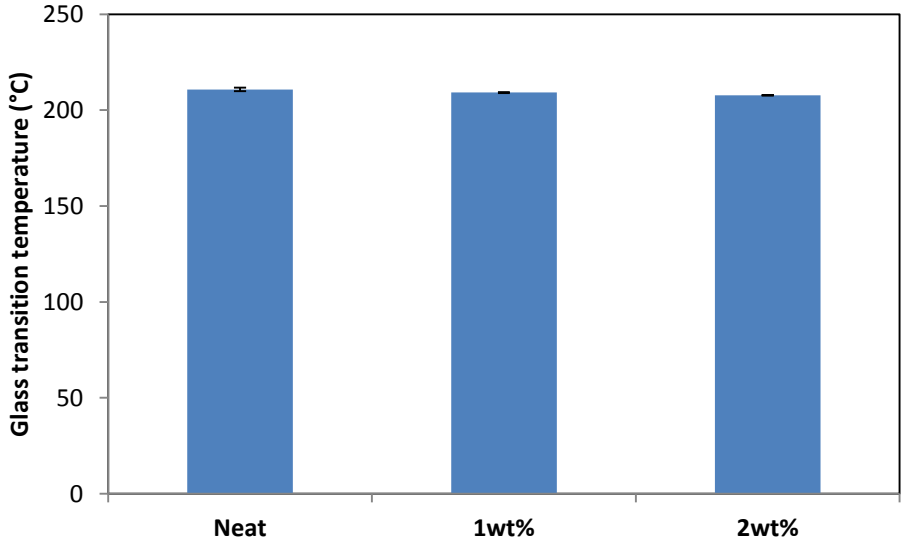

Figure 3-22. T_g's of unfoamed PEI with various MWCNT loadings (2 samples were tested for each condition).

DMA tests were also performed on foamed neat PEI with four different foaming conditions. It was discussed that Sets 1 and 2 had pore size of ~750 nm, and Sets 3 and 4 had that of ~450 nm. Relative density of Sets 1 and 3 was ~65 %, and that of Sets 2 and 4 was ~ 45 %. The results are shown in Figure 3-23. Normalized storage moduli by (relative density)^2 at 50 °C and T_g's are shown in Figures 3-24 and 3-25 under different foaming conditions. The reason for the normalization of storage moduli by (relative density)^2 is that Moore et al. [70] discovered that foam stiffness decreased by (relative density)^2. Therefore, it is reasonable to compare stiffness of polymers with the values normalized by (relative density)^2, when the density of material needs to be considered. Normalized storage moduli of foamed neat PEI were around 2.5 to 2.7 GPa, showing good agreement with that of unfoamed neat PEI. Effects of different foaming conditions (or foam morphology such as cell size and relative density) on the normalized storage moduli of foamed neat PEI was found to be insignificant, as shown in Figure 3-24.

High thermal property from PEI matrix was maintained for foamed neat PEI, showing T_g's around 220 to 225 °C in Figure 3-25. T_g's of the foamed samples were higher than that of unfoamed samples and even that of the reference value (216 °C). This might be because of the following reasons: 1) During the foaming process, the remaining solvent was removed; 2) Due to the decreased thermal conductivity for foams the heat was not effectively delivered to the sample. Effect of different foaming conditions or foam morphology such as the cell size and relative density on the T_g's of the foamed neat PEI was also found to be negligible, as shown in Figures 3-25.

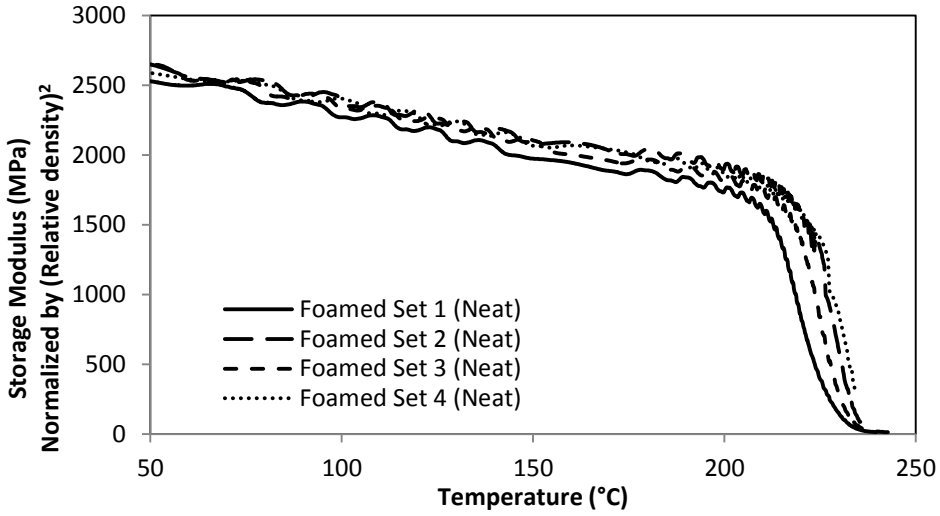

Figure 3-23. DMA results of neat PEI foams with four foaming sets (normalized by (relative density)^2).

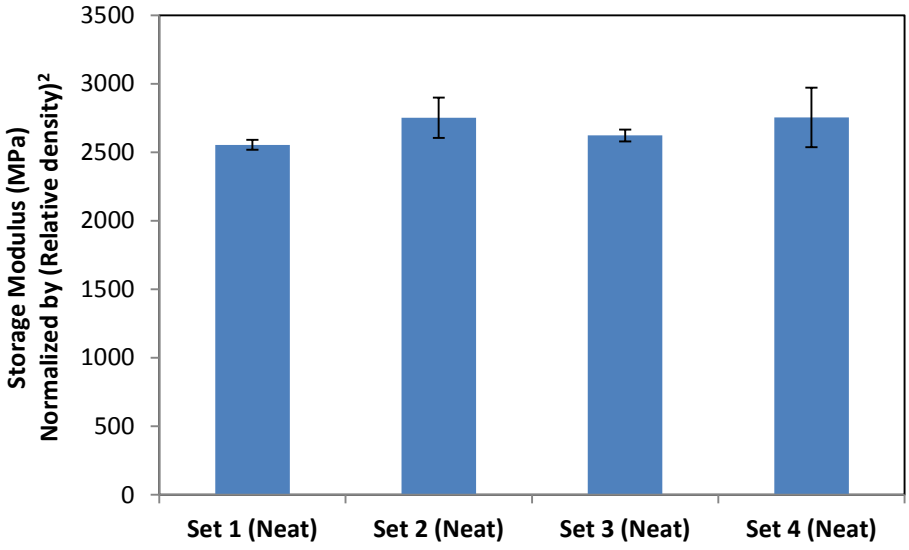

Figure 3-24. Storage moduli of neat PEI foams with four foaming sets (normalized by (relative density)^2) at 50°C (2 samples were tested for each condition).

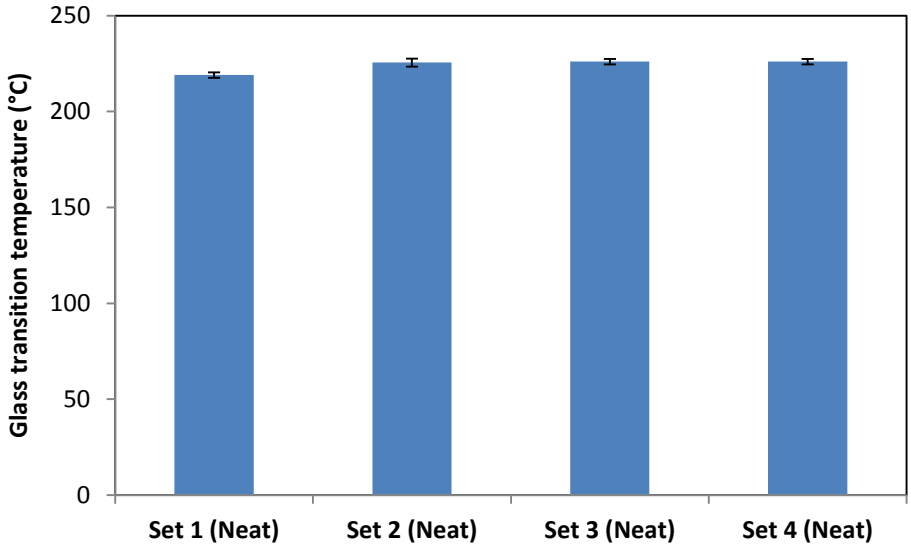

Figure 3-25. T_g's of neat PEI foams under four foaming conditions (2 samples were tested for each condition).

DMA tests were performed for foamed PEI/MWCNT (2 wt%) nanocomposites with four different foaming conditions. The results are shown in Figure 3-26. Normalized storage moduli by (relative density)^2 at 50 °C and T_g's are shown in Figures 3-27 and 3-28, respectively. Normalized storage moduli of foamed PEI/MWCNTs (2 wt%) nanocomposites were between 2.7 to 3.0 GPa, showing good agreement with the storage modulus of unfoamed PEI/MWCNTs (2 wt%) nanocomposites. Effect of different foaming conditions (or foam morphology such as cell size and relative density) on normalized storage moduli of foamed PEI/MWCNTs (2 wt%) nanocomposites was found to be insignificant, similar to the results from foamed neat PEI. The high thermal property

of the PEI matrix was maintained. The T_g of foamed nanocomposites was 225°C, as shown in Figure 3-28.

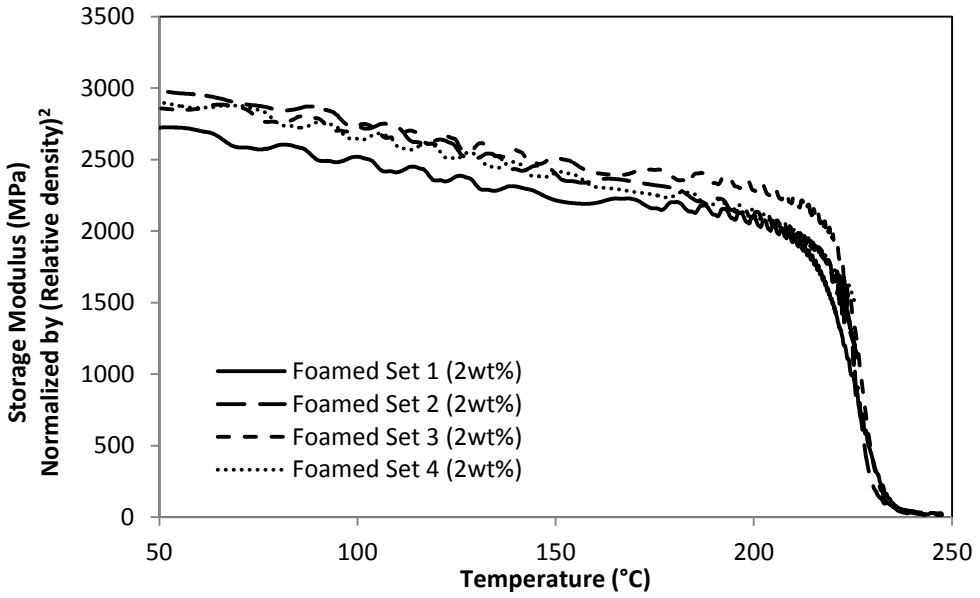

Figure 3-26. Mechanical and thermal property of PEI/MWCNT (2 wt%) nanocomposite foams with four foaming conditions (normalized by (relative density)^2).

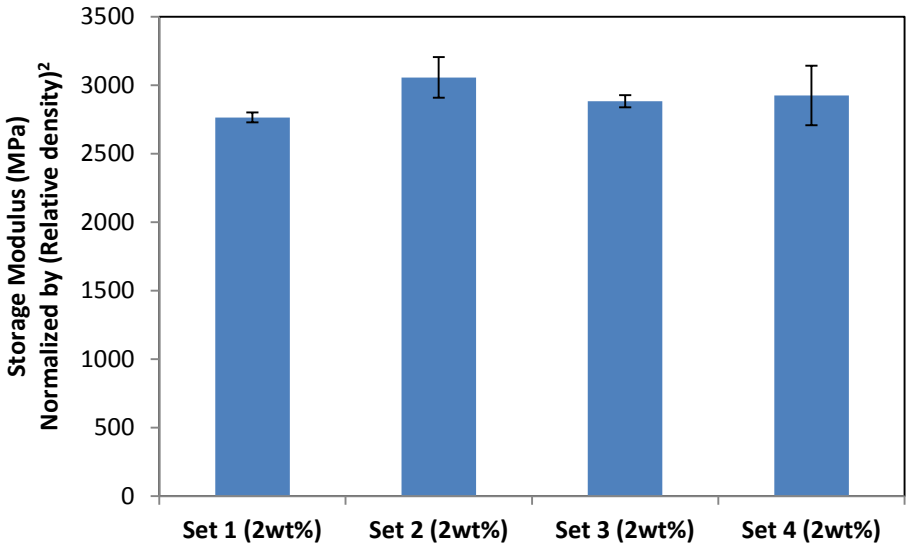

Figure 3-27. Storage moduli of PEI/MWCNT nanocomposite foams under four foaming conditions (normalized by (relative density)^2) at 50 °C.

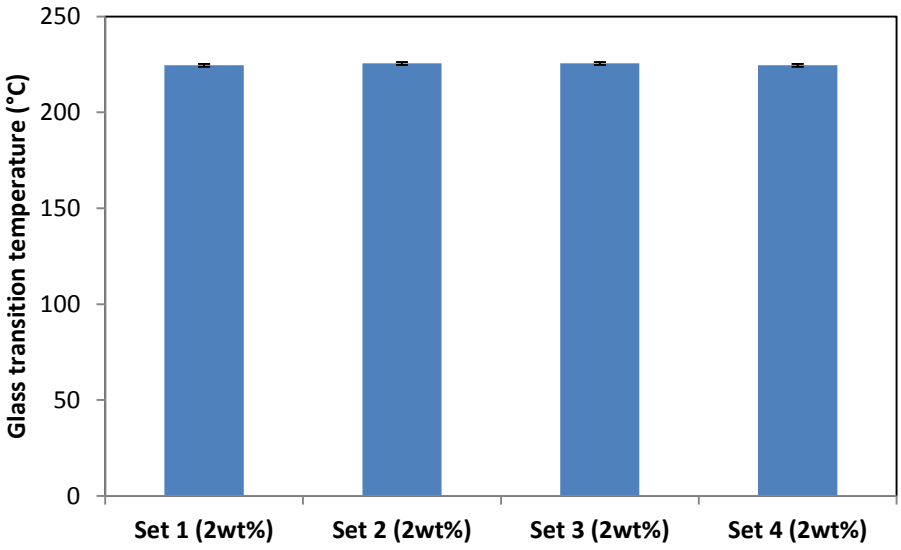

Figure 3-28. T_gs of neat PEI foams with 4 foaming sets (2 samples were tested for each condition).

3.3.3 Electrical Conductivity of Nanocomposites and Foams

Volume electrical conductivity of PEI/MWCNT nanocomposites and their foams were measured. Figure 3-29 shows the volume electrical conductivities of unfoamed PEI/MWCNTs nanocomposites and foamed ones at the saturation pressure of 4 MPa and foaming temperatures of 155 °C (Set 1) and 185 °C (Set 2) with various MWCNT loadings. Set 1 (relative density 65%) and Set 2 (relative density 45%) samples had similar pore sizes (~450 nm). Figures 3-29 shows the effect of foam density on electrical conductivity of nanocomposite foams.

Dramatic increase of electrical conductivity was found for unfoamed nanocomposites between MWCNT loadings of 0 wt% to 0.5 wt%, which indicates that the percolation threshold lies below 0.5 wt% loading. To determine the percolation threshold (φ_c), a power law relation is used as shown in Equation (3-4) [71].

$$Electrical\ conductivity \propto (\varphi - \varphi_c)^t \qquad (3\text{-}4)$$

where φ is the MWCNT loading in wt% and *t* is the critical exponent. t depends on the system dimensionality, and 1.33 is used for a two-dimensional and 2 for a three dimensional system. *t*=2 was used in this study. A log-log plot of conductivity vs. the reduced mass fraction, defined as $(\varphi-\varphi_c)/\varphi_c$, for unfoamed samples is shown in Figure 3-30. A good linear fit was found using the log-log plot, and the percolation threshold φ_c for unfoamed samples was found to be 0.45 wt%.

Electrical conductivities for foamed PEI/MWCNTs nanocomposites are relatively lower than those of the composites, almost by a factor of 100 as shown in Figure 3-29. A similar trend was found from the research for the volume conductivity of

PS/CNT composites and foams by Yang et al. [5]. This could be because of the fact that some of the conducting paths of MWCNTs were broken by the volume expansion due to foaming. Percolation threshold of Set 1 foams was found to be 0.45 wt% which is the same as unfoamed samples, and that of Set 2 foams increased from 0.5 wt% to 1 wt% as shown in Figures 3-31 and 3-32. In addition, the electrical conductivity of Set 2 foams also had slightly lower values than those of Set 1 beyond the percolation threshold. Foamed nanocomposites with a higher density showed a higher electrical conductivity, because more conduction paths were maintained.

The volume electrical conductivity values of unfoamed and foamed nanocomposites obtained when the MWCNT loadings were greater than the percolation thresholds were found to be in the range suitable for electrostatic charge dissipation applications (greater than 10^{-11} S/cm) according to the American National Standard Institute [72]. Therefore, combining with reduced density, the PEI nanocomposite foams could be a possible candidate for low-density electrostatic charge dissipation applications in high temperature situations.

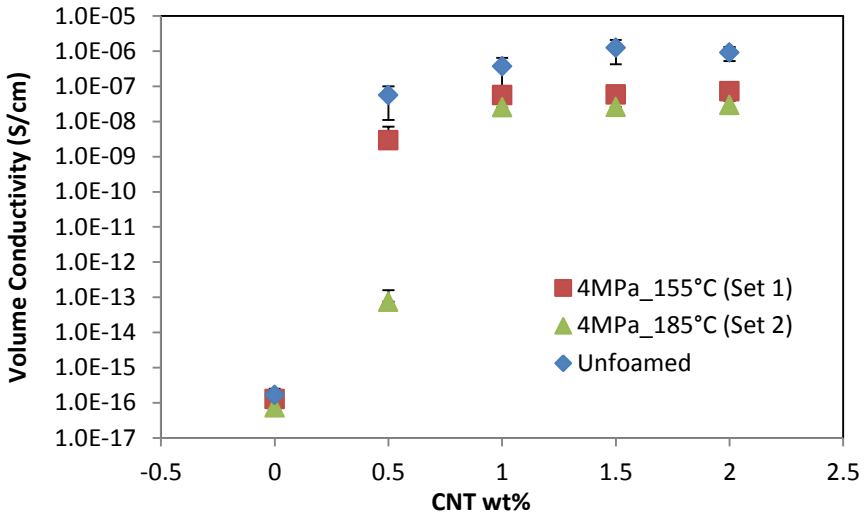

Figure 3-29. Volume DC electrical conductivity of Sets 1 and 2 with various MWCNT loadings.

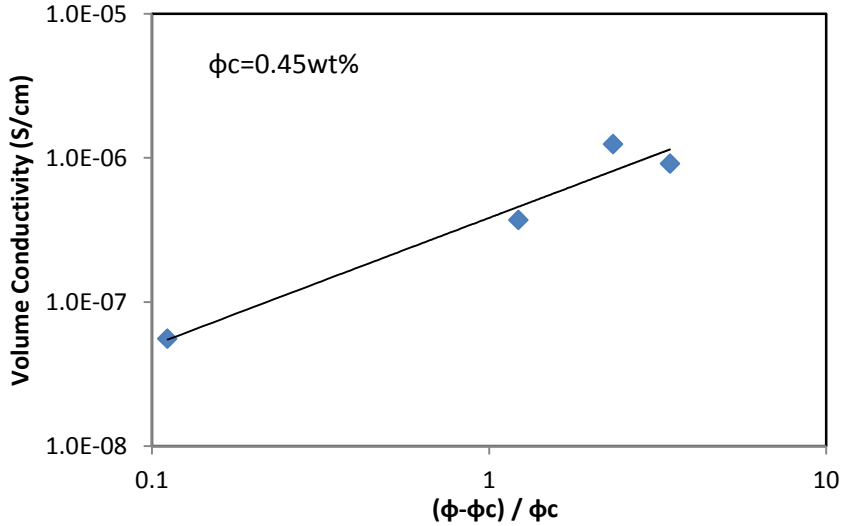

Figure 3-30. A log-log plot of conductivity vs. reduced mass fraction for unfoamed samples. φ_c is the percolation threshold.

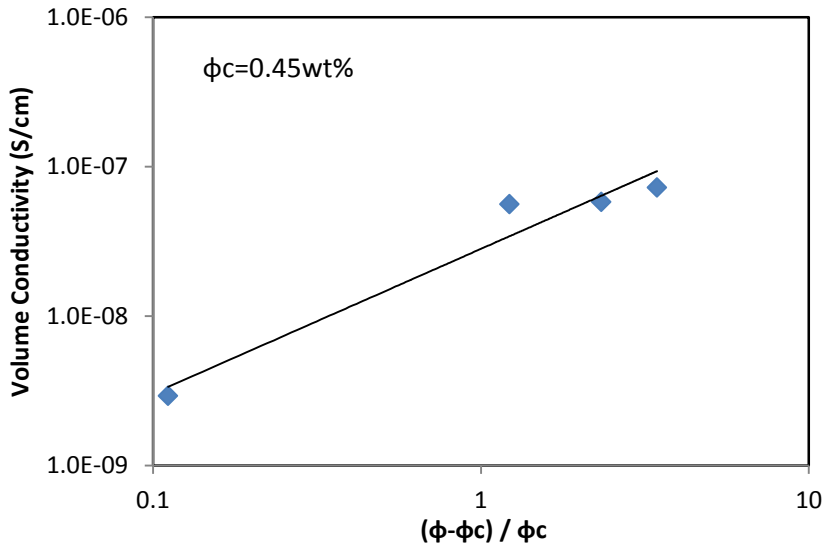

Figure 3-31. A log-log plot of conductivity vs. reduced mass fraction for foamed Set 1 samples. φ_c is the percolation threshold.

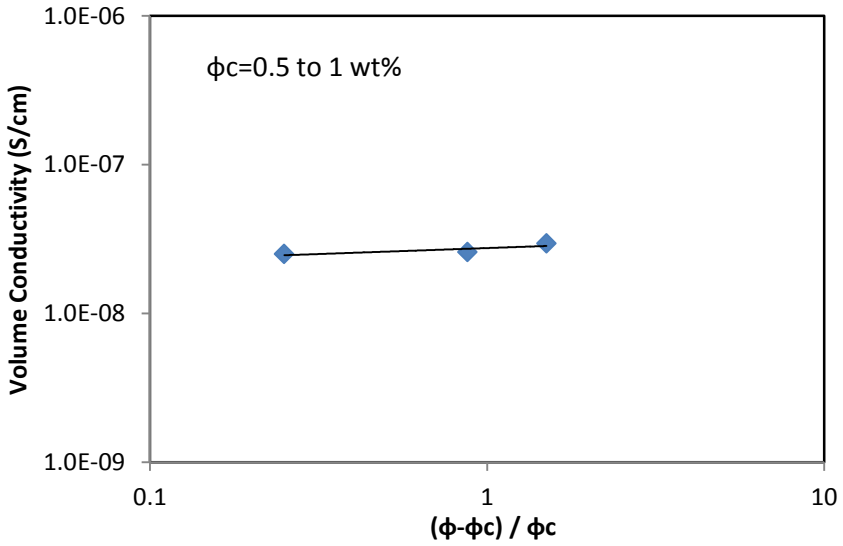

Figure 3-32. A log-log plot of conductivity vs. reduced mass fraction for foamed Set 2 samples. φ_c is the percolation threshold.

At a given volume percent loading, density has little effect on electrical conductivity as shown in Figures 3-33. Filler volume percent was calculated using the following equation (3-4).

$$\text{Volume \%} = \frac{(Filler\ weight\ (g))}{(Filler\ density\ (\frac{g}{cm^3})} \ / \ \frac{(Sample\ weight\ (g))}{(Sample\ density\ (\frac{g}{cm^3})} \qquad (3\text{-}4)$$

where the filler density was 2.1g/cm^3 from the manufacturer. Regardless of the relative density values of unfoamed nanocomposites (relative density 100%), Set 1 (65%), and Set 2 (45%), electrical conductivity from three groups of samples followed the same trend line. At a given volume %, the ratio of MWCNT volume to the sample volume is unchanged regardless of the volume expansion caused by foaming. Therefore, the electrical conductivity of nanocomposite foams can be predicted with the density measurement, provided that electrical conductivity of unfoamed nanocompoistes is known.

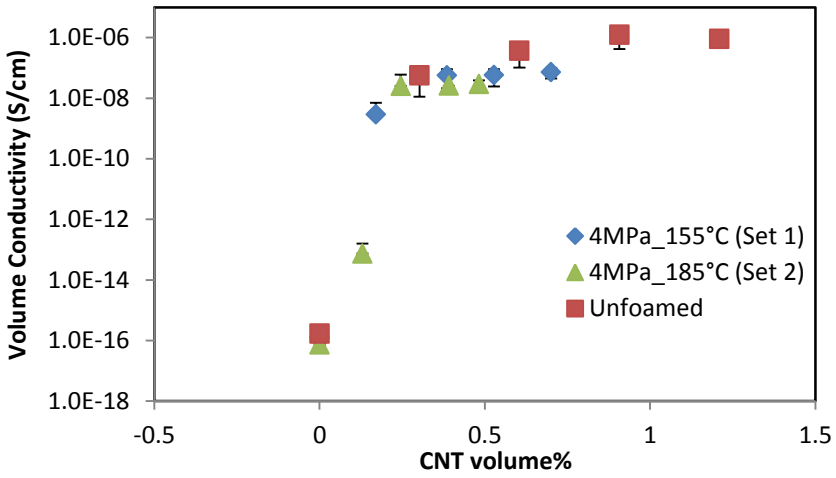

Figure 3-33. Volume DC electrical conductivity of Sets 1 and 2 samples with various MWCNT loadings.

Volume electrical conductivity of Sets 3 and 4 foams were measured. Figures 3-34 shows the volume electrical conductivity of foamed nanocomposites with saturation pressure of 8 MPa and two different foaming temperatures of 155 °C (Set 3) and 185 °C (Set 4), as well as unfoamed PEI/MWCNTs nanocomposites with various MWCNTs loadings. The density effect on electrical conductivity was investigated for large pore (750 nm) groups, including Set 3 (relative density 65%) and Set 4 (relative density 45%) samples. Similar results were found to small pore groups in terms of electrical conductivity and percolation threshold. As density decreased, electrical conductivity dropped and percolation threshold increased. Percolation threshold for Set 3 foams was found to be between 0 wt% and 0.5 wt%, and 0.8 wt% for Set 4 foams as shown in Figures 3-35 and 3-36 according to the power law function fitting using Equation (3-4).

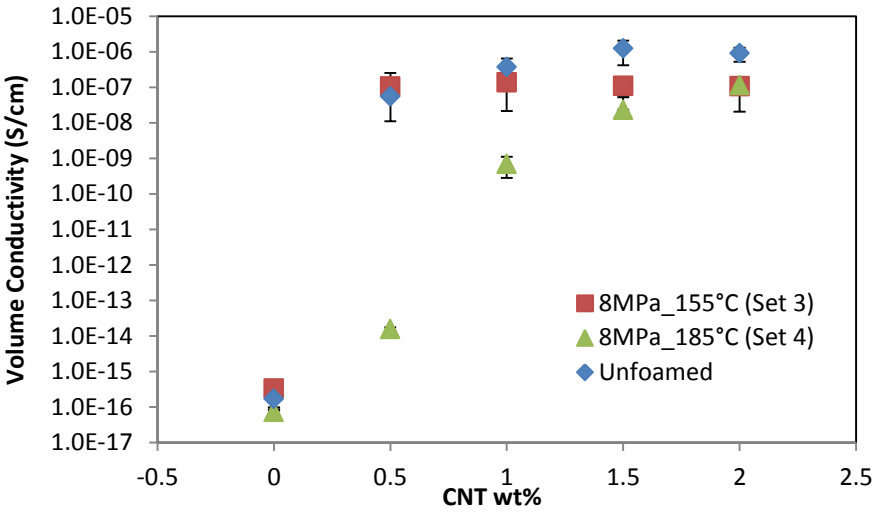

Figure 3-34. Volume DC electrical conductivity of Sets 3 and 4 samples with various MWCNT loadings.

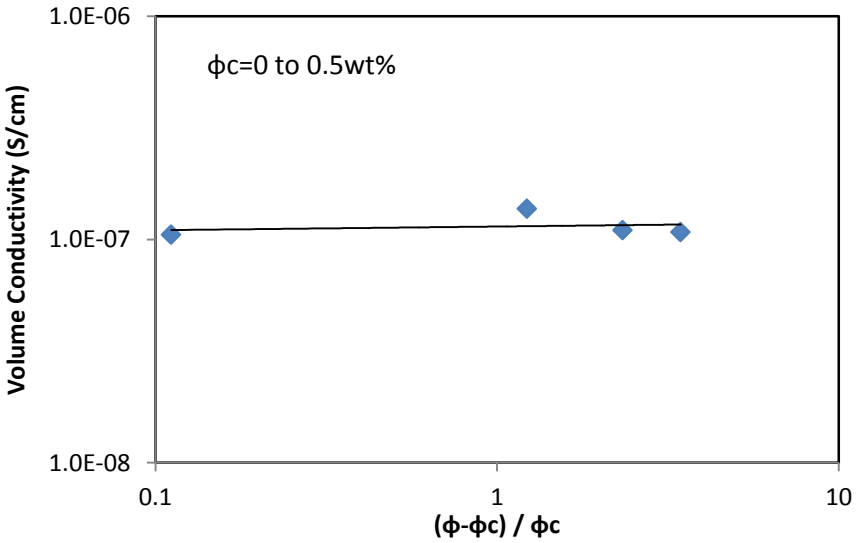

Figure 3-35. A log-log plot of conductivity vs. reduced mass fraction for Set 3 foam samples.

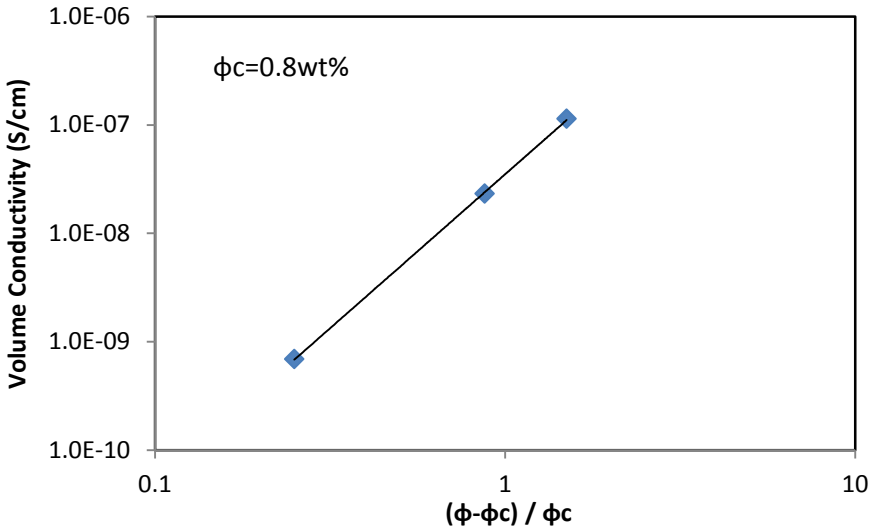

Figure 3-36. A log-log plot of conductivity vs. reduced mass fraction for Set 4 foam samples, which was used to determine the percolation threshold φ_c.

The electrical conductivity of unfoamed nanocomposites and foamed Set 3 and Set 4 samples at given MWCNT volume % also followed the same trend line as shown in Figure 3-37, similar to the results from Set 1 and Set 2 samples as seen in Figure 3-31.

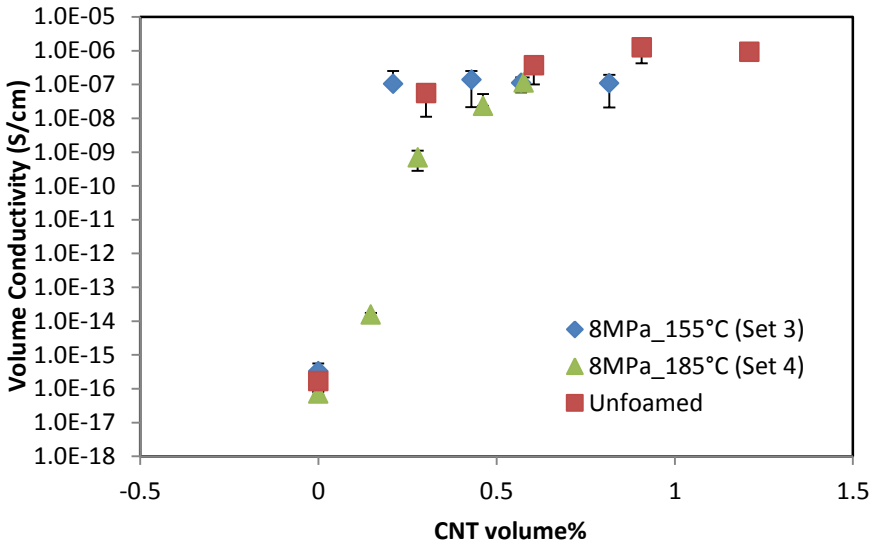

Figure 3-37. Volume DC electrical conductivity of Sets 3 and 4 samples with various MWCNT loadings in volume%.

The cell size effect on electrical conductivity was investigated. Figures 3-38 and 3-39 show the volume electrical conductivity of unfoamed PEI/MWCNTs nanocomposites, and that of foamed nanocomposites with the foaming temperature of 155 ℃ and two different saturation pressures of 4 MPa (Set 1) and 8 MPa (Set 3), under various MWCNT loadings. Figure 3-38 was plotted with the MWCNT loading in wt% and Figure 3-39 was plotted with the MWCNT loading in volume %. Since Set 1 (pore size 750 nm) and Set 2 (pore size 450 nm) samples had a similar relative density (65%), but different pore size, Figures 3-38 and 3-39 shows the effect of pore size on electrical conductivity of the nanocomposite foams. It was found from Figure 3-38 that the electrical conductivities for Set 1 and Set 3 samples were almost identical even though their cell sizes were different at a given wt%. This suggested that there was little effect of cell size on the electrical conductivity of the foamed nanocomposites having a relative density of around 65%. The electrical conductivity of unfoamed nanocomposites and foamed Set 1 and Set 3 samples at a given MWCNT volume % followed the same trend line as shown in Figure 3-39.

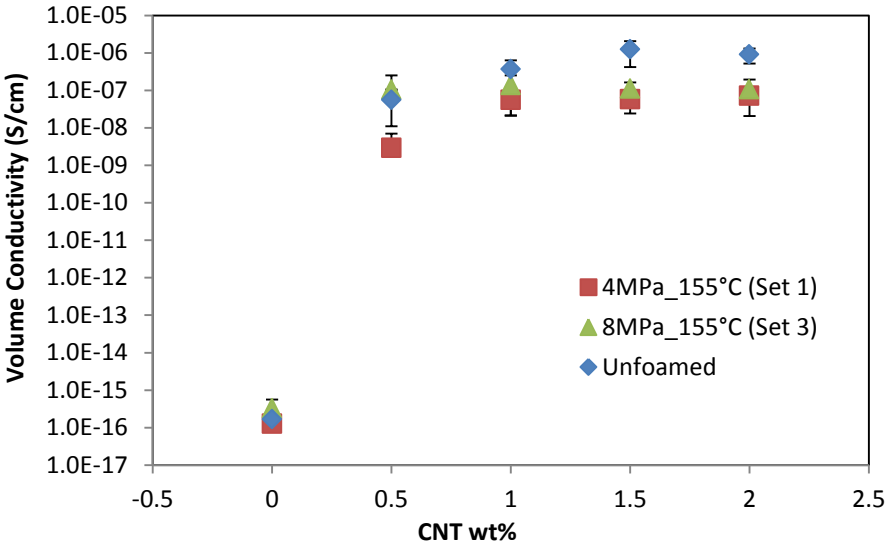

Figure 3-38. Volume DC electrical conductivities of Sets 1 and 3 samples with various MWCNT loadings.

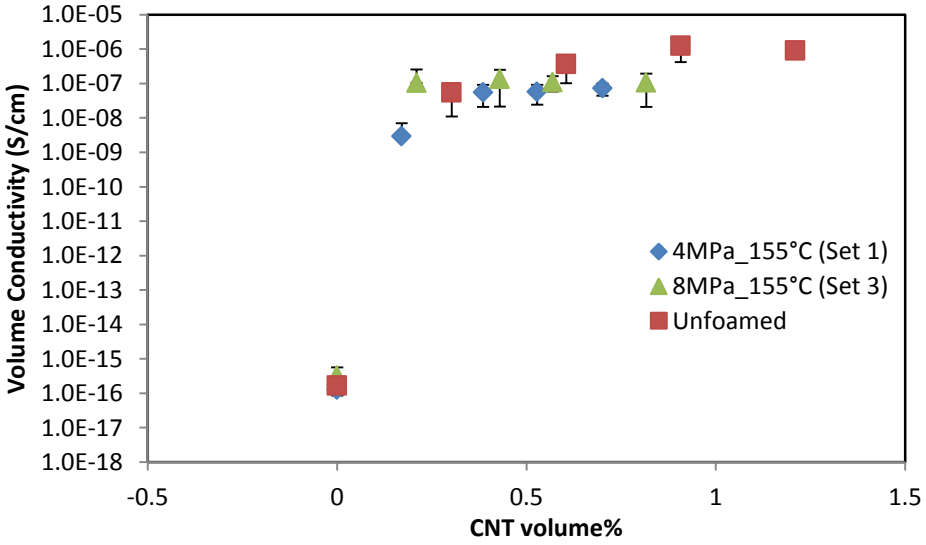

Figure 3-39. Volume DC electrical conductivities of Sets 1 and 3 samples with various MWCNT loadings.

The pore size effect on electrical conductivity was investigated in low density (relative density: ~45%) groups, Set 2 (pore size: ~750 nm) and Set 4 (pore size: ~450 nm). Similar results were found as the high density nanocomposite foams. Figure 3-40 shows that the electrical conductivities of Set 2 and Set 4 samples were also almost identical even though their cell sizes were different at a given wt%, suggesting that there was little effect of cell size on electrical conductivity for the foamed nanocomposites having relative density of around 45%. However, it should be noted that the cell size in this study ranged only from 400 to 800 nm. The electrical conductivity of unfoamed nanocomposites and foamed Set 2 and Set 4 samples at a given MWCNT volume % followed the same trend line, as shown in Figure 3-41.

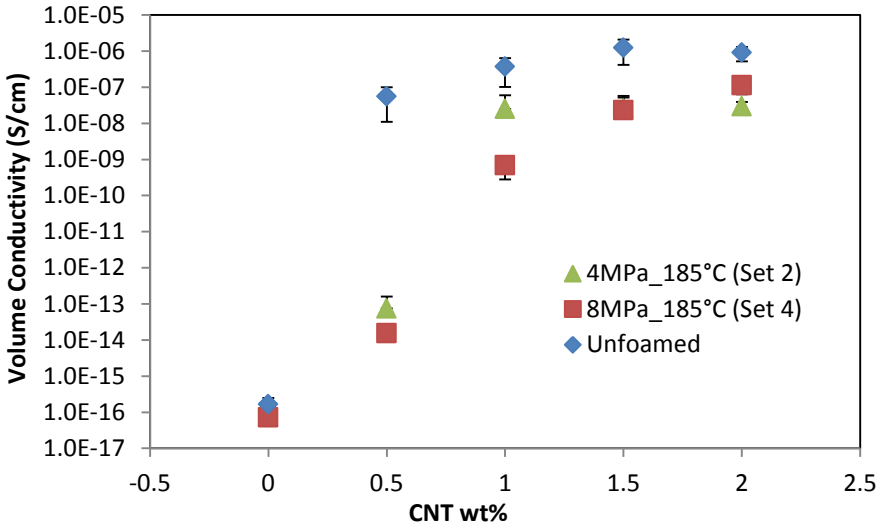

Figure 3-40. Volume DC electrical conductivity of Sets 2 and 4 samples with various MWCNT loadings in wt%.

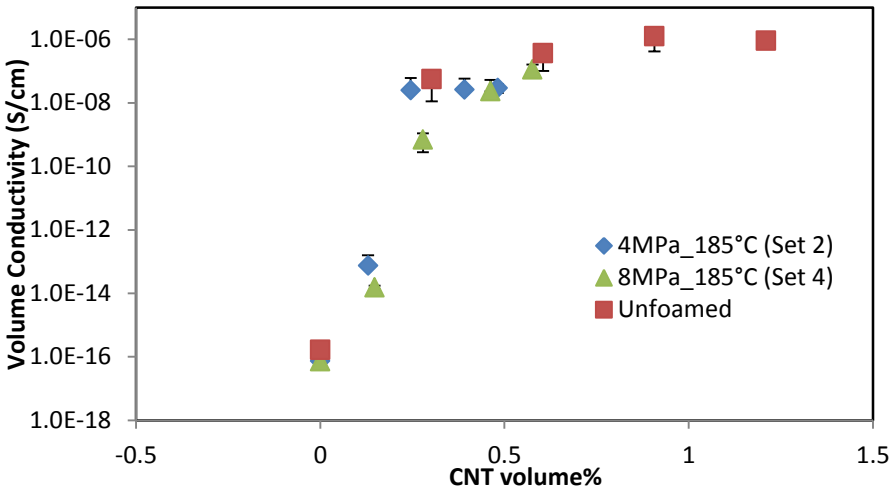

Figure 3-41. Volume DC electrical conductivity of Sets 2 and 4 samples with various MWCNT loadings in volume%.

Figure 3-42 shows the electrical conductivities of all sets of samples at a given weight percent, and the data were used to investigate the effects of foam density, pore size, and filler loading depending on four different foaming conditions on electrical conductivity with the statistical approach. The electrical conductivity data at filler loadings of 0.5wt% and 1.5wt% were used, and the data matrix is shown in Table 3-4. Data analysis software, JMP from SAS, was used to investigate the significance of those factors on electrical conductivity of samples. Interaction effects among those factors were also investigated with full factorial analysis. Table 3-5 shows the effect screening result. For an effect to be statistically significant, Prob>|t| has to be smaller than 0.05. It was found that density, loading, and interaction of density and loading have effects which are statistically significant as shown in Table 3-5. It was found from the Pareto plot as shown

in Figure 3-43 that the filler loading has the most significant effect on increasing electrical conductivity followed by the density of foams. In addition, there was a significant interaction effect between filler loading and density of foams. This interaction effect resulted from the fact that as filler loading increases, the density effect is reduced as shown in Figure 3-42, resulting in negative interaction effect. However, pore size has little effect on electrical conductivity of samples.

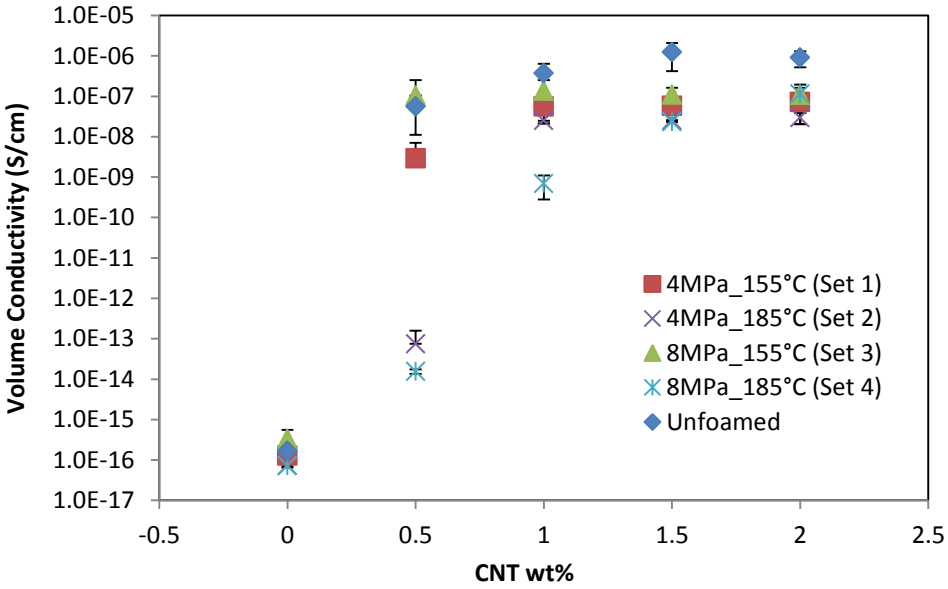

Figure 3-42. Volume DC electrical conductivity of all sets of samples with various MWCNT loadings in wt%.

Table 3-4. Data matrix of factors (filler loading, density, and pore size) on electrical conductivity

	Relative density (%)	Pore size (nm)	Loading (wt%)	Log(Electrical conductivity)
1	45	450	0.5	-13.85138316
2	45	450	1.5	-8.612917919
3	45	750	0.5	-12.87316063
4	45	750	1.5	-8.497005612
5	65	450	0.5	-6.677883606
6	65	450	1.5	-6.832902627
7	65	750	0.5	-8.232964755
8	65	750	1.5	-7.088194781
9	45	450	0.5	-13.77358449
10	45	450	1.5	-7.358431467
11	45	750	0.5	-13.82161694
12	45	750	1.5	-7.315515608
13	65	450	0.5	-14.7363965
14	65	450	1.5	-7.135099585
15	65	750	0.5	-14.05023338
16	65	750	1.5	-7.465370635
17	100	0	0.5	-7.344114896
18	100	0	0.5	-8.012350438
19	100	0	0.5	-6.933706776
20	100	0	0.5	-7.292596828
21	100	0	1.5	-5.658114812
22	100	0	1.5	-5.932268577
23	100	0	1.5	-6.712846408
24	100	0	1.5	-5.84380357

Table 3-5. Effect screening from data analysis using JMP

Response: Conductivity
The estimates are correlated and need a transformation.
The estimates have different variances and need scaling.
Length PSE
0.240461

Transformed Parameter Estimates

Term	Original	Orthog Coded	Orthog t-Test	Prob>|t|
Intercept	-23.66434	-8.835519	-23.6956	<.0001
Density	0.15625	1.653064	4.4333	**0.0004**
Pore Size	-0.00058	0.064147	0.172	0.8656
Density*Pore Size	0.00002	0.057951	0.1554	0.8784
Loading	9.67948	1.797813	4.8215	**0.0002**
Density*Loading	-0.08337	-0.872925	-2.3411	**0.0325**
Pore Size*Loading	-0.00016	-0.061599	-0.1652	0.8709
Density*Pore Size*Loading	-0.00001	-0.015598	-0.0418	0.9672

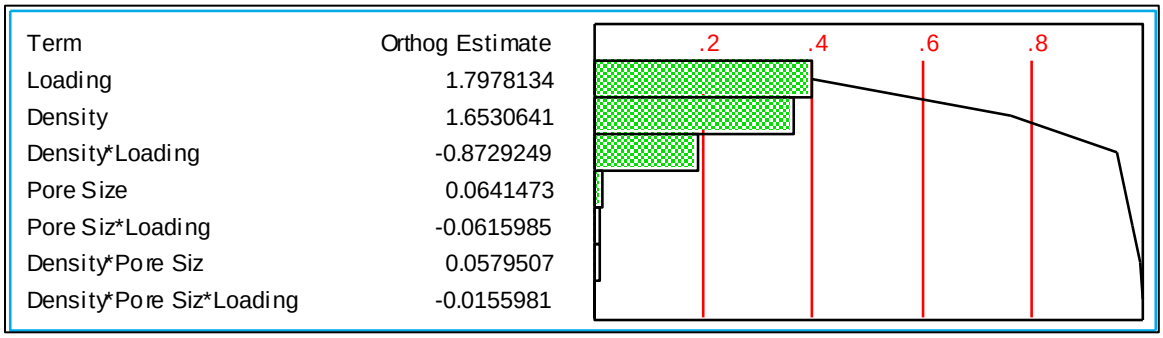

Figure 3-43. Pareto plot of estimates on the significance of factors (filler loading, density, and pore size) on electrical conductivity

Figure 3-44 shows the electrical conductivities of all sets of samples at a given volume percent. The electrical conductivity values followed the same trend line, suggesting that the morphological difference of in PEI nanocomposite foams does not affect the electrical conductivity of samples if they have the same volume percent loading. This phenomenon is going to be discussed in Chapter 5, which studies the electrical conductivity modeling using 3-D Monte Carlo simulation.

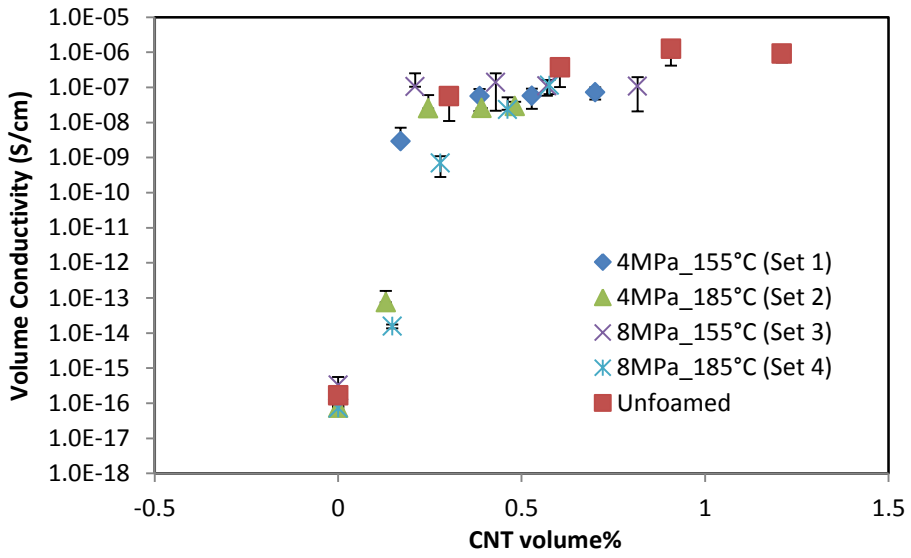

Figure 3-44. Volume DC electrical conductivity of all sets of samples with various MWCNT loadings in volume%.

3.4 SUMMARY AND CONCLUSIONS

PEI/MWCNT nanocomposites and their foams were fabricated using solvent-casting and solid-state foaming. Existence of residual solvent decreased the mechanical and thermal properties of the solvent cast samples. Morphology of the foams including cell size and cell density was examined with respect to different foaming and nanofiller loading conditions. A higher saturation pressure resulted in a smaller cell size and higher cell density. However, the addition of the nanofillers did not affect the cell size and cell density of the foams. It is believed that the increased cell density by heterogeneous nucleation was offset by cell collapsing caused by the residual solvent that was not fully removed from the solvent cast samples. Higher foaming temperatures did not affect the cell density and cell size due to the tradeoff between smaller nuclei and more cell growth.

Mechanical and thermal properties of PEI/MWCNT nanocomposites and foams under different foaming conditions were investigated. Addition of MWCNTs has little effect on increasing the storage modulus of nanocomposite. High thermal property from the PEI matrix was maintained by the PEI/MWCNT nanocomposites and foams. The normalized storage modulus of the foams by (relative density)^2 was in good agreement with their unfoamed counterparts. Cell size has little effect on the thermal and mechanical property of foams in this study.

Volume electrical conductivities of the PEI/MWCNT nanocomposites and foams were measured at various MWCNT loadings. Volume electrical conductivities with the MWCNT loadings beyond the percolation threshold were within the range of electro-

dissipative materials according to the ANSI/ESD standard, which indicates that those foams could be suitable for electrostatic dissipation applications with excellent inherent properties of the high performance polymer matrix. The effect of cell size, cell density, and relative density on the volume electrical conductivity was investigated. No significant effects of cell size and cell density on conductivity were found for the foamed obtained in this study. However, density of the foams affected the electrical conductivity. The higher the density, the less the nanofillers needed to reach percolation. At the same CNT loading in wt%, the higher the density is, the higher the electrical conductivity will be. This is due to the retention of the conducting path in high density foams. However, if the electrical conductivity is plotted against the CNT loading in volume %, the density of foams does not show effect on the electrical conductivity. This phenomenon will be discussed in Chapter 5 with a 3-D Monte Carlo simulation for electrical conductivity of nanocomposite foams.

Chapter 4. Polylactic Acid/Carbon Nanotube Nanocomposite Foams: Fabrication and Characterization

4.1 INTRODUCTION

As discussed in Chapter 3, polymer nanocomposite foams have attracted much interest due to their improved mechanical, thermal, and electrical properties. Early research in this area has focused on improving foam morphology and the mechanical property. Nanoparticles such as nanoclay, carbon nanofiber (CNF), and carbon nanotubes (CNTs) were used with a wide range of polymer matrices to increase the nucleation density, thus reducing the cell size, reinforce the polymer foam, and impart other desirable properties such as fire retardancy [16]. Polymer nanocomposite foams with improved electrical conductivity have recently been developed for lightweight electrostatic discharge (ESD), electromagnetic interference (EMI) shielding, and lightning-strike protection applications [13]. It is well known that a small amount of highly conductive nanoparticles, when well dispersed, could form a conducting network in the polymer matrix, therefore significantly improve the electrical conductivity of the otherwise insulating material. Making these polymer nanocomposites into foams would lead to a new class of multifunctional materials that are both lightweight and electrically conductive. Traditionally, ESD and EMI prevention has relied on metal-based materials, either thin sheet metals or metal coated plastics. These materials suffer from

disadvantages of being heavy, prone to corrosion, and difficult to process. Conductive polymer nanocomposite foams are preferred compared to metal based materials.

Environmental issues have been considered as important factors in plastic manufacturing, due to the increased demand to reduce land fill. Plastic consumption is subjected to increase by a factor of three in the current decade [11]. Especially, for electronics applications, the lifetime of consumer electronics is becoming shorter and the plastics used in electronics products become waste faster. Currently the average lifetime of these product is just a few months [11]. Utilizing biodegradable polymers is considered to be a solution to the plastic waste problems. Therefore, in the area of conductive polymer nanocomposite foams biodegradable polymer matrices can be applied.

Certain biodegradable polymers, such as poly(caprolactone) (PCL) and poly(lactic acid) (PLA) have already been utilized as host matrices for conductive polymer nanocomposite foams, as shown in Table 4-1. PCL has low thermal stability with a glass transition temperature (T_g) of -60 °C and a melting temperature of 65 °C. Among biodegradable polymers, PLA can be derived from renewable sources such as corn starch and has physical properties acceptable for commodity product applications. A few research efforts were found on conductive PLA-based nanocomposite foams, but their electrical properties have not been reported [48,49]. Some reported the conductivity

of unfoamed PLA-based nanocomposites [49, 73, 74]. McCullen et al. [75] reported electrical conductivity of porous PLA/MWCNTs nanocomposites, as shown in Table 4-1; however, they utilized the eletrospinning method to create the porous structure, which could have substantially lower mechanical properties than foams made using other methods, such as solid-state foaming.

In this chapter, PLA/multi-walled carbon nanotubes (MWCNTs) nanocomposite foams were fabricated and their electrical and mechanical properties were characterized. By using PLA as the matrix material, a new environmentally friendly nanocomposite foam material could be developed for lightweight ESD and EMI shielding applications.

Table 4-1. Summary of biodegradable polymer based nanocomposite foams with conductive nanofillers

Matrix	Matrix Tg (°C)	Matrix Tm(°C)	Filler type	Pore size (um)	Relative density (%)	Electrical conductivity	Ref
PCL	-60	65	MWCNT	50-100	15-30	$4x10^{-2}$ S/cm (0.25vol%)-AC	[3]
PLA	60-65	150-180	MWCNT	50-200	20-40	NA	[49]
				2-10	80	NA	[48]
				Electro-spinning	10	10^{-8} S/cm (0.5 wt%)	[75]

4.2 EXPERIMENTAL

4.2.1 Materials

PLA powder (ECORENE^{TM} NW 40) was purchased from ICO Polymers, with an average powder size of 20 μm. PLA is a semi-crystalline thermoplastic material. It is a biodegradable polymer by simple hydrolysis of the ester (CO-O) bond, and it does not require any catalysts for the hydrolysis [76]. The PLA used in this study is derived from natural resources such as corn starch. The molecular structure of PLA is shown in Figure 4-1. The density, mechanical, and thermal properties are shown in Table 4-1. Multi-walled CNTs (MWCNTs) were used in this study as conductive nanofillers. MWCNTs were provided by Bayer Material Science, Germany, with the commercial name of Baytube (C 150 P) (diameter ~15 nm; length 1-10 μm). Baytubes were received as powder agglomerates as shown in Figure 4-2 and individual tubes are shown in Figure 4-3 at a higher magnification. For foaming, industrial grade CO_2 was used as the blowing agent.

Table 4-2. Properties of PLA [47]

Property	Value
Density (g/ml)	1.24
Tensile modulus (GPa)	1.5-2.7
Glass transition temperature (°C)	60-65
Melting temperature (°C)	150-180
Degradation time (Months)	12-18

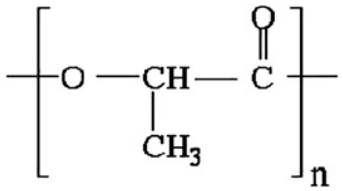

Figure 4-1. PLA structure [47].

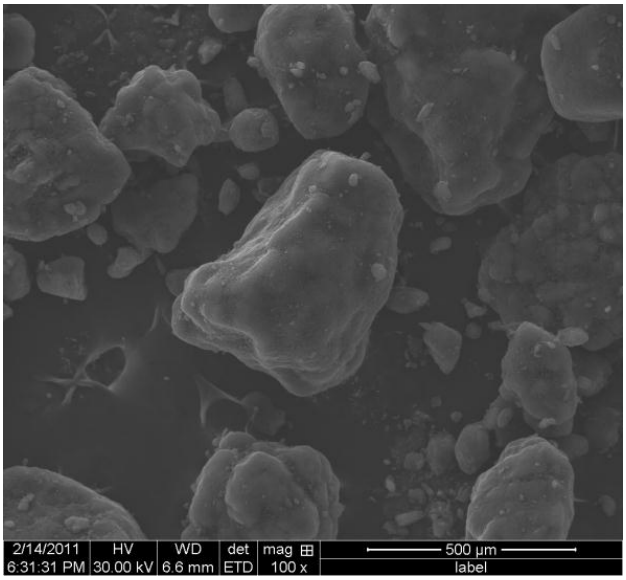

Figure 4-2. SEM of Baytube (Scale bar: 500 µm).

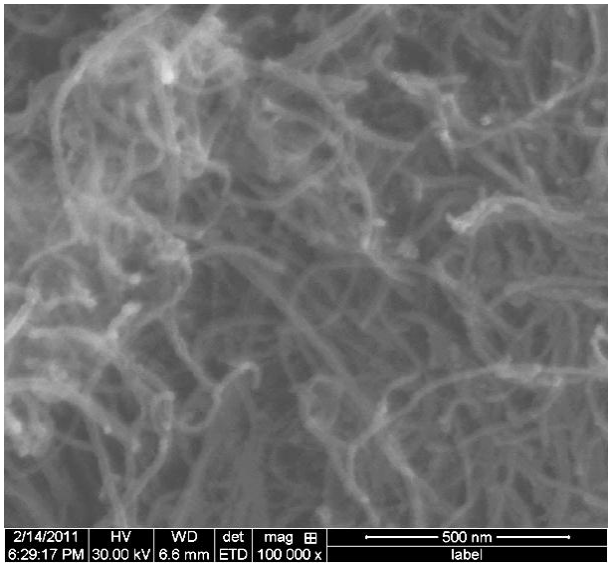

Figure 4-3. SEM of Baytube (Scale bar: 500 nm).

4.2.2 PLA/MWCNT Composite Fabrication

PLA powder and MWCNTs were pre-mixed for 3 minutes using a chrome blade coffee grinder (IDS59, Mr. Coffee, USA) and melt-blended using a twin-screw extruder (Haake Minilab II, Germany). The processing conditions for melt-blending of PLA/MWCNTs are shown in Table 4-2.

Table 4-2. Processing conditions of twin screw extrusion

Screw type	Counter rotating
Screw speed (rpm)	180
Processing temperature (°C)	150
Processing time (min)	10
MWCNTs loading (wt%)	0, 2, 4, and 6

After mixing, blended PLA/MWCNTs nanocomposites are injection molded using a lab-scale injection molder (Haake Mini Jet, Germany). Processing conditions for injection molding of PLA/MWCNTs are shown in Table 4-3.

Table 4-3. Processing conditions of injection molding

Injection pressure (bars)	800
Injection time (sec)	10
Barrel temperature (°C)	200
Mold temperature (°C)	60

Disk-shaped samples were obtained from injection molding, having a diameter of 20 mm and a thickness of 1.4 mm as shown in Figure 4-4.

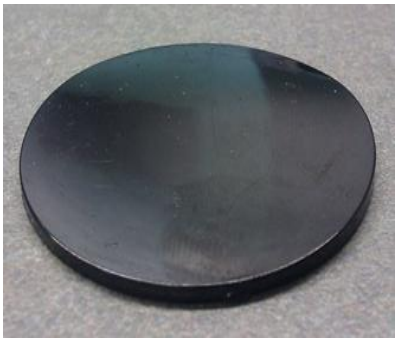

Figure 4-4. Injection molded PLA/MWCNTs nanocomposite sample.

4.2.3 Foaming of Nanocomposites

The PLA/MWCNTs nanocomposites were foamed using the solid-state foaming method as the one used for foaming of PEI/MWCNTs in Chapter 3. In the actual foaming stage, the bath foaming method was used with a foaming fixture as shown in Figure 4-5. Injection molded PLA/MWCNTs nanocomposites having the thickness of 1.4 mm was inserted in the foaming fixture immersed in the oil bath. Foaming fixture had a gap of 2 mm for foam to grow. The oil bath was heated by a hot plate heater and the foaming temperature was controlled by a temperature controller attached. Table 4-3 shows the experimental factors for the foaming of PLA/MWCNTs nanocomposites.

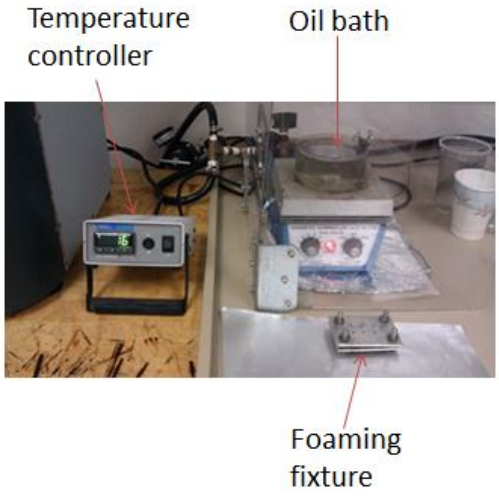

Figure 4-5. A bath foaming setup with the foaming fixture.

Table 4-3. Experimental factors for foaming

Factors	**Values**	
Saturation pressure	2MPa	4MPa
Saturation time	4 days	1 day
Foaming temperature	60-120 °C with an interval of 20 °C	60-140 °C with an interval of 20 °C
Saturation temperature 20 °C, desorption time 10 min, and foaming time 20 sec		

4.2.4 Characterization

Volume DC electrical conductivities of the samples were measured with an Ohmmeter (Super Megohmmeter, Hioki 8220, Japan) with a set of high resolution electrodes (SME 8311, Hioki, Japan). Densities of the samples were measured based on ASTM D792-00 using the equation below.

$$Density = \frac{Wa}{Wa-Ww}(0.9975)\ \ g/cm^3$$

where w_a is the sample weight in air, and w_w is the sample weight when immersed in water. Density measurement was performed with a lab balance (ML53, Mettler Toledo, Switzerland). The ratio of the foamed sample density to that of the unfoamed one is used as the relative density.

Microstructures of the samples were observed using a Quanta 650 FEG scanning electron microscope (FEI Company, USA). The samples were freeze-fractured in liquid nitrogen to avoid damage of the imaging surface by shear force from tools such as scissors. The surfaces to be observed were coated with gold and palladium (Au/Pd) using sputter coater (EMS 500X, Electron Microscopy Sciences, USA) to prevent charging on the surface which is not preferred for imaging.

Thermo-mechanical properties were investigated using a dynamic mechanical analyzer (Q800 DMA, TA instruments, USA) with a temperature ramp rate of 3°C/min, and a frequency of 1 Hz. DMA was used to determine the stiffness and the glass transition temperature of the materials.

4.3 RESULTS AND DISCUSSION

4.3.1 Dispersion of MWCNTs in PLA matrix

MWCNT dispersion in PLA was investigated using SEM images. Figure 4-6 shows a SEM image of a neat PLA sample. Figures 4-7 and 4-8 show SEMs of PLA/MWCNT nanocomposites with filler contents of 4 wt% and 6 wt%, respectively. Compared to the neat PLA, well-dispersed MWCNTs were found in both PLA/MWCNT nanocomposites (4 and 6 wt%), showing that the processing parameters of melt-blending were appropriate for PLA/MWCNT systems in this study. It was shown that MWCNTs are more densely populated in the 6 wt% PLA/MWCNT nanocomposite than the 4 wt% one.

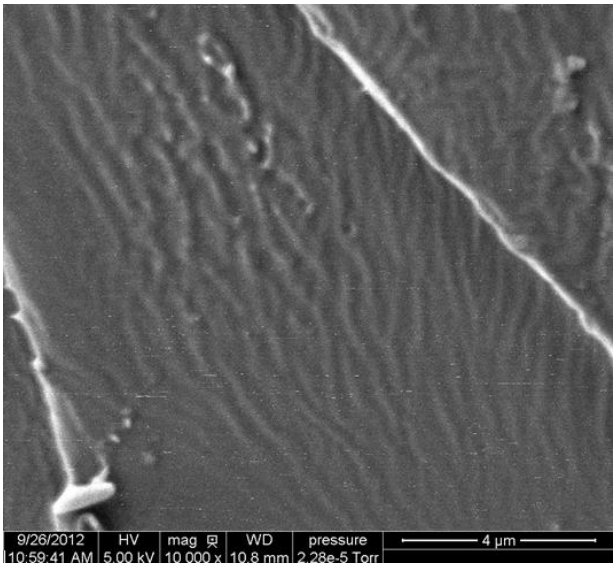

Figure 4-6. An SEM image of neat PLA. Scale bar: 4 µm.

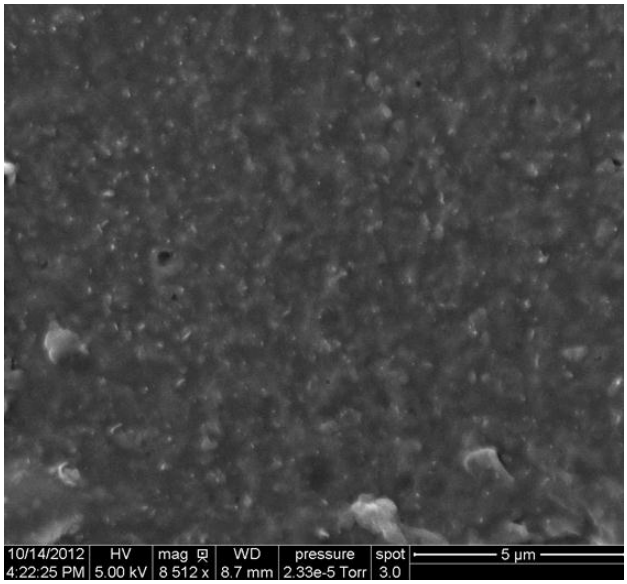

Figure 4-7. An SEM image of PLA/MWCNT (4 wt%). Scale bar: 5 µm.

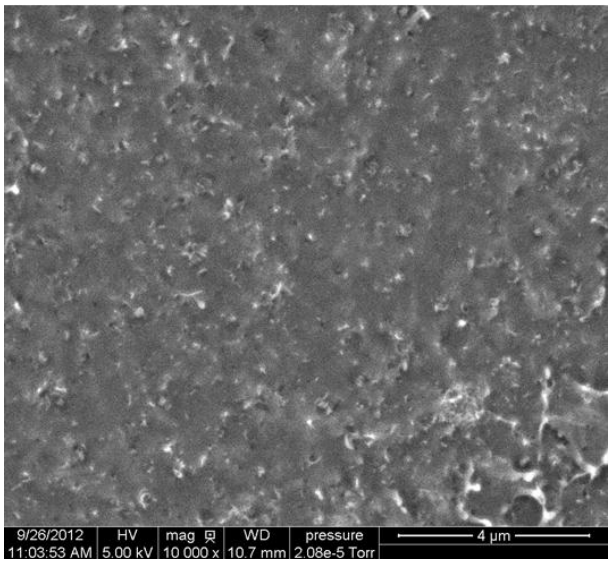

Figure 4-8. An SEM image of PLA/MWCNT (6 wt%). Scale bar: 4 µm.

4.3.2 Effect of foaming conditions on porosity

Effect of different foaming conditions on porosity was investigated. The results are shown in Figure 4-9. Equilibrium CO_2 uptake was around 7% at 2 MPa and 14% at 4 MPa with the saturation time given in Table 4-3. For PLA/MWCNT (6 wt%) nanocomposite foams with a saturation pressure of 2 MPa, porosity increased as foaming temperature increased up to 100 °C, while there was no significant effect of foaming temperature on porosity at the saturation pressure of 4 MPa up 120 °C. For nanocomposite foams foamed with a saturation pressure of 2 MPa, as the foaming temperature increased there was more rapid cell growth due to the combination of a softer matrix and higher kinetic energy of CO_2 at a higher temperature, causing a higher porosity up to the foaming temperature of 100 °C. For the case of the saturation pressure of 4 MPa, porosity was found to be 25% at the foaming temperature of 60 °C. It did not change as the foaming temperature increased up to 120°C. Wang [77] found that CO_2 saturation at 4 MPa increased PLA crystallinity to 27% as shown in Figure 4-10 and that the formation of crystalline phase prevented foaming of thermoplastic polymers [78], causing limited porosity regardless of the foaming temperature. From Matuana's research [79], a maximum porosity of 35% was obtained for PLA with a CO_2 concentration of 16% using various foaming conditions. In the solid state foaming process, as foaming temperature increases the porosity increases up to a certain level and starts to decrease due to cell collapsing [80]. For foams with the saturation pressure of 2 MPa, the maximum porosity was found at the foaming temperature of 100 °C, and the porosity started to decrease afterwards. For foams with saturation pressure of 4 MPa, porosity

appeared to decrease from 140 °C. However, there was essentially no change in the porosity of foams foamed from 120 to 60 °C, indicating that maximum porosity had reached at the foaming temperature of 60 °C. For the rest of study in this chapter, foaming conditions of 2MPa-100°C and 4MPa-120°C were chosen.

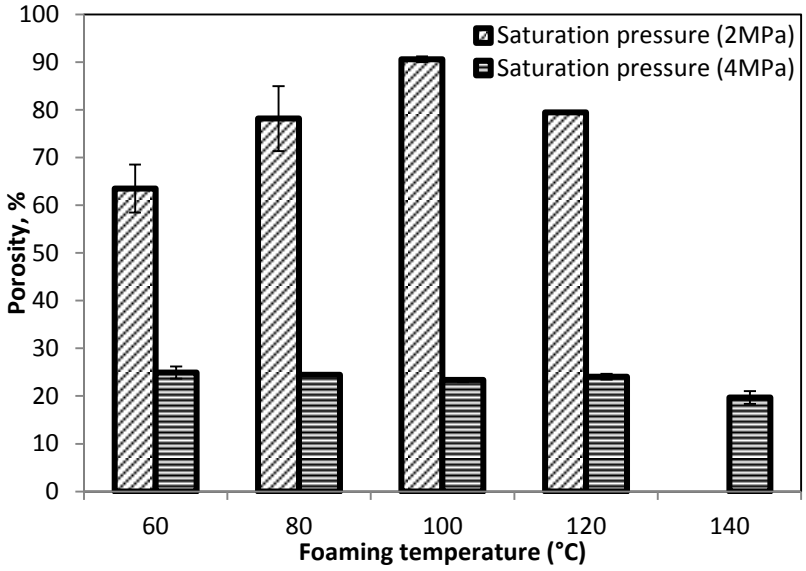

Figure 4-9. Porosity of PLA/MWCNTs (6 wt%) nanocomposite foams at different foaming conditions (2 samples were measured at each condition).

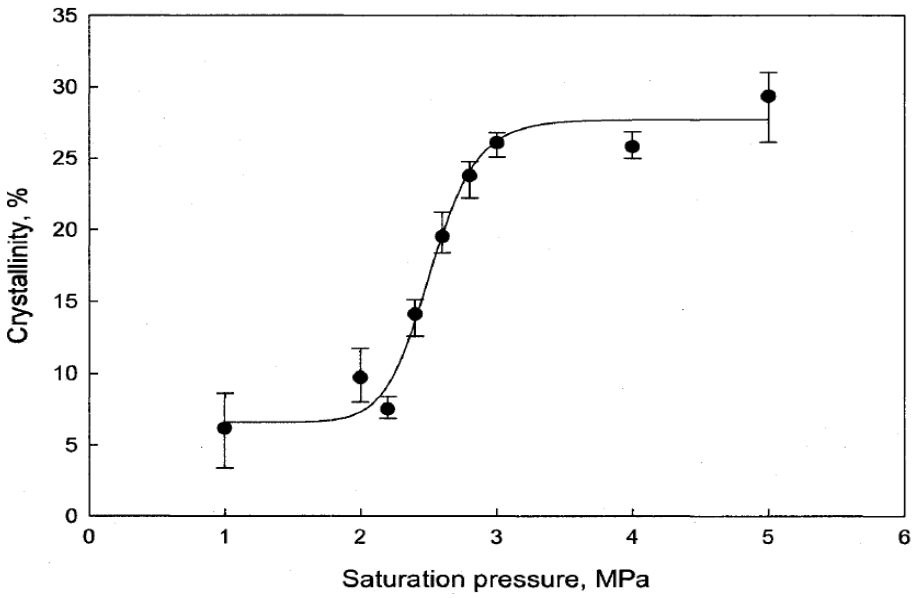

Figure 4-10. PLA crystallinity after CO_2 saturation at different saturation pressures[77].

4.3.3 Effect of MWCNT loading on morphology of nanocomposite foams

The MWCNT loading effect on the porosity of PLA/MWCNT foams was investigated at selected foaming conditions. The results are shown in Figure 4-11. It was found that the porosity slightly increased from 85 to 95% as the MWCNT loading increased from 0 to 4 wt% for foams with the saturation pressure of 2 MPa. A similar phenomenon was found by Rizvi et al. [49], showing decreased foam density as the MWCNT loading increased. For foams with the saturation pressure of 4 MPa, MWCNT loading did not affect the porosity of foams, but stayed at the porosity of around 25%. As discussed before, it is believed that the CO_2 induced crystallization limited the foaming of

PLA and its nanocomposite foams. In general, the effect of MWCNT loading was insignificant for both foam groups with the saturation pressures of 2 and 4 MPa.

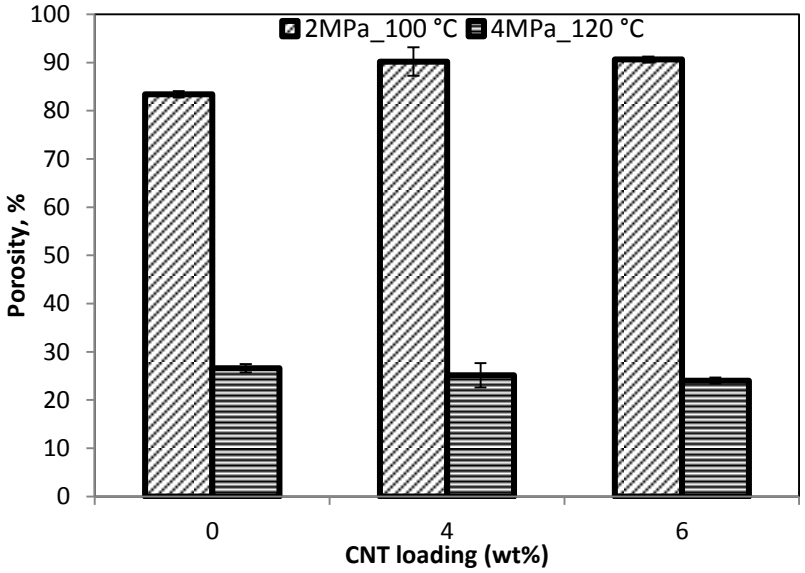

Figure 4-11. Porosity of foams with different filler loadings under selected foaming conditions (2 samples were measured for each condition).

Cell density (# of pores in a unit volume) of nanocomposite foams foamed with the saturation pressure of 2 MPa increased as the MWCNT loading increased from 0 to 4 wt% as compared in Figures 4-12 and 4-13, due to the existence of extra nucleation sites near MWCNTs. Additives cause decreases in the activation energy for nucleus formation. As discussed in Chapter 3, decrease in activation energy for nucleation leads to an increase in nucleation density, causing a larger number of pores [16]. Further addition of MWCNTs up to 6 wt% had little effect on cell density change as shown in Figure 4-14.

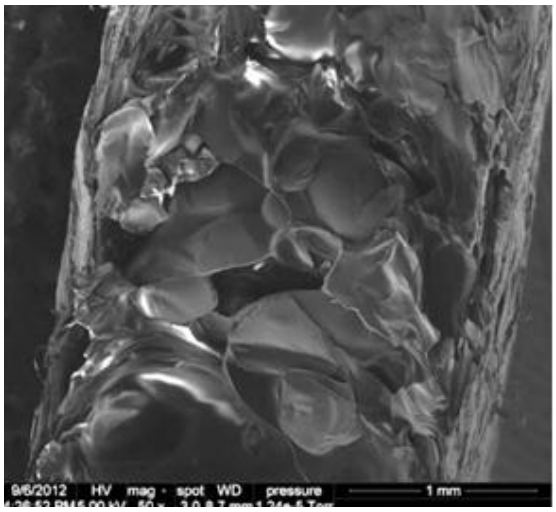

Figure 4-12. An SEM image of a neat PLA foam sample (saturated at 2 MPa, foamed at 100 °C). Scale bar: 1 mm.

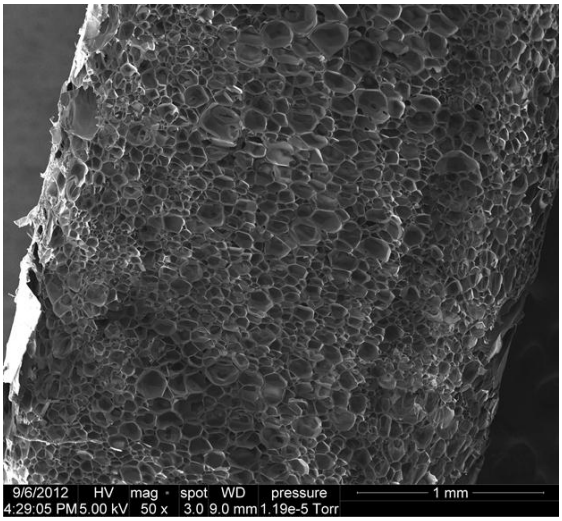

Figure 4-13. An SEM image of a PLA/MWCNT (4 wt%) foam sample (saturated at 2 MPa, foamed at 100 °C). Scale bar: 1 mm.

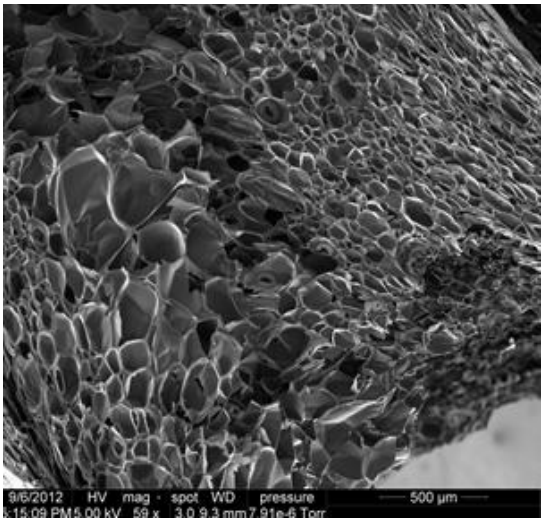

Figure 4-14. An SEM image of a PLA/MWCNT (6 wt%) foam sample (saturated at 2 MPa, foamed at 100 °C). Scale bar: 500 µm.

However, for nanocomposite foams foamed with the saturation pressure of 4 MPa, there was little effect of MWCNT loading on cell density as shown in Figures 4-15, 4-16, 4-17, and 4-18. It is believed that the existence of crystalline phase after CO_2 saturation at 4MPa reduced the effect of MWCNTs loading. For both neat and PLA/MWCNT (6 wt%) foams, porous region was only found in sample skin regions, suggesting that the crystallinity at the skin regions is lower than that in the center region.

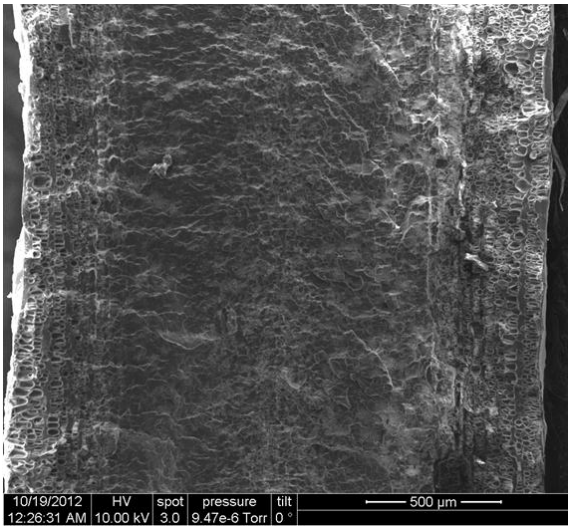

Figure 4-15. An SEM image of a neat PLA foam sample (saturated at 4 MPa, foamed at 120 °C). Scale bar: 500 µm.

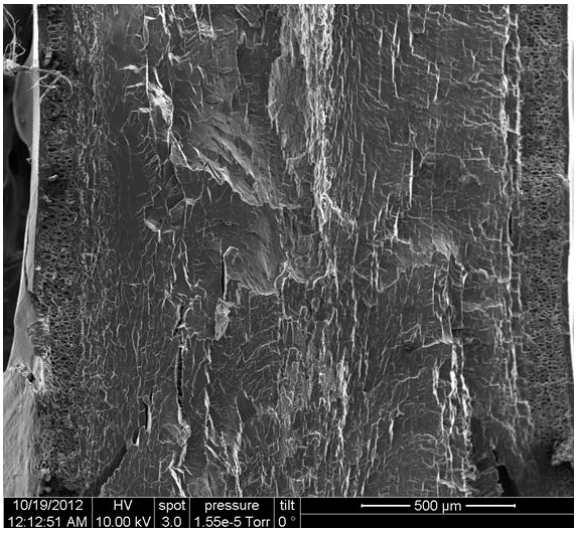

Figure 4-16. An SEM image of a PLA/MWCNT (6 wt%) foam sample (saturated at 4 MPa, foamed at 120 °C). Scale bar: 500 µm.

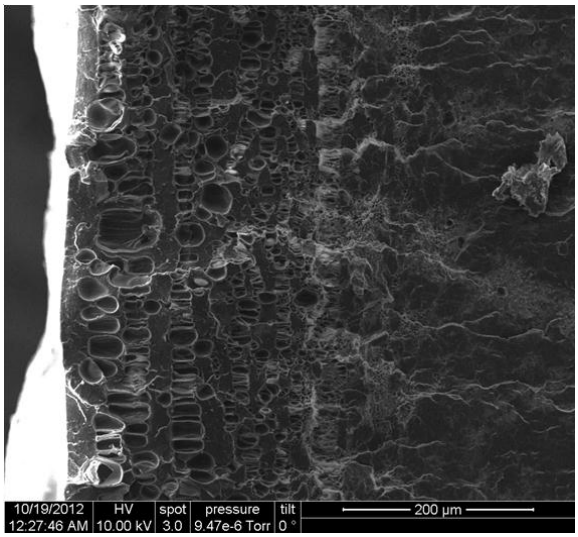

Figure 4-17. An SEM image of a neat PLA foam sample (saturated at 4 MPa, foamed at 120 °C), skin region. Scale bar: 500 µm.

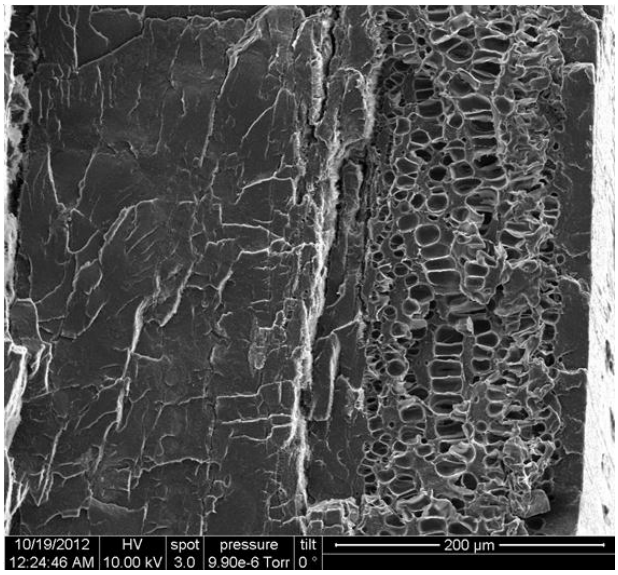

Figure 4-18. An SEM image of a PLA/MWCNT (6 wt%) foam sample (saturated at 4 MPa, foamed at 120 °C), skin region. Scale bar: 500 µm.

4.3.4 Mechanical and thermal properties of PLA/MWCNT nanocomposites and foams

Mechanical and thermal properties of PLA/MWCNT nanocomposites with various MWCNT loadings are shown in Figure 4-19. As the MWCNT loading increased, storage moduli of the nanocomposites increased. There was effective load transfer from polymer matrix to CNTs, causing increases in the stiffness [14]. T_g's of the nanocomposites were at 70 °C.

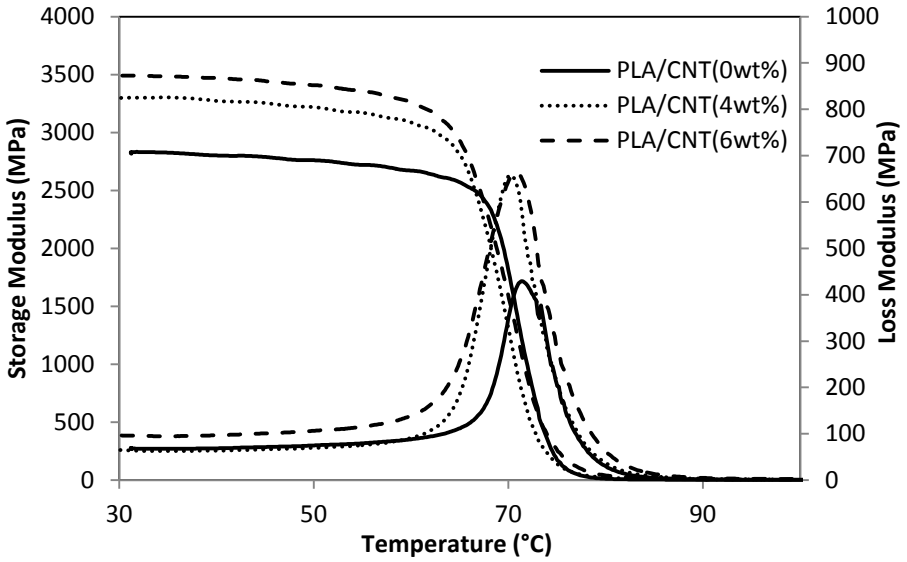

Figure 4-19. Mechanical and thermal property of PLA/MWCNTs nanocomposites with different MWCNTs loadings.

Mechanical and thermal properties of PLA/MWCNT foams with the saturation pressure of 4 MPa are shown in Figure 4-20 at different MWCNT loadings. Foams with the saturation pressure of 2 MPa were not suitable for DMA tests due to the difficulty in clamping the samples. Samples were so soft due to the high porosity that they collapsed during clamping on the DMA fixture. Storage moduli shown in Figure 4-20 were normalized by (relative density)^2. It is shown in Figures 4-19 and 4-20 that the storage moduli are almost identical, showing a good agreement with the Moore's observation [70]. T_g's for nanocomposite foams were found at 75 °C, which is slightly higher than the ones for unfoamed samples. It is believed that foaming caused an increase in the crystallinity of foamed samples, yielding increased T_g's after foaming, as discussed by

Wang [77]. A slight drop in the storage modulus after the elastic region for foamed samples is an indication of increased crystallinity, as compared to the unfoamed samples [82].

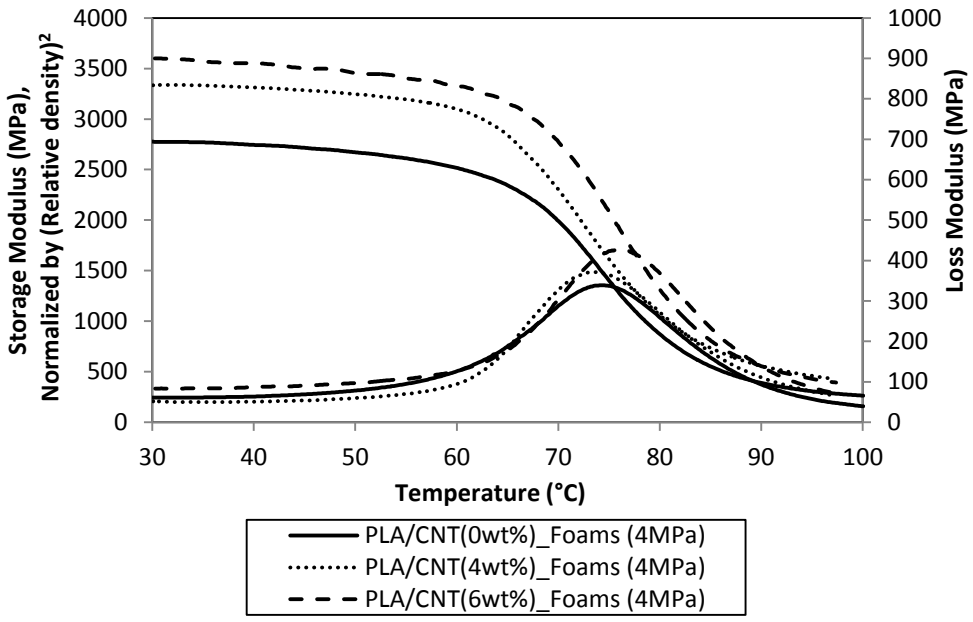

Figure 4-20. Mechanical and thermal properties of unfoamed PLA/MWCNT samples with different loadings.

4.3.5 Electrical property of PLA/MWCNT nanocomposites and foams

Electrical conductivity of PLA/MWCNT nanocomposites and foams with selected foaming conditions (2MPa-100°C and 4MPa-120°C) were investigated at various

MWCNT loadings. Figure 4-21 shows the electrical conductivity behavior as a function of MWCNT loading in wt%. Percolation was found between the MWCNT loadings of 2 to 4 wt%. In general, electrical conductivity of foamed samples had a higher conductivity than unfoamed ones. It was shown in Chapter 3 that electrical conductivity decreased after foaming of PEI/MWCNTs nanocomposites at a given wt%; however, the opposite phenomenon were found in foaming of PLA/MWCNTs nanocomposites, as shown in Figure 4-21. Two possible mechanisms could result in an increased electrical conductivity after foaming. First, MWCNTs aggregated in the cell walls by foaming as shown in Figure 4-22, such that better MWCNT connectivity was achieved by foaming due to the high MWCNT concentration in the solid cell wall portion. For PEI/MWCNT foams, as a comparison, CNTs are randomly distributed after foaming regardless of the foam morphology as shown in Figure 4-23, such that the electrical conductivity significantly dropped due to the diluted MWCNT concentration by volume expansion. Secondly, It was found by Wang [77] that crystallinity of PLA could be increased by foaming due to the stretching and heating effects. Increased crystallinity by foaming could contribute to the increase in electrical conductivity. Unlike other common amorphous polymers, the unique semi-crysalline property of PLA matrix and the increase in crystallinity by foaming could contribute to the increase in electrical conductivity. The volume electrical conductivity values of unfoamed and foamed nanocomposite foams obtained when the MWCNT loadings were greater than the percolation thresholds were found to be in the range suitable for electrostatic charge dissipation applications (greater than 10^{11} S/cm) [72]. Therefore, combining with reduced density, the PLA

nanocomposite foam could be a possible candidate for low-density, biodegradable electrostatic charge dissipation applications. In addition, a novel finding from PLA/MWCNT foams with the saturation pressure of 2 MPa and the foaming temperature of 100 °C was that a reduction of sample weight by 1/10 was achieved without electrical conductivity sacrifice, which is completely different from the behavior of PEI/MWCNT nanocomposite foams.

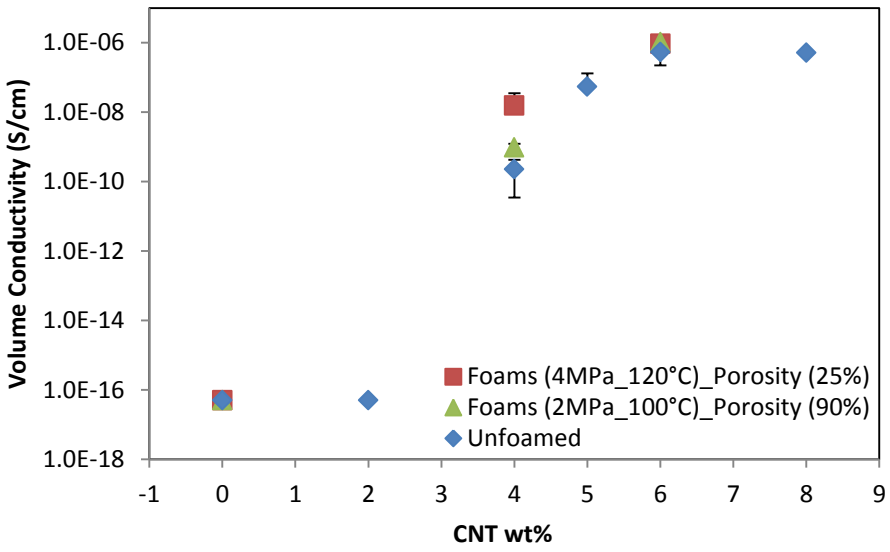

Figure 4-21. Volume DC electrical conductivity with various MWCNT loadings in wt%.

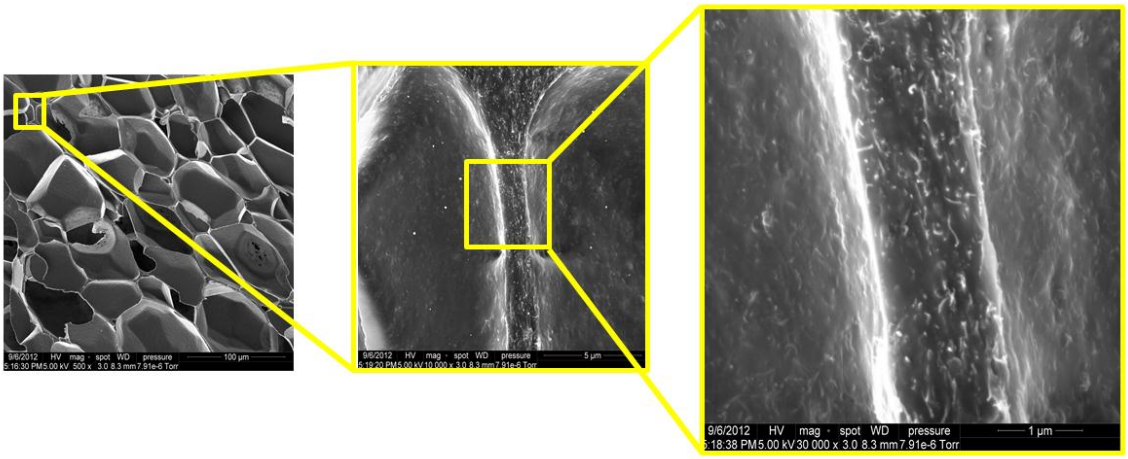

Figure 4-22. SEMs of PLA/MWCNT (6 wt%) foams with the saturation pressure of 2 MPa.

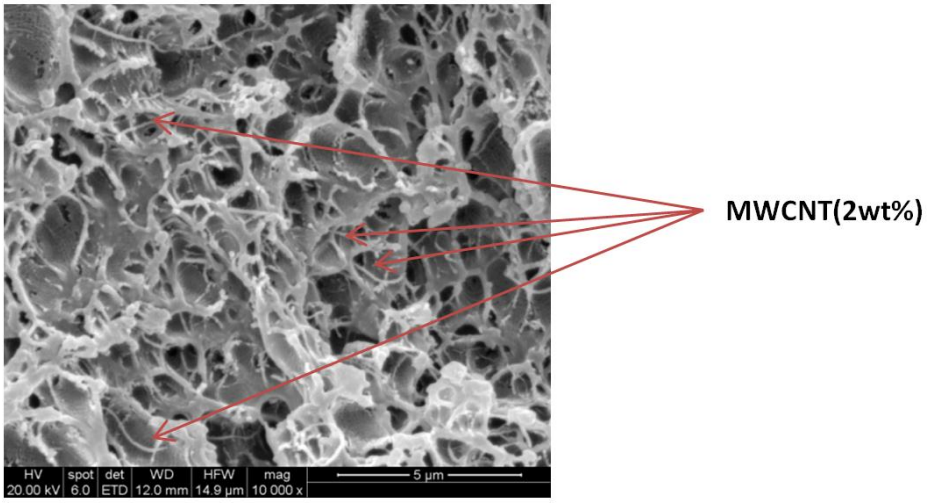

Figure 4-23. An SEM of PEI/MWCNT nanocomposite (2 wt%) foam.

Figure 4-24 shows dramatically increased electrical conductivity as porosity increased with MWCNT loadings in volume%. It was discussed in Chapter 3 that the electrical conductivity of PEI/MWCNT nanocomposites did not change regardless of the porosity at a given volume%, as shown in Figure 4-25. To understand the difference of electrical property for both polymer systems, electrical conductivity modeling will be performed in Chapter 5, and detailed analysis will be dealt with using simulation results.

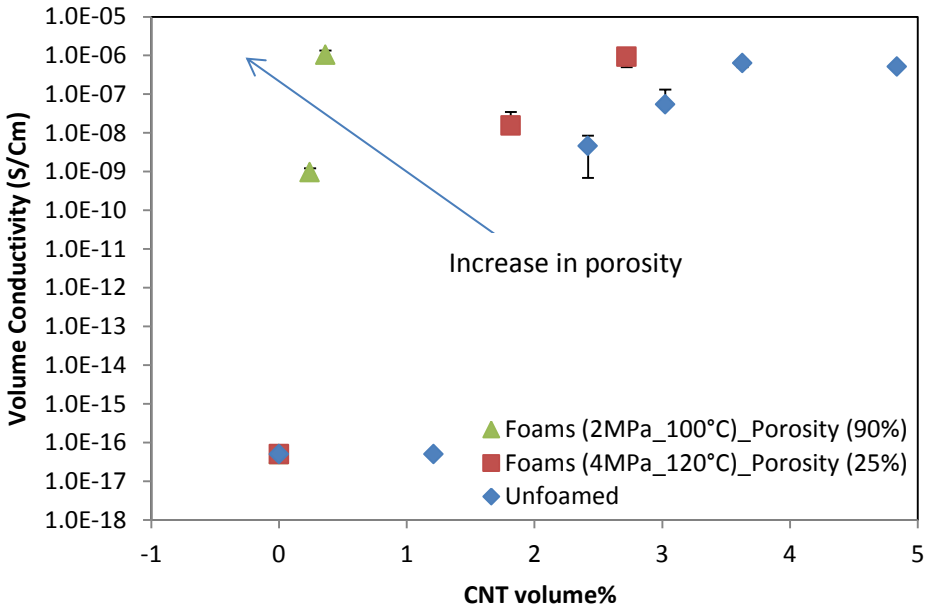

Figure 4-24. Volume DC electrical conductivity with various MWCNT loadings in volume%.

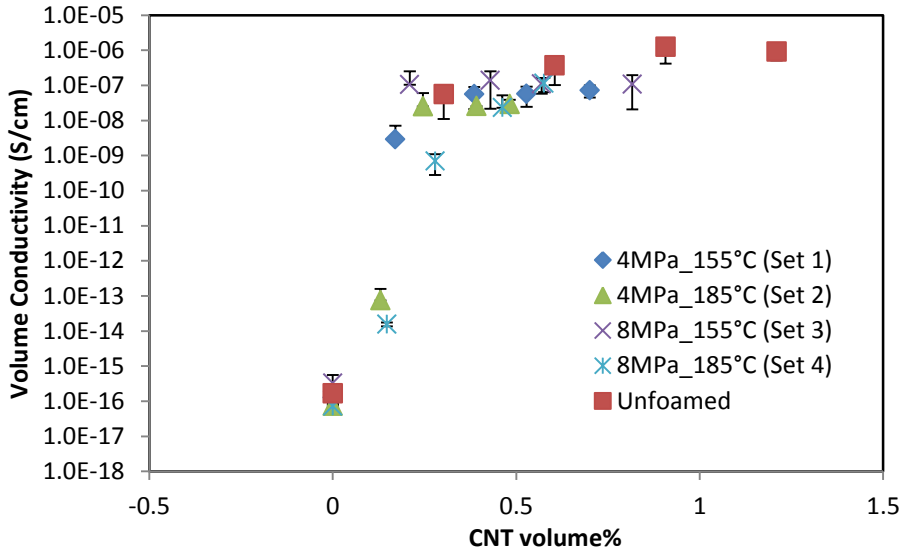

Figure 4-25. Volume DC electrical conductivity of PEI/MWCNT nanocomposites with loadings in volume%.

4.4 SUMMARY AND CONCLUSIONS

PLA/MWCNT nanocomposites and their foams with different foaming conditions were fabricated using melt-blending and solid-state foaming. Effect of foaming conditions on porosity was investigated with PLA/MWCNT nanocomposite foams. For nanocomposite foams with the saturation pressure of 2 MPa, as foaming temperature increased from 60 to 100 °C, the porosity increased then started to decrease due to cell collapsing. For nanocomposite foams with the saturation pressure of 4 MPa, foaming temperature did not affect to the porosity of foams. A constant porosity of around 25% was found with the foaming temperature from 80 to 120 °C. The porosity started to decrease afterwards. The CO_2 induced crystallization limited the foaming of neat PLA and PLA nanocomposites.

The MWCNT loading effect on porosity of PLA/MWCNTs foams was investigated. It was found that the porosity has little effect on porosity of PLA/MWCNT foams. Addition of MWCNTs in PLA significantly increased the cell density of foams at the saturation pressure of 2 MPa due to the lowered activation energy for nuclei formation. For foams with the saturation pressure of 4 MPa, effect of MWCNTs on cell density was insignificant.

Mechanical and thermal properties of PLA/MWCNTs nanocomposites and foams with the saturation pressure of 4 MPa were investigated. Addition of MWCNTs increased storage modulus. The normalized storage modulus of the foam was in a good agreement with their unfoamed counterparts. By foaming, the glass transition temperature increased by 5 °C, due to the increase in crystallinity.

Volume electrical conductivities of PLA/MWCNTs nanocomposites and foams were measured. Volume electrical conductivities with the MWCNT contents beyond the percolation threshold were within the range of dissipative materials according to the ANSI/ESD standard, which indicates that those foams could be suitable for electrostatic charge dissipation applications with their inherent biodegradable property. In general, electrical conductivity of foamed samples had higher conductivity than unfoamed ones compared with the same volume% loading. Especially, the PLA/MWCNT foams with the saturation pressure of 2 MPa and the foaming temperature of 100 °C showed a sample weight reduction by 1/10 without sacrificing the electrical conductivity. This finding could mean materials saving in both MWCNTs and the polymer. Unlike PEI/MWCNT composite foams, the electrical conductivity of PLA/MWCNT foams increased significantly as the porosity increased compared at the same CNT loading in volume%. This phenomenon will be discussed in Chapter 5 with 3D Monte Carlo simulation.

Chapter 5. Electrical Conductivity Modeling of Polymer Nanocomposite Foams

5.1 INTRODUCTION

Polymer nanocomposite foams have attracted tremendous interests due to their improved mechanical, thermal, and electrical properties, in addition to the inherited lightweight benefit of foamed materials [16]. Among different applications, polymer nanocomposite foams with improved electrical conductivity have recently been studied for lightweight electrostatic discharge (ESD), electromagnetic interference (EMI) shielding, and lightning-strike mitigation applications. It is well known that a small amount of highly conductive nanoparticles, when well dispersed, could form a conducting network in the polymer matrix. Making these polymer nanocomposites into foams would generate a new class of lightweight materials that will find many applications in aerospace, automotive, and electronics applications.

A variety of polymer matrices have been used to create foams with conducting fibrous fillers, including multi-walled carbon nanotubes (MWCNTs) and CNF, and their electrical conductivity behaviors have been investigated experimentally in many studies [38]. However, little theoretical effort has been found to understand and predict electrical conductivity of polymer nanocomposite foams.

In spite of the lack of theoretical studies on conductive foamed polymer nanocomposites, there are many efforts devoted to understanding and predicting electrical behaviors of unfoamed polymer nanocomposites with fibrous fillers using Monte-Carlo simulation. The Monte-Carlo simulation method to understand electrical conductivity behaviors with randomly distributed fibrous fillers consists of three steps in general: model generation with randomly distributed fibrous fillers in a finite volume, equivalent resistor network construction, and electrical conductivity calculation.

Pioneering work was done by Pike and Seager in 1974 [50]. They considered nanofillers as straight sticks having a fixed length and zero width in a two dimensional (2D) space. Studies in the 2D space were found in [51,52,83,84] and in 3D space were found in [53,54,85-87] with straight sticks as nanofillers by varying the filler length and alignment of fillers. It was found that a longer filler length and the isotropy (not aligned) of fillers were beneficial for electrical performance. In [55,56,88-92], the nanofiller waviness in 3D was considered since in reality the fibers in polymer matrix have a certain waviness. It was found from simulations that as the aspect ratio (filler length/diameter) increased and the waviness decreased, the electrical conductivity improved [51-56,83-92].

In this chapter, modeling and simulation of electrical conductivity of polymer nanocomposite foams was performed using 3D Monte-Carlo simulation. Wavy fibers

having a width of the tube diameter were used for the modeling. Two cases of foam generation mechanisms were considered. In the first case, fibers were distributed randomly regardless of the foam morphology after foaming due to the small enough pore size compared to the nanofiller size. In this case, the only event happened after foaming was volume expansion, such that only the distance between tubes increased accordingly. In the second case, nanofillers are not in the spherical pores, but are densely packed in the cell walls. These two different foaming mechanisms are modeled, and the numerical results from simulations were validated with the experimental data. Effects of foam density, pore size, and filler aspect ratio on the electrical performance were investigated for the two different foaming mechanisms, respectively.

5.2 MODELING

5.2.1 Generating geometrical model in a Representative Volume Element (RVE)

A geometrical model was generated with randomly distributed fibrous fillers in the Monte Carlo simulation. A generated model was scaled down to a reasonably small unit, so called a representative volume element (RVE), which can represent the entire system due to the computational efficiency. An initial point was generated in a RVE box as described in the Equation (5-1) below, where r is a random number greater than 0 and less than 1, and L is the length of the RVE cube edge. From the initial point, the second point was allocated following Equation (5-2), where φ and Θ are two randomly generated angles and l is the segment length of a carbon nanotube. The second point is another point having the distance of l from the initial point. The orientation is defined by the two angles of φ and Θ. The third point is allocated similarly following Equation (5-3) with a transformation matrix **T** as shown in Equation (5-4) with restricted Θ value, which is $(\pi/8)\cdot(\text{rand})$, where rand is a random number between 0 and 1, in this study to control tube straightness. The number of segments for a tube is chosen as six. Figure 5-1 shows the description of tube generation [91].

$$\begin{pmatrix} X(0) \\ Y(0) \\ Z(0) \end{pmatrix} = L * \begin{pmatrix} r \\ r \\ r \end{pmatrix} \qquad (5\text{-}1)$$

$$\begin{pmatrix} X(1) \\ Y(1) \\ Z(1) \end{pmatrix} = \begin{pmatrix} X(0) \\ Y(0) \\ Z(0) \end{pmatrix} + l * \begin{pmatrix} \sin\theta\cos\varphi \\ \sin\theta\sin\varphi \\ \cos\theta \end{pmatrix} \quad (5\text{-}2)$$

$$\begin{pmatrix} X(2) \\ Y(2) \\ Z(2) \end{pmatrix} = \begin{pmatrix} X(1) \\ Y(1) \\ Z(1) \end{pmatrix} + T * l * \begin{pmatrix} \sin\theta\cos\varphi \\ \sin\theta\sin\varphi \\ \cos\theta \end{pmatrix} \quad (5\text{-}3)$$

$$T = \begin{pmatrix} \cos\theta & 0 & \sin\theta \\ 0 & 1 & 0 \\ -\sin\theta & 0 & \cos\theta \end{pmatrix} \begin{pmatrix} \cos\varphi & -\sin\varphi & 0 \\ \sin\varphi & \cos\varphi & 0 \\ 0 & 0 & 1 \end{pmatrix} \quad (5\text{-}4)$$

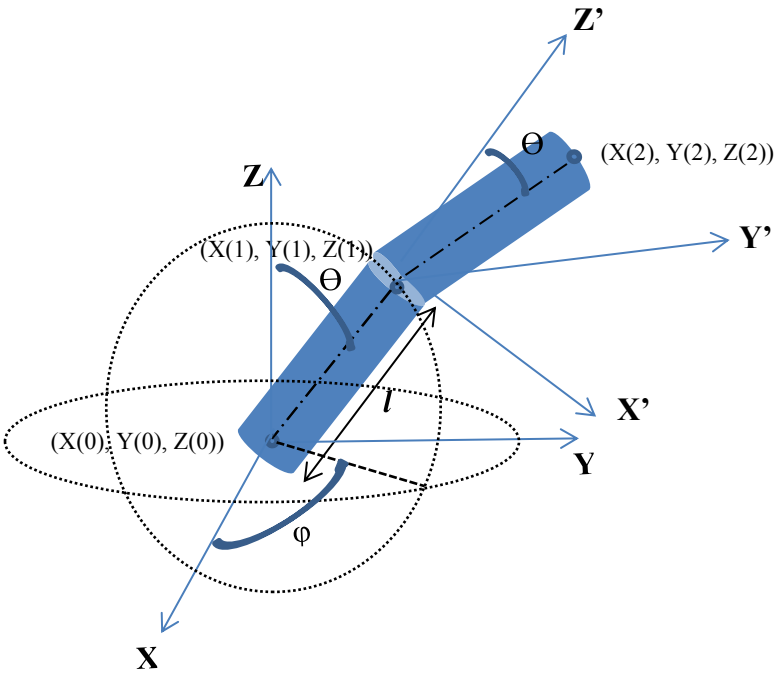

Figure 5-1. A description of tube generation.

The total number of MWCNTs used in the simulation was determined by the weight of MWCNTs used, the density of the MWCNTs (2.1 g/cm^3 which is provided by Cheap Tubes, Inc.), and the dimensional information of the tube. Since the tube length used in the simulation was considered to be fixed, the total number of tubes used in the simulation can be calculated using Eqn. (5-5),

$$\text{Total number of tubes (n)} = \frac{\text{n}l\ (\text{cm})}{l\ (\text{cm})} \qquad (5\text{-}5)$$

where l is the length of a tube, and nl is the summation of all the tubes in the system. The total length of tubes (nl) in the system can be calculated using Eqn. (5-6),

$$\text{n}l\ (\text{cm}) = \frac{\text{w (g)}}{\text{A (cm}^2\text{)}\times\text{d (g/cm}^3\text{)}} \qquad (5\text{-}6)$$

where w is the total weight of tubes used in the system, A is the cross sectional area, and d is the density of the tubes.

Geometric models for possible cases (Case 1 and Case 2) were generated with randomly distributed MWCNTs, as shown in Figure 5-2. In Case 1, the tubes were distributed randomly regardless of the foam morphology after foaming due to the small enough pore size compared to the nanofiller size. In this case, the only event happened after foaming was volume expansion, such that only the distance between the tubes increased accordingly. To model Case 1, the same number of tubes was randomly distributed in an expanded RVE according to the corresponding porosity. In Case 2, nanofillers are not in the spherical pore, and are densely packed in the solid regions.

During the foaming process with the Case 2 mechanism, nanofillers were pushed to the interstitial volumes by bubble growth. To model Case 2, a sphere was generated inside the RVE as a pore, and the tubes were not allowed inside the pore.

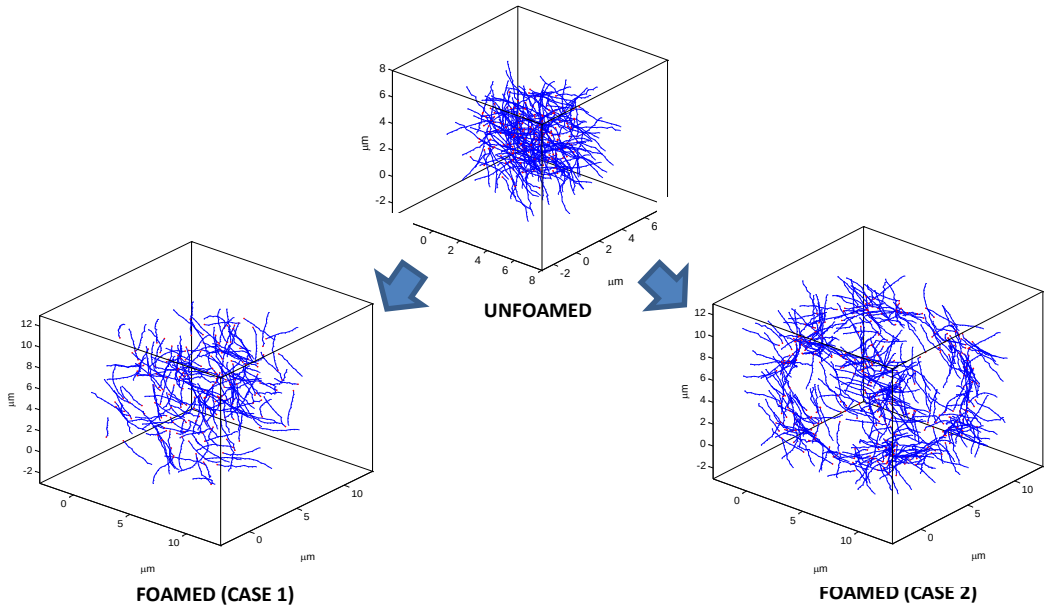

Figure 5-2. RVE cubes with CNTs for unfoamed, Case 1 foamed, and Case 2 foamed nanocomposites.

5.2.2 Equivalent network formation

To determine the connectivity the dispersed tubes, distance measurements were performed between each line segment of tubes as shown in Figure 5-3 [94]. And two line segments from tubes P and Q are described as shown in Eqns. (5-7) and (5-8),

$$P(s) = P_0 + s(P_1 - P_0) = P_0 + s\boldsymbol{p} \qquad (5\text{-}7)$$

$$Q(t) = Q_0 + t(Q_1 - Q_0) = Q_0 + t\boldsymbol{q} \qquad (5\text{-}8)$$

where 0 <= (s , t) <= 1, Using these two line vector equations, a new vector

$$\bar{U} = Q_0 - P_0 + t\boldsymbol{q} - s\boldsymbol{p}$$

is generated starting from a segment of P to a segment of Q. The minimum distance between the two segments was evaluated using $\bar{\mathbf{U}}$ by calculating its magnitude. In the case where 0 <= (s , t) <= 1 is not satisfied, use a dot product property of the vector which shown in Eqn. (5-9).

$$|\bar{U}|^2 = \bar{U} \bullet \bar{U} = (Q_0 - P_0 + t\boldsymbol{q} - s\boldsymbol{p}) \bullet (Q_0 - P_0 + t\boldsymbol{q} - s\boldsymbol{p}) \qquad (5\text{-}9)$$

which is a quadratic function of s and t to evaluate the minimum distance. By taking a derivative of the obtained quadratic function, the minimum distance can be evaluated when the derivative is set to 0 [94]. This distance evaluation process was the most time consuming part in the simulation. Each tube had 6 segments, such that to evaluate the distance between two tubes, Eqn. (5-9) has to be evaluated 6^2 times. For distance evaluation among N tubes, the equation has to be evaluated 6^N times.

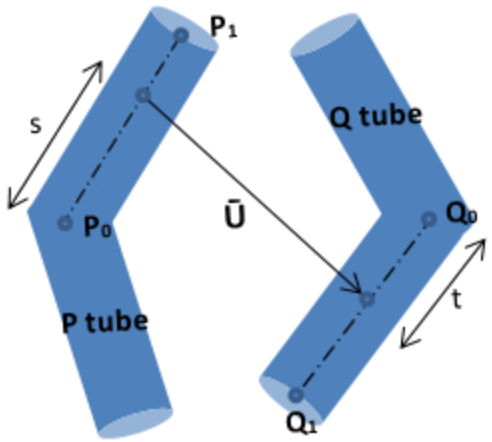

Figure 5-3. The distance between two tubes.

If the distance is less than the diameter of the MWCNT, the tubes are considered in contact. Electron hopping is considered if the gap between the two tubes is up to 2 nm which is considered as the maximum separation for electron tunneling in the polymer carbon nanotube composite system [46]. Since the diameter of the tubes is 20 nm, the total separation of two fibers needs to be less than 22 nm to be considered conducting and contributing to forming a resistor network.

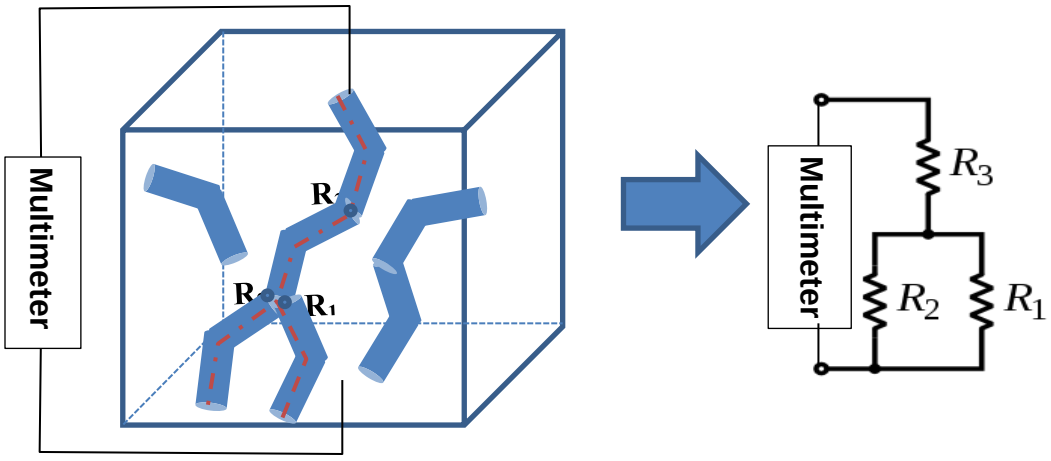

Figure 5-4. Equivalent resistor network.

The distance evaluation among tubes allows to determine which tubes are connected. After determining which tubes constructed a cluster, it was evaluated whether the cluster spans from one side of the RVE to the opposite side. If so, an equivalent resistor network was generated using the information from the connected cluster as shown in Figure 5-4. A circuit file was generated with the information obtained from the network, and was utilized in a circuit analysis software to calculate the net resistance.

To evaluate the net resistance of the system, three types of resistance need to be considered in the network system as following.

1) Tube resistance (10 kΩ, for a tube having a length of 6 μm and a diameter of 20 nm [93])
2) Direct contact resistance (100 kΩ – 3.4 MΩ [95])
3) Tunneling resistance (10^{11} - 10^{13}Ω [87, 96])

The tube resistance can be ignored since it has a negligible value compared to the direct contact and tunneling resistance. The direct contact resistance of the tubes and the tunneling resistance between tubes form the total contact resistance. However, for polymer nanocomposite systems, it is well known that CNTs cannot directly contact each other and there should be a gap of around 1 nm because the tubes are often wrapped with polymer chains [92]. Therefore, the tunneling resistance plays a dominant role in the net resistance of the system [96].

In this study, the minimum distance between the tubes due to the wetting of CNTs by polymer chains was taken as 1.3 nm. The diameter of a typical polymer chain is a few tenths of nanometers [97]. For example, the diameter of polyethylene oligomer is 0.4 nm [98]. Yu et al. estimated the diameter of epoxy oligomer to be 0.5 nm, since the epoxy resins are polymerized from chains with epoxied end groups which are more complex

[93,99]. PEI has a more complex molecular structure than epoxy, such that the gap between the CNTs for PEI composites is assigned with 1.3 nm.

Simmon [100] developed a tunneling resistance model as a function of the separation distance that was used in this study to determine tunneling resistance.

$$\mathrm{R}_{tunnel} = \frac{\rho_{tunnel}}{A_c}$$

where

R_{tunnel} = tunneling resistance

$A_c(\text{area of the contact}) = d^2$

$\rho_{tunnel}(\text{tunneling resistivity } (\Omega \cdot cm^2)) = \frac{U}{J}$

where

d is the diameter of the carbon nanotube (20 nm in this study)

$$U = \frac{e}{C} = \frac{et}{A_c K \varepsilon_0}$$

$$J = 6.2 \times 10^{10} \times \Delta t - 2[w \times \exp\left(-1.025 \times \Delta t \times w^{\frac{1}{2}}\right) - (w + \mathrm{U}) \times \exp\left(-1.025 \times \Delta t \times (\mathrm{w} + \mathrm{U})^{\frac{1}{2}}\right)]$$

$$\mathrm{w} = w_0 - \left(\frac{U}{2t}\right) \times (t_1 + t_2) - \frac{5.75}{K \times \Delta t} \times \ln \frac{t_2(\mathrm{t} - t_1)}{t_1(\mathrm{t} - t_2)}$$

$$t_1 = \frac{6}{K w_0}$$

$$t_2 = t\left[1 - \frac{46}{(3w_0Kt + 20 - 2UKt)}\right] + \frac{6}{Kw_0}$$

where

e is the unit electric charge

C is capacitance

ε_0 is the electrical permittivity of vacuum (8.85×10^{-14} F/cm)

K is the dielectric constant of the polymer matrix

t is the thickness of the insulation layer

$\Delta t = t_2 - t_1$ is the difference of the limits of barrier at Fermi level

w_0 is the work function of CNTs which is around 5eV

According to the equation, a tunneling resistance plot is generated for epoxy and PEI based material systems as shown in Figure 5-5. It was shown that the effect of filler diameter is significant to determine tunneling resistance of polymer nanocomposites than the types of the matrix materials. For PEI/MWCNTs nanocomposite and foam simulations, since the diameter of MWCNTs used was 20 nm, relevant curves from Figure 5-5 was used to determine the tunneling resistance. It was assigned that the minimum distance between the tubes by wetting of PEI polymer chains was 1.3 nm. According to the minimum distance, a corresponding resistance of 1.45×10^{11} Ω was

determined from the tunneling resistance plot. Even though the two tubes overwrapped when the distance between the tubes was less than the diameter of the tubes (20 nm), those two tubes should be considered to be separated with the distance of 1.3 nm. Therefore, if the distance between the tubes is 0 nm to 21.3 nm (summation of the tube diameter and the minimum separation due to the polymer wetting), the resistance of 1.45 X 10^{11} Ω was assigned for the total contact resistance. If the distance between the tubes is 21.3 nm to 22 nm, distance-dependent tunneling resistance needs to be assigned. However, for the net resistance evaluation in this study, this resistance was ignored, since majority of the contacts (21.3 nm/22 nm) have the minimum tunneling resistance of 1.45 X 10^{11} Ω, which will have the dominant effect on the contact resistance. Foygel et al. [87] estimated the contact resistance for polyimide CP2/SWCNTs system to be 10^{13} Ω. In this study, a lower resistance value resulted from the larger diameter of MWCNTs according to Figure 5-5. The total resistance of the system was evaluated with the information of the network cluster based on the distances determined. The circuit analysis software Multisim 12 from National Instrument was used to calculate the net resistance. Detailed procedure of using Multisim 12 is described in Appendix A.1.

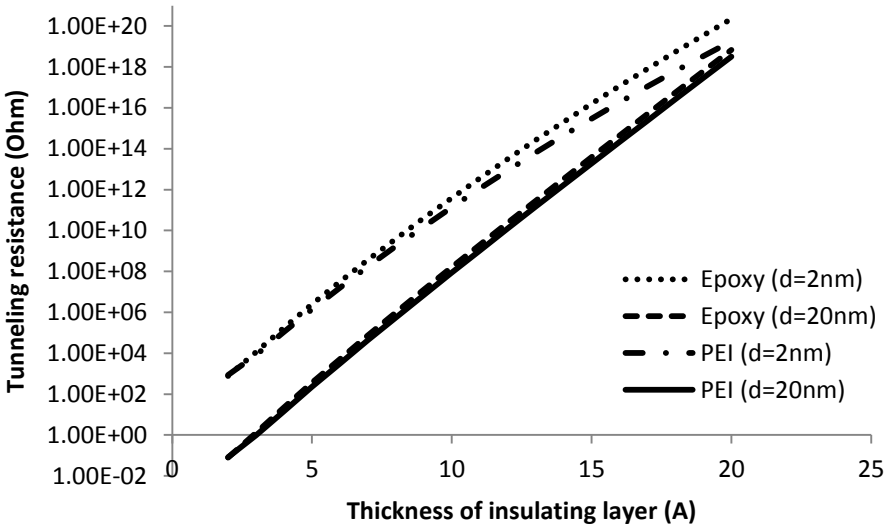

Figure 5-5. Tunneling resistance depending on the thickness of insulation layer for nanocomposites having different filler diameter. (K for epoxy and PEI was 3.98 and 3.15 respectively)

With this modeling method, electrical percolation and conductivity simulations for both foaming mechanisms were conducted. The effects of foam density and pore size (if applicable) on electrical performances were investigated.

5.3 RESULTS AND DISCUSSION

5.3.1 RVE size effect

The RVE size effect on the electrical conductivity was investigated to check whether the RVE size affect to the simulation results. In the simulation, RVE sizes of 4, 5, 7, and 10 μm were used in a polymer nanocomposite system with the carbon nanotube length of 3 μm. The ratio of the RVE size to the CNT length used in this study was 1.3, 1.7, 2.3, and 3.3. Physically, in the first two cases, at least two tubes are needed for making a conduction path. Three and four tubes are needed to make conduction path for the third and the fourth case, respectively. The RVE size range used in this study allowed the consideration of many different conduction path formation situations. The simulation result is shown in Figure 5-6. There was no significant effect of RVE size on electrical conductivity behavior of polymer nanocomposites from 4 μm to 10 μm RVE size. Therefore, the simulation result suggested that in general, there was no significant RVE size effect on the electrical conductivity of polymer nanocomposites with the ratio of CNT to RVE edge length of 1.3 to 3.3. In the following analysis, RVE sizes within the range discussed in this section are used for the simulations.

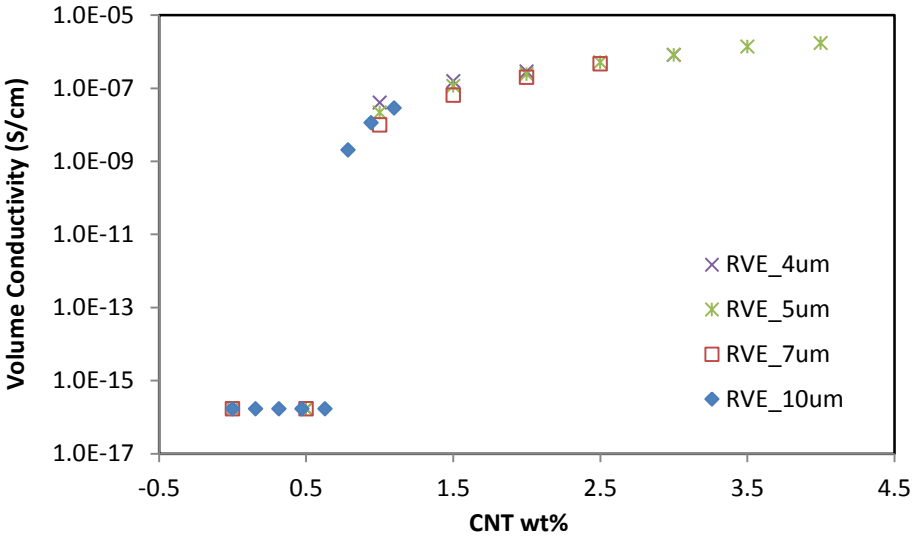

Figure 5-6. Representative Volume Element (RVE) size effect on the volume conductivity of unfoamed PEI/MWCNTs nanocomposites having a filler length of 3 μm and the diameter of 20 nm.

5.3.2. Validation of the models

Electrical conductivity of unfoamed and foamed samples from experiments and those from the simulation were compared. For the unfoamed case, the carbon nanotube length L of 3, 4.5, and 6 um were used and the simulation results are shown in Figure 5-7. The simulation results and experimental results were in good agreement when L was 6 µm. With low filler lengths, electrical conductivity decreases, and percolation threshold increases especially when the filler length is 0.5L. It has been discussed that lower aspect ratio of nanofillers would decrease electrical property [93].

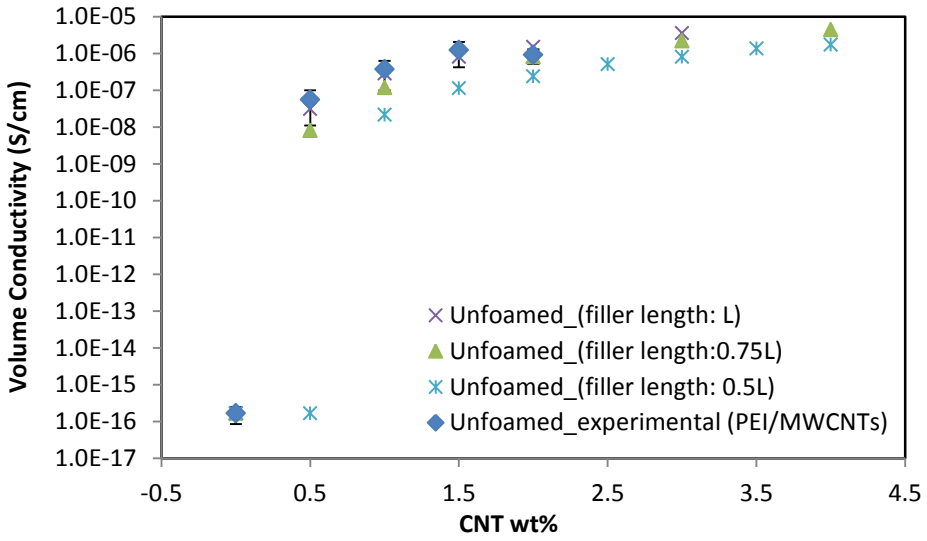

Figure 5-7. Electrical conductivity from experimental and modeling results for unfoamed cases, L=6 µm.

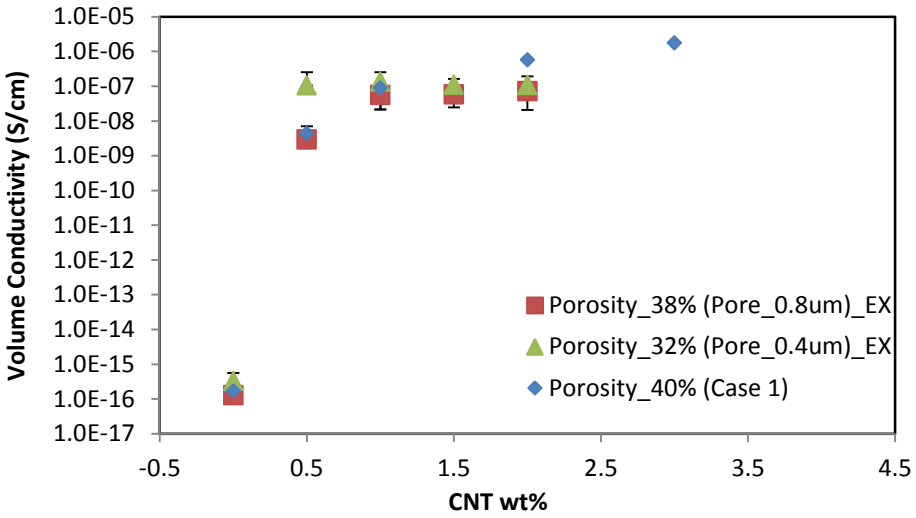

Figure 5-8. Electrical conductivity from experimental and modeling results for foamed cases, L=6 μm.

With selected L=6 μm, simulation for foam Case 1 was performed and compared with the experimental data from PEI/MWCNTs nanocomposite foams discussed in Chapter 3. Simulation results for Case 1 and experimental data with the porosity of around 40% are shown in Figure 5-8. It is reasonable to use foaming mechanism Case 1 to represent the PEI/MWCNTs nanocomposite foams based on the SEM observation of the fabricated PEI/MWCNTs nanocomposite foams, as shown in Figure 5-9. The pore size was small enough compared to the MWCNTs size, and the nanofillers were randomly distributes. This configuration is consistent to the assumption of the foaming mechanism Case 1.

The simulation results were in good agreement with the experimental results, as shown in Figure 5-8. Percolation thresholds from both experimental and modeling were found between MWCNTs loading of 0 wt% to 0.5 wt%, and the electrical conductivity was also similar to each other. Therefore, the models for unfoamed and Case 1 foamed samples were validated. Based on the validated modeling procedures, prediction of electrical percolation and conductivity will be performed for foams foamed by both Case 1 and Case 2, varying foam porosity and pore size.

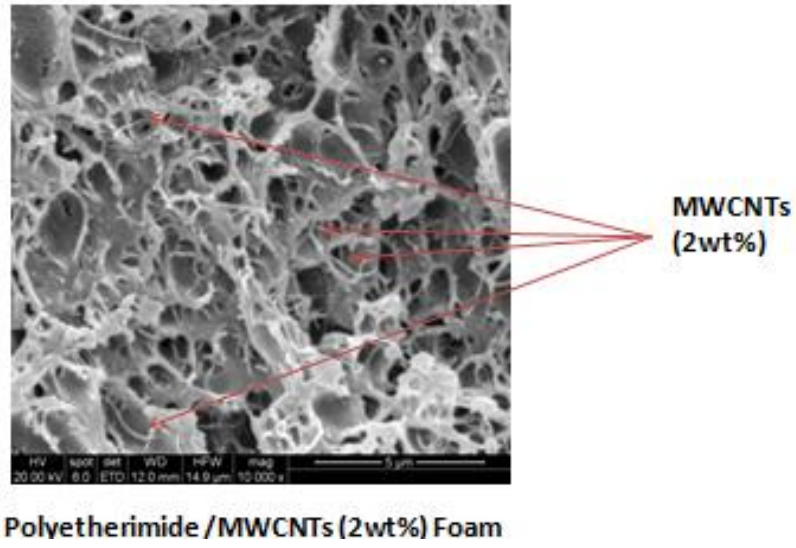

Figure 5-9. A SEM of PEI/MWCNTs (2 wt%) foam.

5.3.3. Porosity effect on electrical conductivity of foams

5.3.3.1 Case 1

Electrical conductivity plots of foams for Case 1 model with porosity of 40% and 80% were obtained from simulations as shown in Figure 5-10 in wt% and Figure 5-11 in volume%. As porosity increased, the electrical conductivity decreased at given wt% as expected, and the percolation threshold increased as shown in Figure 5-10. This is because by foaming with Case 1 model, the same amount of MWCNTs from unfoamed model is distributed in an expanded volume, resulting in increased distance between tubes, therefore, causing decreased electrical conductivity. In terms of percolation threshold, the probability for MWCNTs to form a network decreased due to the less dense population of MWCNTs. More fillers are needed to reach a percolation point.

At a given volume%, porosity did not affect to the electrical conductivity as shown in Figure 5-11. Regardless the porosity of foams, electrical conductivity values followed a trend line. This is because the fillers are randomly distributed and a decrease in tube density (# of tubes in a unit volume) by foaming is exactly proportional to the decrease in electrical conductivity. In this model, provided there is an electrical conductivity plot for unfoamed case at different volume percent, it is possible to predict the electrical conductivity of foamed samples after foaming process if the porosity information is provided.

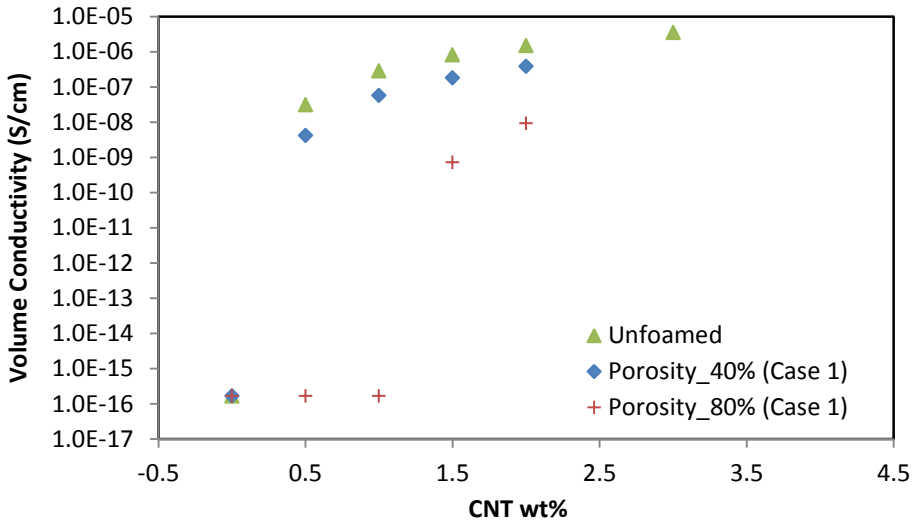

Figure 5-10. Electrical conductivity of foams for Case 1 model plotted against wt%.

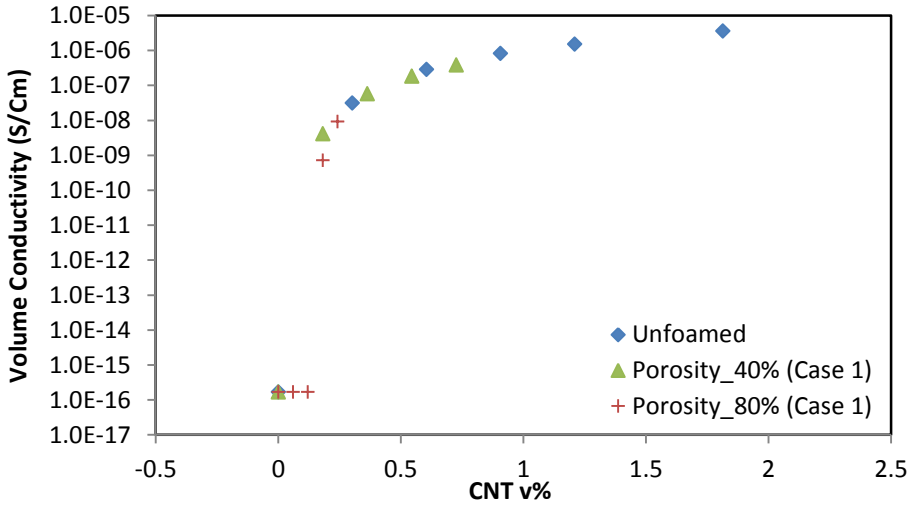

Figure 5-11. Electrical conductivity of foams Case 1 model plotted against volume%.

5.3.3.2 Case 2

Electrical conductivity simulation results of nanocomposite foams for Case 2 with different porosity (40, 80, and 90%) with the pore size of 8 μm is shown in Figure 5-12, and with the pore size of 16 μm is shown in Figure 5-13 in wt%. It was shown from both plots that no significant electrical conductivity change was found as porosity increased to 40%. Further increase in porosity decreased the electrical conductivity of nanocomposite foams. Electrical conductivity comparison for foams having the same porosity of 40 % which were foamed with Case 1 and Case 2 was shown in Figure 5-14, and that for foams with the porosity of 80% were shown in Figure 5-15. It was found that electrical conductivity drop by foaming mechanism Case 2 was less significant than that by foaming mechanism Case 1 under the same porosity as shown in Figures 5-14 and 5-15. This is because, by foaming Case 2, carbon nanotubes were pushed out by bubble generation resulting in filler aggregation in the cell wall region, while nanofillers in foam Case 1 are distributed everywhere randomly. In foam Case 2, nanofillers are only distributed in the solid part having higher filler density to form network easily.

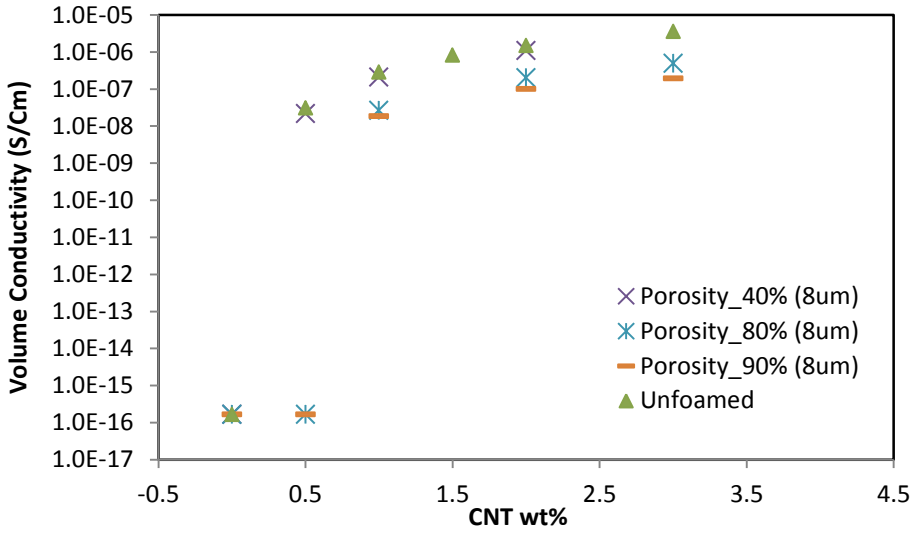

Figure 5-12. Electrical conductivity of foams for Case 2 model at given wt%.

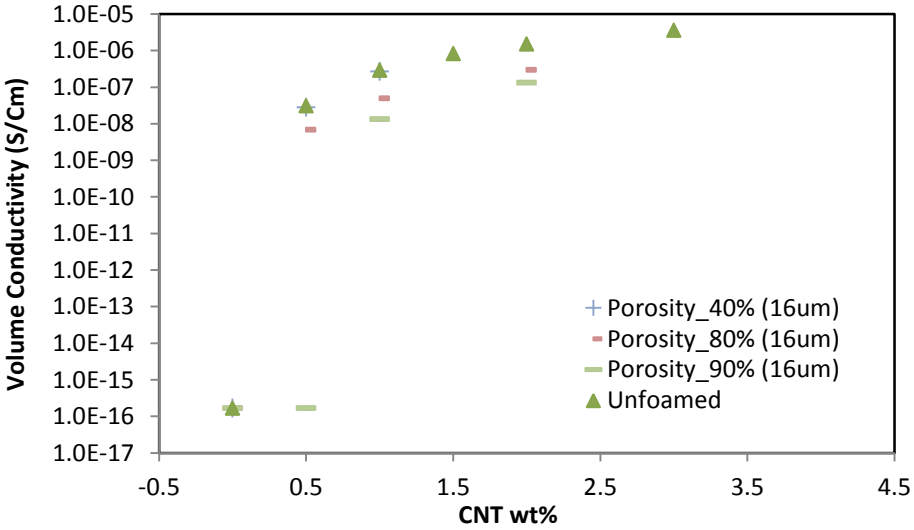

Figure 5-13. Electrical conductivity of foams for Case 2 model at given wt%.

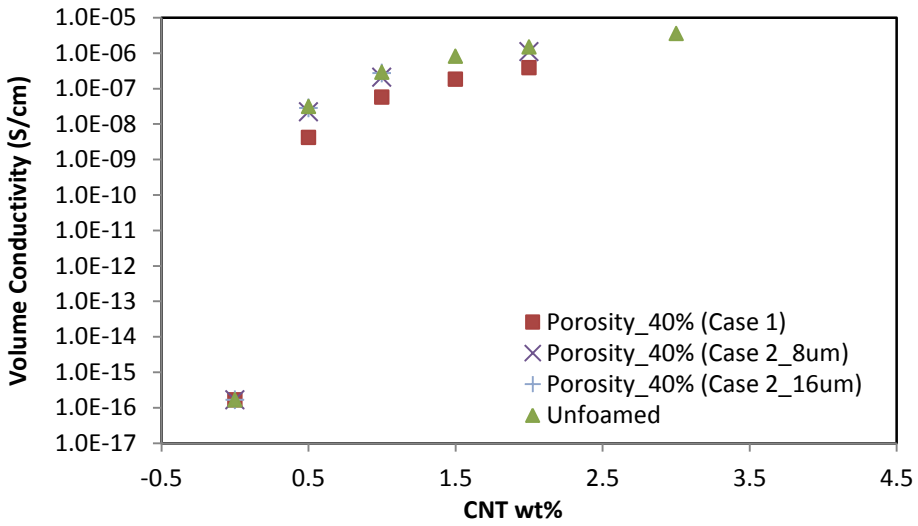

Figure 5-14. Electrical conductivity of foam Case 1 and Case 2 models under the same porosity of 40%.

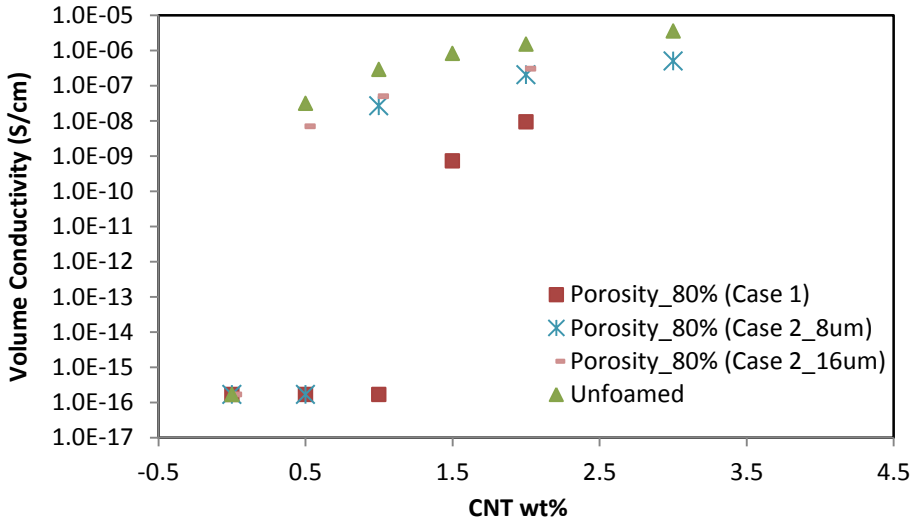

Figure 5-15. Electrical conductivity of foam Case 1 and Case 2 models under the same porosity of 80%.

However, at a given volume%, as porosity increases, electrical conductivity increases as well, as shown in Figure 5-16, while there was no porosity effect on electrical conductivity of Case 1 foams as shown in Figure 5-11. This is because, volume expansion rate and decrease in probability for tubes to form network by expansion are not proportional anymore for Case 2 foams, but the latter term is less compared to the former term causing increase in conductivity at a given volume%. This phenomenon is promising in such applications as light-weight ESD and EMI shielding, because as the product becomes lighter, electrical performance gets better at a given product volume with the same amount of MWCNTs consumption.

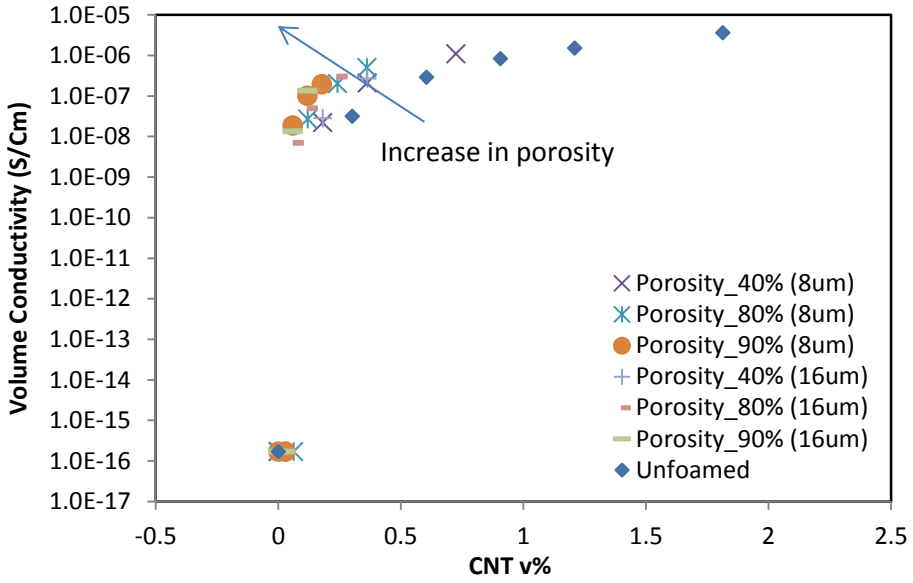

Figure 5-16. Electrical conductivity of foams Case 2 model at given volume%.

Figure 5-17 shows volume electrical conductivity of PLA/MWCNTs nanocomposites foams plotted against volume%. It was shown that as porosity increased, electrical conductivity increased as well. Figure 5-18 shows the SEMs of PLA/MWCNTs (6 wt%) foams. It was shown that MWCNTs were aggregated in the cell wall region which follows foam Case 2 model, causing electrical conductivity increase as porosity increase at a given volume%.

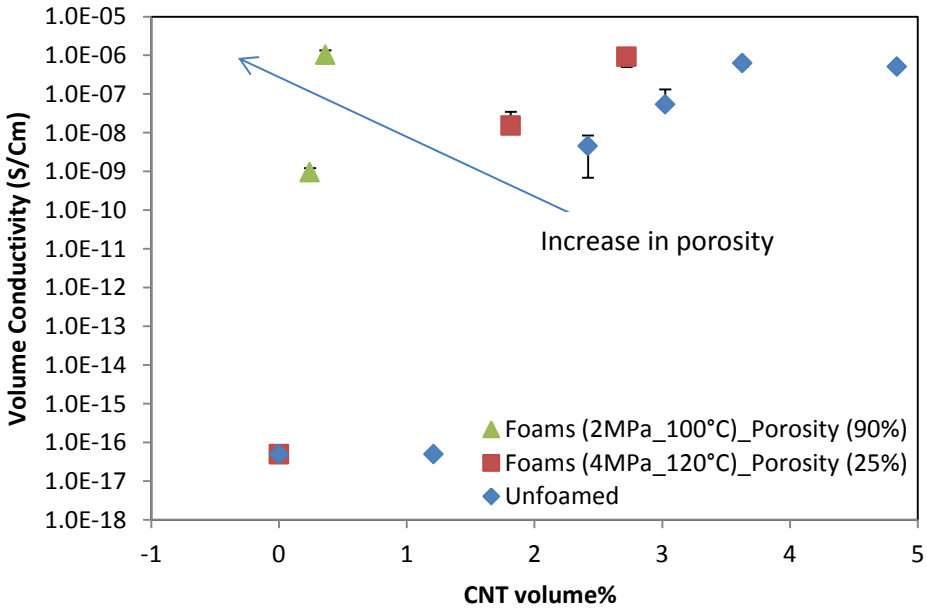

Figure 5-17. Volume DC electrical conductivity of PLA/MWCNTs foams with various MWCNT loadings plotted against CNT volume%.

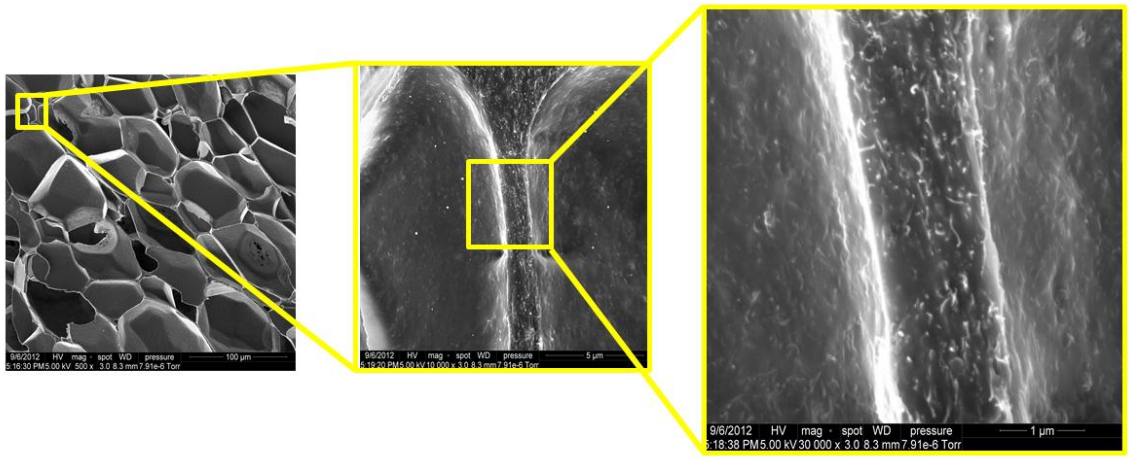

Figure 5-18. SEMs of PLA/MWCNTs (6 wt%) foams. (Also shown as Figure xxx. Figure reproduced here for convenient illustration)

5.3.4. Pore size effect on electrical conductivity of foams

5.3.4.1. Case 1

Pore size effect on electrical conductivity for Case 1 was not evaluated since the assumption for the Case 1 model did not include pore structure in the foam.

5.3.4.1. Case 2

Pore size effect on electrical conductivity for Case 2 foam was evaluated at a fixed porosity under two different filler length conditions as shown in Figures 5-19 and 5-20. A trend was found that as porosity increased the electrical conductivity increased and

percolation threshold decreased, showing improved electrical property. However, beyond the percolation threshold, the effect of pore size on the electrical conductivity seemed not significant, at least for the 6 μm tube length case. For a short tube length L=3 μm, there was conductivity difference observed both at and beyond the percolation threshold, as shown in Figure 5-20. In this case, however, the pore size changed from 4 μm to 24 μm, instead of an 8 to 24 μm change for the 6 μm tube length case. Three and six times pore size difference resulted in very little change in electrical conductivity as shown in Figures 5-19 and 5-20. However, there was a trend in increase of electrical conductivity and decrease in percolation threshold as pore size increases such that foams with the pore size of a few hundred of microns could show significant effect. The simulation was limited due to the extremely long computational time.

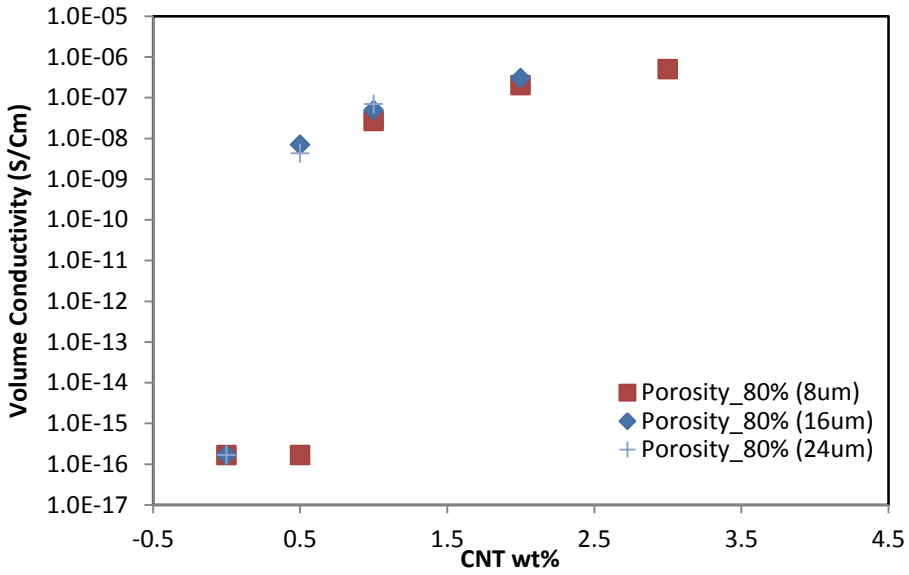

Figure 5-19. Electrical conductivity of foams for Case 2 model at given wt%. Tube length: 6 µm.

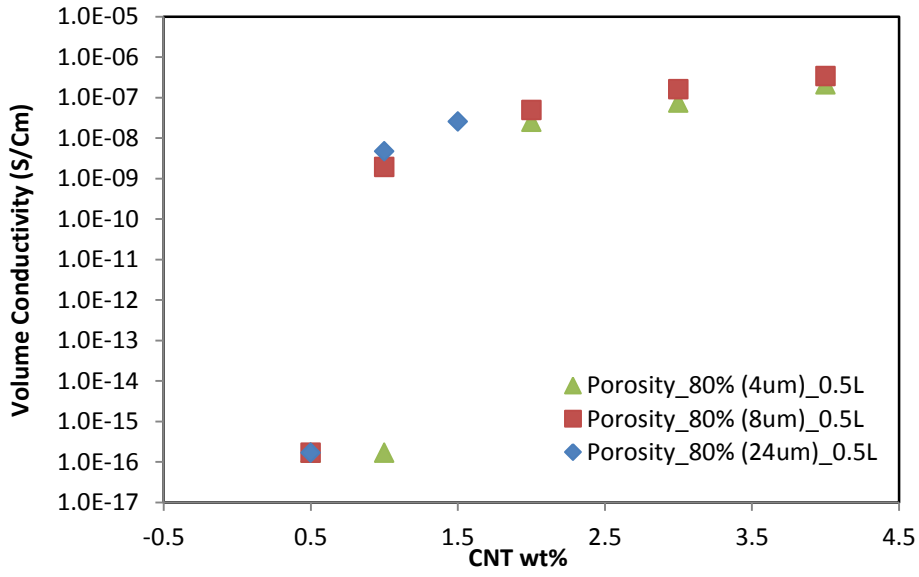

Figure 5-20. Electrical conductivity of foams for Case 2 model at given wt%. Tube length: 0.5L=3 µm.

5.4 SUMMARY AND CONCLUSIONS

A Monte Carlo simulation model was developed to understand and predict the electrical conductivity of polymer/MWCNTs nanocomposite foams. Two different foam morphologies were considered, designated as Case 1: volume expansion without nanotubes rearrangement and Case 2: nanotube aggregated in cell walls. Simulation results from unfoamed nanocomposites and Case 1 model were validated with the experimental data. The results were in good agreement with those from PEI/MWCNTs nanocomposites. Porosity effects on electrical conductivity were investigated for both Case 1 and Case 2 models. For the Case 1 model, the electrical conductivity decreased as the porosity increased at a given wt%. However, there was no porosity effect on electrical conductivity at a given volume%. At a given volume%, the electrical conductivity was identical regardless of the porosity. This result allows predicting electrical conductivity of foams by density only, if the unfoamed conductivity is known. For the Case 2 model, the electrical conductivity did not decrease as the porosity increased. On the other hand, the electrical conductivity actually decreased for foams with certain high porosities. This result is interesting, since it suggests that it is achievable to reduce the density without sacrificing the electrical conductivity by foaming with the Case 2 foaming mechanism. At a given volume%, as porosity increased, the electrical conductivity could also increase.

Chapter 6. Electrical Conductivity Prediction for Foamed Polymer Nanocomposites Using Finite Element Modeling

6.1 INTRODUCTION

In Chapter 5, the electrical conductivity modeling and simulation for polymer nanocomposite foams were developed using Monte-Carlo simulation. The simulation method were validated and used to predict the electrical property of polymer nanocomposite foams with different foaming mechanisms, which are Case 1 (volume expansion without nanotubes rearrangement) and Case 2 (nanotubes are aggregated in the cell wall). However, for the Case 2 model with a large pore size, a large size of representative volume element (RVE) and thus a large number of nanofillers are also needed. Therefore, there is a limitation on computational efficiency with a large RVE. For example, if the size of RVE is small enough so that the number of required nanofillers is less than 1000, the computation takes only a few hours to complete on a high performance computing system of Mechanical Engineering department in the University of Texas at Austin (Two dualcore 3.73 Xeon processors and 24 GB of shared memory). However, as the number of fillers increased to 10000, the computational time increases to a week.

In this chapter, electrical conductivity prediction of foamed polymer nanocomposites with finite element modeling (FEM) is proposed. The results obtained

from FEM are compared to those from the Monte-Carlo simulation method. The feasibility of using FEM to predict electrical conductivity of foamed polymer nanocomposites is discussed.

6.2 METHOD

Commercially available finite element analysis package, COMSOL 4.2, was used for electrical conductivity analysis. Foam geometric models were generated according to the pore size and porosity of the foams and meshed with triangular elements as shown in Figure 6-1. Unfoamed electrical conductivity data which is obtained from the previously Monte-Carlo simulation method were used to assign the material property of the solid portion of the foam.

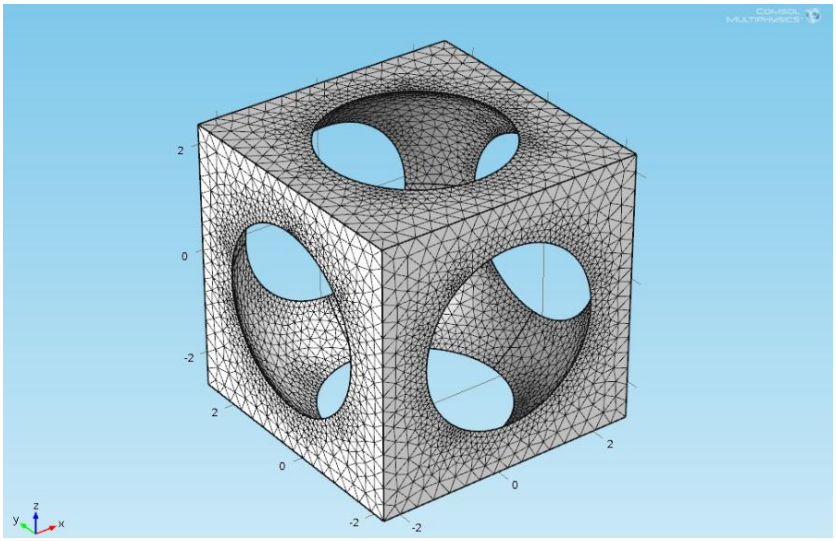

Figure 6-1. Triangular elements used in the meshed model in COMSOL.

Electric potential of 1 MV was applied to one side of the foam structure, and the opposite side was grounded. The result of the electric potential in the structure is shown in Figure 6-2. Electrical current density was obtained from the ground side, and was surface-integrated to get the current. With the obtained current data, a resistance of the structure was calculated using Ohm's law (V=I·R). The calculated resistance was converted to conductivity according to the sample dimension using Equation (6-1) below

$$\sigma = \frac{1}{\rho} = \frac{1}{R \times L} \qquad (6\text{-}1)$$

where σ is the electrical conductivity, ρ is the electrical resistivity, R is the electrical resistance, and L is the RVE cube edge length.

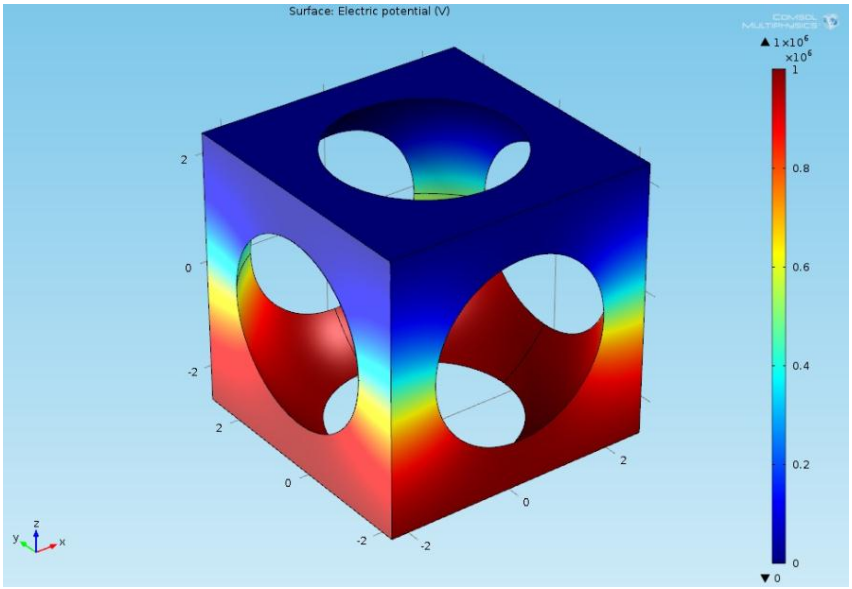

Figure 6-2. A simulation result of electric potential in the foam structure from COMSOL.

6.3 Results and Discussion

The electrical conductivity results obtained from FEM were compared with those from Monte-Carlo simulation performed using MATLAB. Electrical conductivity values for unfoamed polymer nanocomposites to be used as material constants are shown in Figure 6-3, which were obtained from the Monte-Carlo simulation method described in Chapter 5 with the filler length of 3 μm in a polyetherimide matrix.

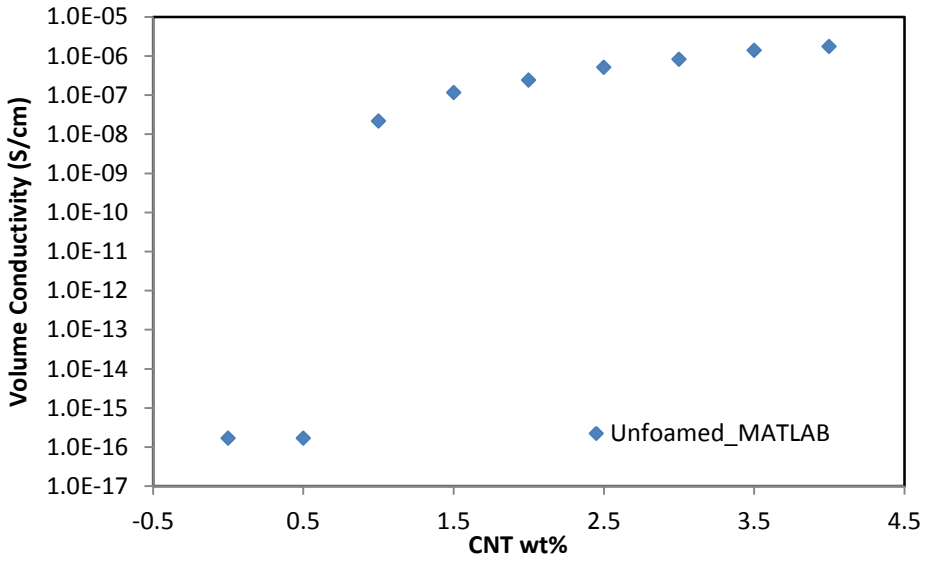

Figure 6-3. Electrical conductivity of unfoamed polymer nanocomposites from the Monte-Carlo simulation.

Figure 6-4 shows the electrical conductivity comparison using the two different simulation methods for Case 2 foams having a filler loading of 2 wt% and different pore sizes and porosities. Figure 6-5 is for Case 2 foams having a filler loading of 4 wt%. It was shown in both figures that the FEM method was able to predict the electrical conductivity of foams well with provided electrical conductivity of the corresponding unfoamed sample. The predicted electrical conductivity by FEM was slightly lower than that by Monte-Carlo simulation. However, this shows the feasibility to predict electrical conductivity of foamed polymer nanocomposites with minimal computational efforts.

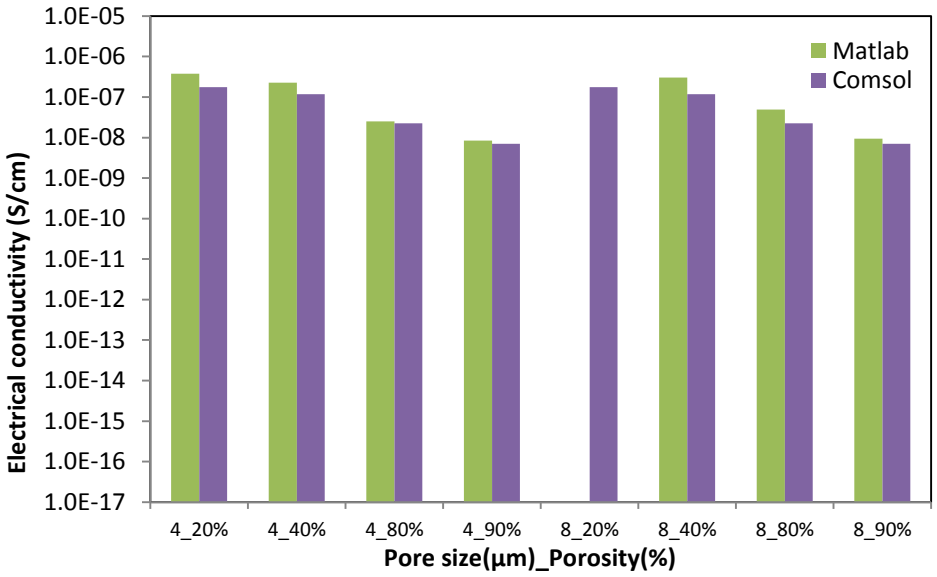

Figure 6-4. Electrical conductivity comparison under two simulation methods for Case 2 foams having filler loading of 2 wt%.

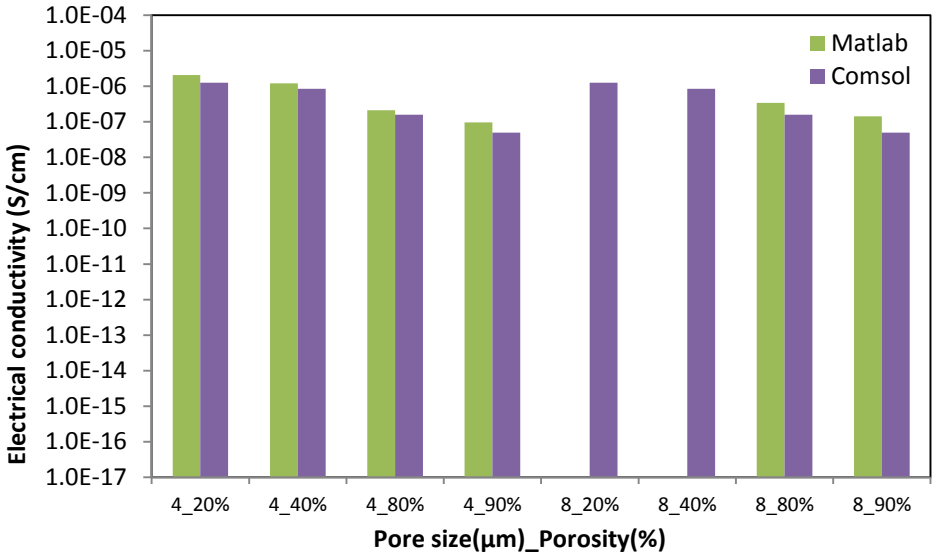

Figure 6-5. Electrical conductivity comparison under two simulation methods for Case 2 foams having filler loading of 4 wt%.

Figure 6-6 shows the electrical conductivity of Case 2 foams having filler loading of 2 wt% at given porosity with different pore sizes (4, 8, and 100 μm) using COMSOL, and Figure 6-7 is for electrical conductivity of Case 2 foams having filler loading of 4 wt% at given porosity with different pore sizes. It is seen from both figures that there was no pore size effect found from FEM simluation. However, it was found from the Monte-Carlo simulation in Chpater 5 that there was a pore size effect on the electrical conductivity. As the pore size increased, the percolation threshold decreased and the electrical conductivity increased slightly. However, this trend was not able to be found from the COMSOL simulation. It is obvious that this method could not detect the pore size effect on electrical conductivity, because it considered the solid portion of the foam as one homogenous conductive material, such that at a given porosity, proportional change in dimensions could not result in change in electrical conductivity. In the Monte-Carlo simulation, the nanocomposites and foams were considered as heterogeous material systems having multiple phases includng the matrix and fillers. Therefore, more detailed analysis regarding morphological effects were able to be analiyzed, showing a change in electrical conductivity after the percolation threshold for different pore size foams.

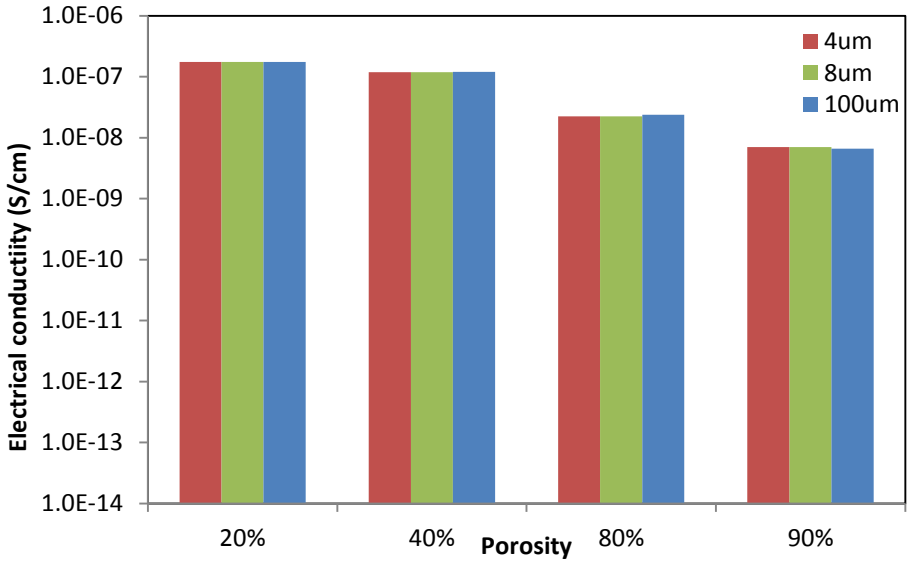

Figure 6-6. Electrical conductivity comparison of Case 2 foams having a filler loading of 2 wt% under different pore sizes at given porosity using COMSOL.

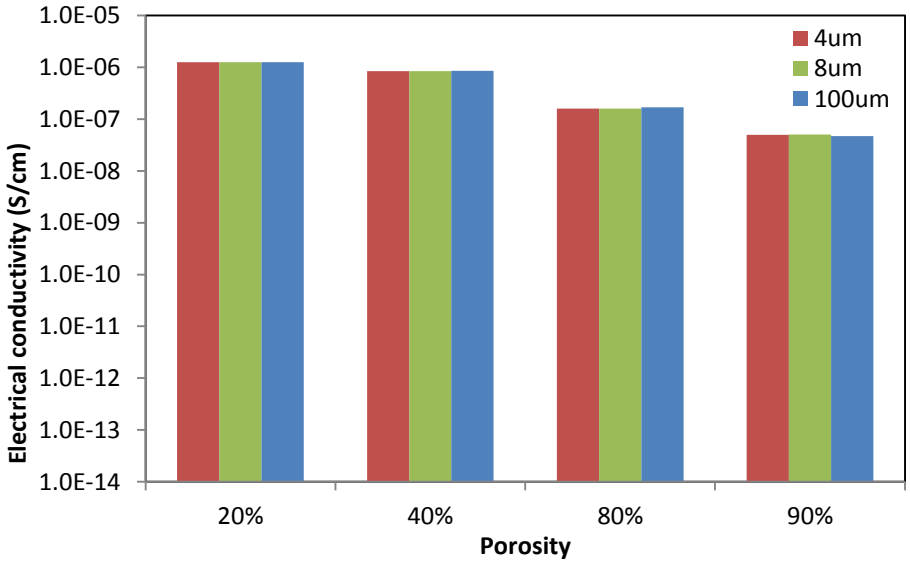

Figure 6-7. Electrical conductivity comparison of Case 2 foams having a filler loading of 4 wt% under different pore size at given porosity using COMSOL.

Figures 6-8 and 6-9 show the electrical conductivity of Case 2 foams having different pore sizes as predicted using FEM and Monte-Carlo (MC) simulation at given porosity values of 40% and 80%, respectively. Filler loadings of 1 to 4 wt% were used for FEM simulations for both figures. Since the FEM simulation could not identify the pore size effect on the electrical conductivity, the electrical conductivity of foams having the pore size of 4 μm was plotted on both figures to represent the electrical conductivity from COMSOL simulations. It was found from both figures that after the percolation threshold, electrical conductivity obtained from COMSOL was very close to the one from MATLAB simulation. However, this is only true when the pore size is small. The electrical conductivity of Case 2 foams having smaller pore size (close to filler length) from the MC simulation was more consistent with the conductivity from the FEM simulation. MC simulation has shown that there is a pore size effect in the electrical conductivity of nanocomposite foams. FEM based simulation is not able to show the difference. In addition, the limitation of the FEM simulation also include that it is not possible to determine the electrical percolation threshold. The FEM simulation can be utilized only when the percolation threshold of Case 2 foams were determined by the MC simulation.

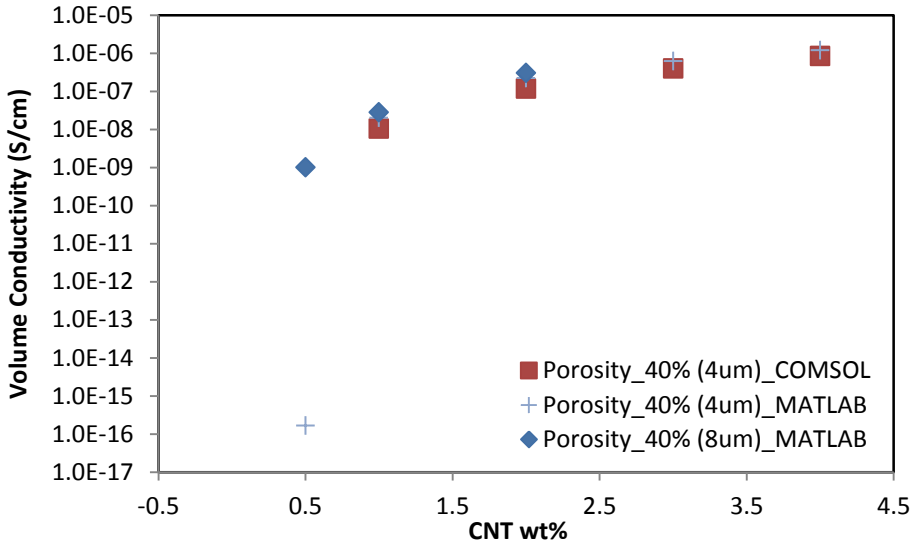

Figure 6-8. Electrical conductivity of Case 2 foams at a porosity of 40% using COMSOL and MATLAB.

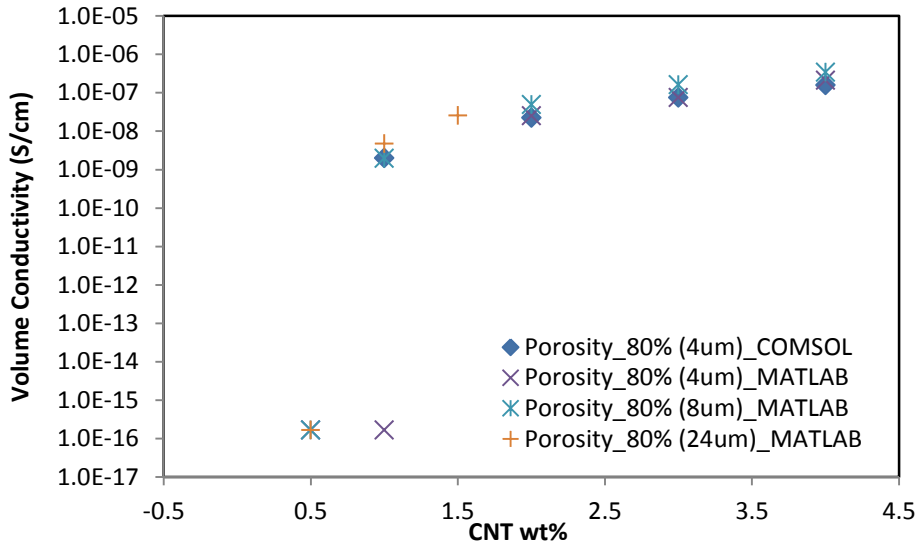

Figure 6-9. Electrical conductivity of Case 2 foams at a porosity of 80% using COMSOL and MATLAB.

6.4 SUMMARY AND CONCLUSIONS

Electrical conductivity prediction of foamed polymer nanocomposites using FEM was performed. The results obtained from FEM were compared with those from the Monte-Carlo simulation method. Feasibility of using FEM to predict the electrical conductivity of foamed polymer nanocomposites was discussed. FEM was able to predict the electrical conductivity of polymer nanocomposite foams represented by the Case 2 model with various porosities. However, it could not capture the pore size effect in the electrical conductivity prediction. The FEM simulation can be utilized to predict the electrical conductivity of Case 2 foams when the percolation threshold is determined by Monte-Carlo simulation to save the computational time. This has only been verified when the pore size is small in the range of a few micrometers.

Chapter 7. Summary and Future Work

7.1 SUMMARY

Polymer nanocomposite foams using high performance polymer and bio-degradable polymer with carbon nanotubes were fabricated, and the effects of foam density and pore size on physical properties were investigated. Especially, the effects of density and pore size on electrical conductivity of polymer nanocomposite foams were investigated both experimentally and theoretically. The accomplishments of the research are summarized as follows.

- PEI/MWCNT nanocomposites and their foams were fabricated using solvent-casting and solid-state foaming. It was found that the existence of residual solvent decreased the mechanical and thermal properties of the solvent cast samples. Mechanical and thermal properties of PEI/MWCNT nanocomposites and foams under different foaming conditions were investigated. Addition of MWCNTs has little effect on increasing the storage modulus of the nanocomposites. High thermal property of the PEI matrix was maintained by the PEI/MWCNT nanocomposites and foams. The normalized storage modulus of the foams was in good agreement with their unfoamed counterparts. Cell size has little effect on the thermal and mechanical property of foams in this study.

Volume electrical conductivities of the PEI/MWCNT nanocomposites and foams were measured at various MWCNT loadings. Volume electrical conductivities with the MWCNT loadings beyond the percolation threshold were within the range of electro-dissipative materials according to the ANSI/ESD standard, which indicates that those foams could be suitable for electrostatic dissipation applications with excellent inherent properties from the high performance polymer matrix. The effect of cell size, cell density, and relative density on the volume electrical conductivity was investigated. No significant effects of cell size and cell density on conductivity were found for the PEI/MWCNT foams obtained in this study. However, density of the foams affected the electrical conductivity. The higher the density, the less the nanofillers needed to reach percolation. At the same CNT loading in wt%, the higher the density is, the higher the electrical conductivity will be. This is due to the retention of the conducting path in high density foams. However, if the electrical conductivity is plotted against the CNT loading in volume%, the density of foams does not show effect on the electrical conductivity.

- PLA/MWCNT nanocomposites and their foams with different foaming conditions were fabricated using melt-blending and solid-state foaming. Effects of foaming conditions on porosity were investigated for PLA/MWCNT nanocomposite

foams. Mechanical and thermal properties of PLA/MWCNT nanocomposites and foams were characterized. Addition of MWCNTs increased the storage modulus. The normalized storage modulus of foams by (relative density)^2 was in a good agreement with their unfoamed counterparts. By foaming, the glass transition temperature increased by 5 °C. Volume electrical conductivities of PLA/MWCNT nanocomposites and foams were measured. Volume electrical conductivities with the MWCNT contents beyond the percolation threshold were within the range of dissipative materials according to the ANSI/ESD standard, which indicates that those foams could be suitable for electrostatic charge dissipation applications with their inherent biodegradable property. In general, the electrical conductivity of foamed samples had a higher conductivity than unfoamed ones. Especially, PLA/MWCNT foams with the saturation pressure of 2 MPa and foaming temperature of 100 °C showed a weight reduction by 1/10 without electrical conductivity sacrifice, which is beneficial in terms of materials saving. At a given volume%, as porosity increased the electrical conductivity increased significantly.

- A Monte Carlo simulation model was developed to understand and predict the electrical conductivity of polymer/MWCNT nanocomposite foams. Two different foam morphologies were considered, designated as Case 1: volume expansion without nanotubes rearrangement, and Case 2: nanotube aggregation in cell walls.

Simulation results for unfoamed nanocomposites and Case 1 foams were validated with the experimental data. The results were in good agreement with those from the PEI/MWCNT samples. Porosity effects on electrical conductivity were investigated for both Case 1 and Case 2 models. For the Case 1 model, the electrical conductivity decreased as porosity increased at a given loading in wt%. However, there was no porosity effect on electrical conductivity at a given volume%. At a given volume%, the electrical conductivity was identical regardless of the porosity. This result allows predicting electrical conductivity of Case 1 foams by density only if the unfoamed conductivity is known. For the Case 2 model, electrical conductivity did not decrease as the porosity increased. On the other hand, it increased at certain loadings. This result is interesting, since it suggests that it is achievable to reduce the density without sacrifice the electrical conductivity by foaming with the Case 2 foaming mechanism. This type of foams are promising in such applications as lightweight ESD and EMI shielding, because as the product becomes lighter, electrical performance gets better at a given product volume with the same amount of MWCNT loading.

- Electrical conductivity prediction of foamed polymer nanocomposites using the FEM method was performed. The results obtained from FEM were compared with those from the Monte-Carlo simulation method. It was found that FEM was

able to predict the electrical conductivity of polymer nanocomposite foams that could be represented with the Case 2 model when the pore size is small. However, it could not capture the pore size effect. FEM simulation can be utilized to predict the electrical conductivity of Case 2 foams when the percolation threshold is determined by the Monte-Carlo simulation to save the computation time for foams. .

7.2 FUTURE WORK

The current research has paved the way for further study, which could include the following.

7.2.1 Validation of Case 2 model

In the simulation study using the Monte-Carlo method, Case 2 model was used for electrical conductivity prediction without the model validation. Model validation was performed with unfoamed and foamed PEI/MWCNTs nanocomposites. Case 2 model was generated with the assumption that PEI/MWCNTs nanocomposites were foamed having large pores in the structure, and MWCNTs cannot be present in the pore region. Miller et al. found that solid state foaming of neat PEI gave the maximum pore size of around 4 μm [101]. Pore size is expected to be smaller if nanofillers are incorporated. Instead of solid state foaming, using chemical foaming method, PEI/MWCNTs nanocomposites foams could be fabricated having the Case 2 structure with larger pore sizes (4 μm and larger), such that the model Case 2 could be validated with the experimental results.

7.2.2 Simulation of Case 2 model with large pore size (a few tens or hundreds of microns)

In the current simulation study with Monte-Carlo simulation, there was limitation on the computational time for Case 2 model simulation with large pores due to the large number of nanofillers. The most time-consuming step during the simulation was the

distance evaluation among tube segments. The computational time increases exponentially as the number of tubes increases. To investigate the pore size effect, it could be considered to simplify wavy tubes to straight sticks such that the computational time could be reduced dramatically.

7.2.3 EMI shielding effectiveness

Thomassin et al. [3] found that foaming of conductive nanocomposites not only decrease the density of the product, but also increase the ability to absorb electromagnetic waves instead of reflecting them in EMI shielding applications. Their objective of study was to investigate the effect of foaming itself on EMI shieling effectiveness. It would be worth studying the effect of different foaming mechanisms discussed in this study (Case 1 and Case 2) on EMI shielding effectiveness. In addition, in the same foaming mechanism group, effects of foam density or pore size could be also investigated. By doing these, it is expected to find out what would be the most important contribution among foaming-related factors to the EMI shielding effectiveness.

Appendix

A.1 Resistance measurement procedures using multisim 12 (National instrument)

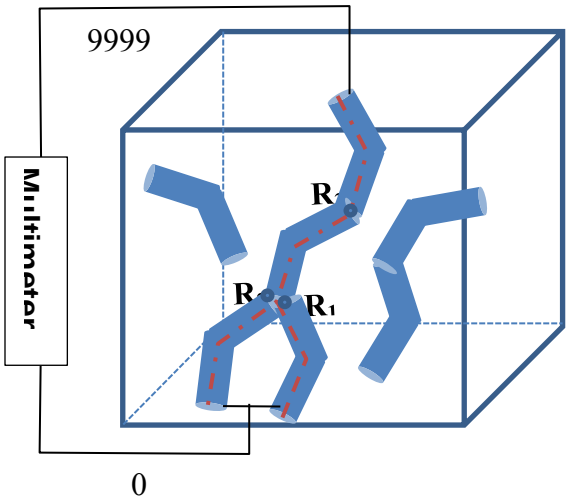

Figure A-1. Equivalent resistor network

MATLAB simulation determines the connectivity among each tube by distance measurements and this information can be used to construct SPICE (Simulation Program for Integrated Circuits Emphasis) code for resistors as shown below.

Resistor name, node number, node number, resistance value

Node numbers can be replaced by tube numbers which are connected and resistance value also can be assigned as discussed in Chapter 5. Tubes extruded on one side of the RVE cube are connected to the '9999' node, and the tubes extruded to the opposite side of the RVE cube are connected to the '0' node. This can be done by

converting those tube numbers to 9999 and 0 for corresponding sides when the total number of tubes used was less than 10000.

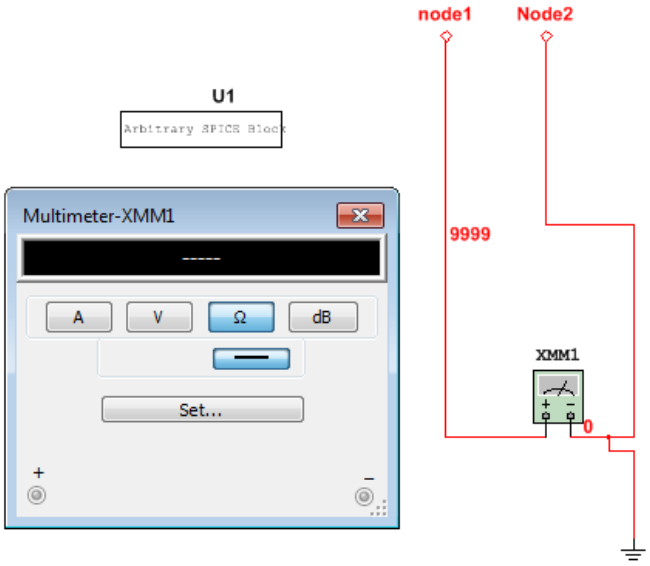

Figure A-2. A schematic of Multisim 12 to get net resistance of the system

Modified SPICE file is loaded to “Arbitrary SPICE Block” and a multimeter is connected to two nodes which are extruded to the opposite side of RVE cube and the net resistance is measured as shown in Figure A-2.

References

1. Li, N., Y. Huang, F. Du, X. He, X. Lin, H. Gao, Y. Ma, F. Li, Y. Chen and P. C. Eklund "Electromagnetic interference (EMI) shielding of single-walled carbon nanotube epoxy composites." *Nano letters* **6**(6) (2006): 1141-1145.

2. Zhang, H. B., Q. Yan, W. G. Zheng, Z. He and Z. Z. Yu "Tough Graphene− Polymer Microcellular Foams for Electromagnetic Interference Shielding." *ACS Applied Materials & Interfaces* **3**(3) (2011): 918-924.

3. Thomassin, J. M., C. Pagnoulle, L. Bednarz, I. Huynen, R. Jerome and C. Detrembleur "Foams of polycaprolactone/MWNT nanocomposites for efficient EMI reduction." *Journal of Materials Chemistry* **18**(7) (2008): 792-796.

4. Rizvi, R., J. K. Kim and H. Naguib "Synthesis and characterization of novel low density polyethylene–multiwall carbon nanotube porous composites." *Smart Materials and Structures* **18** (2009): 104002.

5. Yang, Y., M. Gupta, K. Dudley and R. Lawrence "Novel Carbon Nanotube-Polystyrene Foam Composites for Electromagnetic Interference Shielding." *Nano Lett* **5**(11) (2005): 2131-2134.

6. Yang, Y., M. Gupta, K. Dudley and R. Lawrence "Conductive carbon nanofiber–polymer foam structures." *Advanced materials* **17**(16) (2005): 1999-2003.

7. Xu, X., Z. Li, L. Shi, X. Bian and Z. Xiang "Ultralight Conductive Carbon Nanotube–Polymer Composite." *Small* **3**(3) (2007): 408-411.

8. Fletcher, A., M. C. Gupta, K. L. Dudley and E. Vedeler "Elastomer foam nanocomposites for electromagnetic dissipation and shielding applications." *Composites Science and Technology* **70**(6) (2010): 953-958.

9. Huynen, I., N. Quiévy, C. Bailly, P. Bollen, C. Detrembleur, S. Eggermont, I. Molenberg, J. M. Thomassin, L. Urbanczyk and T. Pardoen "Multifunctional hybrids for electromagnetic absorption." *Acta Materialia* **59**(8) (2011): 3255-3266.

10. Eswaraiah, V., V. Sankaranarayanan and S. Ramaprabhu "Functionalized Graphene–PVDF Foam Composites for EMI Shielding." *Macromolecular Materials and Engineering* **296**(10) (2011): 894-898.

11. Irimia-Vladu, M., E. D. Glowacki, G. Voss, S. Bauer and N. S. Sariciftci "Green and biodegradable electronics." *Materials Today* **15**(7-8) (2012): 340-346.

12. Koo, J. H. *Polymer nanocomposites: processing, characterization, and applications*, McGraw-Hill New York.(2006)

13. Iijima, S. "Helical microtubules of graphitic carbon." *nature* **354**(6348) (1991): 56-58.

14. Coleman, J. N., U. Khan, W. J. Blau and Y. K. Gun'ko "Small but strong: a review of the mechanical properties of carbon nanotube–polymer composites." *Carbon* **44**(9) (2006): 1624-1652.

15. Popov, V. N. "Carbon nanotubes: properties and application." *Materials Science and Engineering: R: Reports* **43**(3) (2004): 61-102.

16. Lee, L. J., C. C. Zeng, X. Cao, X. M. Han, J. Shen and G. J. Xu "Polymer nanocomposite foams." *Composites Science and Technology* **65**(15-16) (2005): 2344-2363.

17. Vaia, R. A., B. B. Sauer, O. K. Tse and E. P. Giannelis "Relaxations of confined chains in polymer nanocomposites: Glass transition properties of poly (ethylene oxide) intercalated in montmorillonite." *Journal of Polymer Science Part B: Polymer Physics* **35**(1) (1997): 59-67.

18. Kumar, S., B. Li, S. Caceres, R. Maguire and W. Zhong "Dramatic property enhancement in polyetherimide using low-cost commercially functionalized multi-walled carbon nanotubes via a facile solution processing method." *Nanotechnology* **20** (2009): 465708.

19. Koegler, W., C. Patrick, M. Cima and L. Griffith "Carbon dioxide extraction of residual chloroform from biodegradable polymers." *Journal of biomedical materials research* **63**(5) (2002): 567-576.

20. Andrews, R., D. Jacques, M. Minot and T. Rantell "Fabrication of carbon multiwall nanotube/polymer composites by shear mixing." *Macromolecular Materials and Engineering* **287**(6) (2002): 395-403.

21. Pötschke, P., A. R. Bhattacharyya, A. Janke and H. Goering "Melt mixing of polycarbonate/multi-wall carbon nanotube composites." *Composite Interfaces* **10**(4-5) (2003): 389-404.

22. Huang, X., S. Lewis, W. J. Brittain and R. A. Vaia "Synthesis of polycarbonate-layered silicate nanocomposites via cyclic oligomers." *Macromolecules* **33**(6) (2000): 2000-2004.

23. Cua, E. Polyetherimide-Silver Nanoparticle Nanofoamed Nanocomposites for Water Filtration Applications. *Department of Mechanical Engineering*. Seattle, University of Washington. **Master of Science** (2010)**:** 81.

24. Throne, J. L. *Thermoplastic foam extrusion: an introduction*, Hanser Gardner Publications.(2004)

25. Klempner, D., V. Sendijarevic, V. Sendijarevi c and R. Aseeva *Handbook of polymeric foams and foam technology*, Hanser Gardner Publications.(2004)

26. Guo, Z. Experimental analysis of polymer nanocomposite foaming using carbon dioxide. *Chemical and Biomolecular Engineering*. Columbus, The Ohio State University. **Doctor of Philosophy** (2008).

27. Lee, J. W. S. and C. B. Park "Use of Nitrogen as a Blowing Agent for the Production of Fine-Celled High-Density Polyethylene Foams." *Macromolecular Materials and Engineering* **291**(10) (2006): 1233-1244.

28. Lee, S. T. *Foam extrusion: principles and practice*, CRC.(2000)

29. Park, C. B., D. F. Baldwin and N. P. Suh "Effect of the pressure drop rate on cell nucleation in continuous processing of microcellular polymers." *Polymer Engineering & Science* **35**(5) (2004): 432-440.

30. Holl, M., V. Kumar, J. Garbini and W. Murray "Cell nucleation in solid-state polymeric foams: evidence of a triaxial tensile failure mechanism." *Journal of materials science* **34**(3) (1999): 637-644.

31. Vaccaro, N. Polyetherimide Carbon Nanofiber Nanofoamed Nanocomposites. *Mechanical Enginering*. Seattle, University of Washington. **Master of Science** (2010).

32. Ibeh, C. and M. Bubacz "Current trends in nanocomposite foams." *Journal of Cellular Plastics* **44**(6) (2008): 493.

33. Porter, D. A. and K. E. Easterling *Phase transformations in metals and alloys*, CRC.(1992)

34. Ham, F. S. "Diffusion-Limited Growth of Precipitate Particles." *Journal of applied physics* **30**(10) (1959): 1518-1525.

35. Strauss, W. and N. A. D'Souza "Supercritical CO2 processed polystyrene nanocomposite foams." *Journal of Cellular Plastics* **40**(3) (2004): 229.

36. Nam, P. H., P. Maiti, M. Okamoto, T. Kotaka, T. Nakayama, M. Takada, M. Ohshima, A. Usuki, N. Hasegawa and H. Okamoto "Foam processing and cellular structure of polypropylene/clay nanocomposites." *Polymer Engineering & Science* **42**(9) (2002): 1907-1918.

37. Taki, K., T. Yanagimoto, E. Funami, M. Okamoto and M. Ohshima "Visual observation of CO2 foaming of polypropylene-clay nanocomposites." *Polymer Engineering & Science* **44**(6) (2004): 1004-1011.

38. Mitsunaga, M., Y. Ito, S. S. Ray, M. Okamoto and K. Hironaka "Intercalated polycarbonate/clay nanocomposites: nanostructure control and foam processing." *Macromolecular Materials and Engineering* **288**(7) (2003): 543-548.

39. Fu, J. and H. E. Naguib "Effect of nanoclay on the mechanical properties of PMMA/clay nanocomposite foams." *Journal of Cellular Plastics* **42**(4) (2006): 325-342.

40. Jo, C. and H. E. Naguib "Effect of Nanoclay and Foaming Conditions on the Mechanical Properties of HDPE–Clay Nanocomposite Foams." *Journal of Cellular Plastics* **43**(2) (2007): 111-121.

41. Lee, Y., K. Wang, C. Park and M. Sain "Effects of clay dispersion on the foam morphology of LDPE/clay nanocomposites." *Journal of applied polymer science* **103**(4) (2006): 2129-2134.

42. Lee, L., J. Shen and H. Xiangmin *Nucleation and reinforcement of carbon nanofibers on polystyrene nancomposite foam*. ANTEC-CONFERENCE PROCEEDINGS-. (2005)

43. Chen, L., R. Ozisik and L. S. Schadler "The influence of carbon nanotube aspect ratio on the foam morphology of MWNT/PMMA nanocomposite foams." *Polymer* **51**(11) (2010): 2368-2375.

44. Rizvi, R., J. K. Kim and H. Naguib "Synthesis and characterization of novel low density polyethylene–multiwall carbon nanotube porous composites." *Smart Materials and Structures* **18**(10) (2009): 104002.

45. Sorrentino, L., M. Aurilia, L. Cafiero and S. Iannace "Nanocomposite foams from high-performance thermoplastics." *Journal of applied polymer science* **122**(6) (2011): 3701-3710.

46. Sorrentino, L., M. Aurilia and S. Iannace "Polymeric foams from high-performance thermoplastics." *Advances in Polymer Technology* **30**(3) (2011): 234-243.

47. Armentano, I., M. Dottori, E. Fortunati, S. Mattioli and J. Kenny "Biodegradable polymer matrix nanocomposites for tissue engineering: A review." *Polymer Degradation and Stability* **95**(11) (2010): 2126-2146.

48. Pilla, S., A. Kramschuster, S. Gong, A. Chandra and L. Turng "Solid and microcellular polylactide-carbon nanotube nanocomposites." *International Polymer Processing* **22**(5) (2007): 418.

49. Rizvi, R., O. Khan and H. E. Naguib "Development and characterization of solid and porous polylactide-multiwall carbon nanotube composites." *Polymer Engineering & Science* **51**(1) (2010): 43-53.

50. Pike, G. and C. Seager "Percolation and conductivity: A computer study. I." *Physical review B* **10**(4) (1974): 1421.

51. Balberg, I., N. Binenbaum and C. Anderson "Critical behavior of the two-dimensional sticks system." *Physical Review Letters* **51**(18) (1983): 1605-1608.

52. Du, F., J. E. Fischer and K. I. Winey "Effect of nanotube alignment on percolation conductivity in carbon nanotube/polymer composites." *Departmental Papers (MSE)* (2005): 79.

53. Balberg, I., N. Binenbaum and N. Wagner "Percolation thresholds in the three-dimensional sticks system." *Physical Review Letters* **52**(17) (1984): 1465.

54. Ounaies, Z., C. Park, K. Wise, E. Siochi and J. Harrison "Electrical properties of single wall carbon nanotube reinforced polyimide composites." *Composites Science and Technology* **63**(11) (2003): 1637-1646.

55. Yi, Y., L. Berhan and A. Sastry "Statistical geometry of random fibrous networks, revisited: Waviness, dimensionality, and percolation." *Journal of applied physics* **96** (2004): 1318.

56. Hu, N., Z. Masuda, C. Yan, G. Yamamoto, H. Fukunaga and T. Hashida "The electrical properties of polymer nanocomposites with carbon nanotube fillers." *Nanotechnology* **19** (2008): 215701.

57. Cao, X., L. James Lee, T. Widya and C. Macosko "Polyurethane/clay nanocomposites foams: processing, structure and properties." *Polymer* **46**(3) (2005): 775-783.

58. Chandra, A., S. Gong, M. Yuan, L. S. Turng, P. Gramann and H. Cordes "Microstructure and crystallography in microcellular injection-molded polyamide-6 nanocomposite and neat resin." *Polymer Engineering & Science* **45**(1) (2005): 52-61.

59. Di, Y., S. Iannace, E. D. Maio and L. Nicolais "Poly (lactic acid)/organoclay nanocomposites: thermal, rheological properties and foam processing." *Journal of Polymer Science Part B: Polymer Physics* **43**(6) (2005): 689-698.

60. Mahfuz, H., V. K. Rangari, M. S. Islam and S. Jeelani "Fabrication, synthesis and mechanical characterization of nanoparticles infused polyurethane foams." *Composites Part A: Applied Science and Manufacturing* **35**(4) (2004): 453-460.

61. Sinha Ray, S. and M. Okamoto "New polylactide/layered silicate nanocomposites, 6." *Macromolecular Materials and Engineering* **288**(12) (2003): 936-944.

62. Vanvuchelen, J., C. Perugini, M. Deweerdt, L. Chen and T. Burnham "Microcellular PVC foam for thin wall profile." *Journal of Cellular Plastics* **36**(2) (2000): 148.

63. Yuan, M., L. S. Turng, S. Gong, D. Caulfield, C. Hunt and R. Spindler "Study of injection molded microcellular polyamide-6 nanocomposites." *Polymer Engineering & Science* **44**(4) (2004): 673-686.

64. Zeng, C., X. Han, L. Lee, K. Koelling and D. Tomasko *Structure of nanocomposite foams*. (2001)

65. Zeng, C., X. Han, L. J. Lee, K. W. Koelling and D. L. Tomasko "Polymer–clay nanocomposite foams prepared using carbon dioxide." *Advanced materials* **15**(20) (2003): 1743-1747.

66. Zeng, C., N. Hossieny, C. Zhang and B. Wang "Synthesis and processing of PMMA carbon nanotube nanocomposite foams." *Polymer* **51**(3) (2010): 655-664.

67. Liu, T., Y. Tong and W. Zhang "Preparation and characterization of carbon nanotube/polyetherimide nanocomposite films." *Composites Science and Technology* **67**(3-4) (2007): 406-412.

68. Sasaki, M., S. Takishima and H. Masuoka "Supercritical carbon dioxide extraction of benzene in poly (vinyl acetate) and polystyrene (Part 2)." **33**(5) (1990): 304-310.

69. Jacobs, M. (2005). "Carbon dioxide pressure-temperature phase diagram." from http://en.wikipedia.org/wiki/File:Carbon_dioxide_pressure-temperature_phase_diagram.svg.

70. Moore, D. and M. Iremonger "The prediction of the flexural rigidity of sandwich foam mouldings." *Journal of Cellular Plastics* **10**(5) (1974): 230-236.

71. Bauhofer, W. and J. Z. Kovacs "A review and analysis of electrical percolation in carbon nanotube polymer composites." *Composites Science and Technology* **69**(10) (2009): 1486-1498.

72. "American National Standard Institute (ANSI/ESD) S541-2008." (2008).

73. Villmow, T., P. Pötschke, S. Pegel, L. Häussler and B. Kretzschmar "Influence of twin-screw extrusion conditions on the dispersion of multi-walled carbon nanotubes in a poly (lactic acid) matrix." *Polymer* **49**(16) (2008): 3500-3509.

74. Kobashi, K., T. Villmow, T. Andres and P. Pötschke "Liquid sensing of melt-processed poly (lactic acid)/multi-walled carbon nanotube composite films." *Sensors and Actuators B: Chemical* **134**(2) (2008): 787-795.

75. McCullen, S. D., K. L. Stano, D. R. Stevens, W. A. Roberts, N. A. Monteiro-Riviere, L. I. Clarke and R. E. Gorga "Development, optimization, and characterization of electrospun poly (lactic acid) nanofibers containing multi-walled carbon nanotubes." *Journal of applied polymer science* **105**(3) (2007): 1668-1678.

76. Garlotta, D. "A literature review of poly (lactic acid)." *Journal of Polymers and the Environment* **9**(2) (2001): 63-84.

77. Wang, X. Solvent-free Fabrication of Porous Polymer for Tissue Engineering Applications. *Department of Mechanical Engineering*. Seattle, University of Washington. **Doctor of Philosophy** (2007)**:** 167.

78. Liao, X., A. V. Nawaby and H. E. Naguib "Porous poly (lactic acid) and PLA-nanocomposite structures." *Journal of applied polymer science* (2012).

79. Matuana, L. "Solid state microcellular foamed poly (lactic acid): Morphology and property characterization." *Bioresource technology* **99**(9) (2008): 3643-3650.

80. Krause, B. Polymer Nanofoams. *Chemical Engineering*. Enschede, The Netherlands, University of Twente. **Doctor of Philosophy** (2001)**:** 176.

81. Zhou, C., P. Wang and W. Li "Fabrication of functionally graded porous polymer via supercritical CO_2 foaming." *Composites Part B: Engineering* **42**(2) (2011): 318-325.

82. TA instrument. *Dynamic Mechanical Analysis: Basic theory and applications training*.(2011)

83. Natsuki, T., M. Endo and T. Takahashi "Percolation study of orientated short-fiber composites by a continuum model." *Physica A: Statistical Mechanics and its Applications* **352**(2) (2005): 498-508.

84. Wu, S. H., I. Masaharu, T. Natsuki and Q. Q. Ni "Electrical conduction and percolation behavior of carbon nanotubes/UPR nanocomposites." *Journal of reinforced plastics and composites* **25**(18) (2006): 1957-1966.

85. Taya, M. and N. Ueda "Prediction of the in-plane electrical conductivity of a misoriented short fiber composite: fiber percolation model versus effective medium theory." *Journal of Engineering Materials and Technology* **109** (1987): 252.

86. Lee, Y. H. and H. Kim "Three-dimensional electrical percolation behaviour in conductive short-fibre composites." *Journal of materials science* **30**(12) (1995): 3033-3036.

87. Foygel, M., R. Morris, D. Anez, S. French and V. Sobolev "Theoretical and computational studies of carbon nanotube composites and suspensions: Electrical and thermal conductivity." *Physical review B* **71**(10) (2005): 104201.

88. Dalmas, F., R. Dendievel, L. Chazeau, J. Y. Cavaillé and C. Gauthier "Carbon nanotube-filled polymer composites. Numerical simulation of electrical conductivity in three-dimensional entangled fibrous networks." *Acta Materialia* **54**(11) (2006): 2923-2931.

89. Lu, W., T. W. Chou and E. T. Thostenson "A three-dimensional model of electrical percolation thresholds in carbon nanotube-based composites." *Applied Physics Letters* **96** (2010): 223106.

90. Ma, H. and X. L. Gao "A three-dimensional Monte Carlo model for electrically conductive polymer matrix composites filled with curved fibers." *Polymer* **49**(19) (2008): 4230-4238.

91. Narayanunni, V., H. Gu and C. Yu "Monte Carlo simulation for investigating influence of junction and nanofiber properties on electrical conductivity of segregated-network nanocomposites." *Acta Materialia* (2011).

92. Sun, X. and M. Song "Highly conductive carbon nanotube/polymer nanocomposites achievable?" *Macromolecular Theory and Simulations* **18**(3) (2009): 155-161.

93. Yu, Y. Modeling of mechanical dampling and electrical properties of carbon nanotube reinforced composites. *Department of Mechanical Engineering*. Houston, University of Houston. **Doctor of Philosophy** (2010)**:** 192.

94. Sunday, D. (2006). "Distance between two line segments." from http://softsurfer.com/Archive/algorithm_0106/algorithm_0106.htm#dist3D_Segment_to_Segment.

95. Fuhrer, M., J. Nygård, L. Shih, M. Forero, Y. G. Yoon, H. J. Choi, J. Ihm, S. G. Louie, A. Zettl and P. L. McEuen "Crossed nanotube junctions." *Science* **288**(5465) (2000): 494-497.

96. Li, C., E. T. Thostenson and T. W. Chou "Dominant role of tunneling resistance in the electrical conductivity of carbon nanotube–based composites." *Applied Physics Letters* **91**(22) (2007): 223114-223114-223113.

97. Reneker, D. H. and I. Chun "Nanometre diameter fibres of polymer, produced by electrospinning." *Nanotechnology* **7**(3) (1999): 216.

98. Hentschke, R., B. L. Schürmann and J. P. Rabe "Molecular dynamics simulations of ordered alkane chains physisorbed on graphite." *The Journal of chemical physics* **96**(8) (1992): 6213-6221.

99. Stevens, M. P. *Polymer Chemistry*, Oxford University Press.(1999)

100. Simmons, J. G. "Electric tunnel effect between dissimilar electrodes separated by a thin insulating film." *Journal of applied physics* **34**(9) (1963): 2581-2590.

101. Miller, D., P. Chatchaisucha and V. Kumar "Microcellular and nanocellular solid-state polyetherimide (PEI) foams using sub-critical carbon dioxide I. Processing and structure." *Polymer* **50**(23) (2009): 5576-5584.